ABSTRACT

Title of Dissertation: MINIMALLY INVASIVE NEUROCHEMICAL SENSING SYSTEMS FOR *IN VITRO* AND *IN VIVO* INVESTIGATION OF SEROTONERGIC MODULATION

Jinjing Han, Doctor of Philosophy, 2023

Dissertation Directed By: Dr. Reza Ghodssi
Department of Electrical and Computer Engineering
Institute for System Research

Serotonin (5-hydroxytryptamine, 5-HT) plays a crucial role as a monoamine neurotransmitter, regulating various behavioral and physiological functions in the brain and peripheral systems. Its effects encompass emotions, behaviors, gastrointestinal motility, hemostasis, and cardiovascular function. Dysregulation of the serotonergic system and imbalances in 5-HT levels have been associated with psychiatric disorders, underscoring its potential as a biomarker for conditions like anxiety disorders, depression, Alzheimer's disease, and impulsive aggressiveness. However, the precise mechanisms by which 5-HT modulates these physiological conditions and behavioral processes remain unknown, necessitating the use of sensing tools to monitor 5-HT dynamics in specific locations. Traditional techniques such as high-performance liquid chromatography (HPLC) and enzyme-linked immunosorbent assay (ELISA) have been employed to measure 5-HT concentrations in biological samples. However, these offline methods only provide information at the end of an experiment and lack spatial and temporal resolution. Due to the rapid extracellular

release and uptake of 5-HT, there is a clear need for detection techniques with high spatiotemporal resolution to investigate serotonergic modulations.

This dissertation focuses on the development of minimally invasive neurochemical sensing systems to address challenges related to real-time 5-HT sensing and facilitate *in vitro* and *in vivo* investigation of serotonergic modulation. Two sensing systems were developed. For *in vitro* 5-HT sensing, surface-modified microelectrodes with single carbon fiber were developed and integrated with a portable potentiostat for point-of-care (POC) applications. These microelectrodes were tested for detecting *in vitro* cell-secreted 5-HT and 5-HT in homogenized crayfish nerve cord samples. The portable system exhibited a sensitivity of 74 nM/μM with a limit of detection (LOD) of 140 nM. Moreover, it was tested for detecting 5-HT in artificial urine, showcasing its application as a POC device for early diagnosis of 5-HT syndrome from urine tests. For *in vivo* 5-HT sensing, surface-modified microelectrodes with multiple carbon fibers were developed to enhance mechanical robustness specifically for *in vivo* applications. After integration with a miniature PCB, the device was able to co-detect dopamine (DA) and 5-HT at sub-micromolar concentrations with wireless communication. The integrated untethered implantable system demonstrated its capabilities for *in vivo* simultaneous monitoring of DA and 5-HT in freely moving crayfish during injection events. Overall, these developed systems offer electrochemical 5-HT sensing solutions for both *in vitro* and *in vivo* applications, providing reliable tools to obtain real-time 5-HT dynamics information with high spatial resolution. This capability significantly enhances our ability to investigate precise 5-HT signaling and mechanism underlying serotonergic modulation in the disorder development and behavioral processes.

MINIMALLY INVASIVE NEUROCHEMICAL SENSING SYSTEMS FOR IN VITRO AND IN VIVO INVESTIGATION OF SEROTONERGIC MODULATION

By

Jinjing Han

Dissertation submitted to the Faculty of the Graduate School of the
University of Maryland, College Park, in partial fulfillment
of the requirements for the degree of
Doctor of Philosophy
2023

Advisory Committee:
Professor Reza Ghodssi, Chair
Professor Pamela Abshire
Professor Kevin Daniels
Professor Timothy Horiuchi
Professor Jens Herberholz, Dean's Representative

Dedication

To my parents and family,

who have supported and fueled my journey,

and

to Mingqian (Erica),

who completed my soul.

This achievement is as much yours as mine.

所爱隔山海

山海亦可平

Acknowledgements

I would like to express my gratitude to my advisor, Professor Reza Ghodssi, for his guidance throughout the development of this work. Together with Professor Jens Herberholz, they have provided a valuable sounding board in the larger scheme of our research goals. I would also like to extend my thanks to Professors Pamela Abshire, Timothy Horiuchi, and Kevin Daniels for their roles as members of my thesis committee and for their valuable feedback on this dissertation.

I am deeply appreciative of the contributions made by both former and current members of the MEMS Sensors and Actuator Lab (MSAL) at every stage of this project. Specifically, I would like to acknowledge Drs. Pradeep Rajasekaran and Ashley Chapin as the originators of the serotonin sensing project and for their development of the electrochemical sensing platform for serotonin detection in cell culture environments. They also played a crucial role in mentoring me and teaching me the fundamentals of electrochemistry early on in my career. I would also like to acknowledge Dr. Justin Stine for his work in developing the customized potentiostat circuit and for his guidance in implementing cyclic voltammetry measurements and wireless communication functions. I am grateful for the unwavering support from all the members of MSAL, including Josh Levy, Michael Straker, Sydney Overton, Brian Holt, and Katie Ruland, who have consistently provided their presence and feedback. I would also like to express my appreciation to former MSAL members, Dr. Sanwei Liu, Dr. Sangwook Chu, Dr. George Banis, Dr. Ryan Huiszoon, and Dr. Santiago Botasini for their mentorship. Special thanks go to Peiyao Jia for her invaluable assistance in editing and organizing documents.

Furthermore, the direct collaborations I have had with the Herberholz lab, the Losert lab, and the Bentley lab have significantly enhanced the quality of my work and have led to exciting discussions and future directions. I would like to extend my heartfelt gratitude, particularly to Ta-

wen Ho and Dr. Herberholz, for their significant contributions in assisting with crayfish surgeries and experiments.

I would like to acknowledge and thank the technical staff at the FabLab, AIMLab, and Terrapin Works for their unwavering support in maintaining fabrication equipment, providing training for these processes, and offering fabrication assistance when needed. I am also grateful for the assistance provided by the administrative staff in ISR and ECE, especially Regina King, Carla Scarbor, Julianna Bynoe, Emily Irwin, and Melanie Prange, who have ensured the smooth functioning of our operations and provided helpful assistance during times of need.

Lastly, I owe a tremendous debt of gratitude to my parents, Jiazhen and Li, who have been unwavering in their support of my education and have made it possible for me to succeed. I would also like to express my heartfelt appreciation to my aunt and uncle, Xin and Xing, as well as my grandparents, Keming and Lian, for their constant encouragement and life guidance. Most importantly, I want to thank Mingqian for her love, which has brought fulfillment to my life.

Table of Contents

List of Tables

List of Figures

List of Abbreviations

5-HT: Serotonin

CNS: Central nervous system

HPLC: High-performance liquid chromatography

ELISA: Enzyme-linked immunosorbent assay

CFME: Carbon fiber microelectrode

PCB: Printed circuit board

SERT: Serotonin transporter

5-HTR: Serotonin receptor

CNT: Carbon nanotube

LOD: Limit of detection

LOQ: Limit of quantification

5-HIAA: 5-Hydroxyindoleacetic acid

UA: Uric acid

DA: Dopamine

NE: Norepinephrine

ADN: Adenosine

CV: Cyclic voltammetry

AFE: Analog front-end

BLE: Bluetooth Low Energy

MCU: Microcontroller unit

3D printing: 3-dimensional printing

Ipa: Oxidation peak current

Epa: Oxidation peak potential

SSRI: Selective serotonin reuptake inhibitors

5-HTTP: 5-Hydroxytryptophan

TPH: Tryptophan hydroxylase

MAO: Monoamine oxidase

MAOI: Monoamine oxidase inhibitor

FSCV: Fast-scan cyclic voltammetry

DPV: Differential pulse voltammetry

CA: Chronoamperometry

GCE: Glassy carbon electrode

CPE: Carbon paste electrode

SPCE: Screen-printed carbon electrode

AA: Ascorbic acid

PEDOT: Poly(3,4-ethylenedioxythiophene)

WE: Working electrode

RE: Reference electrode

CE: Counter electrode

TIA: Transimpedance amplifier

ADC: Analog-to-digital converter

ASIC: Application-specific integrated circuit

COTS: Commercial off-the-shelf

PSS: Polystyrene sulfonate

VTA: Ventral tegmental area

LED: Light-emitting diode

POC: Point of care

SEM scanning electron microscopy

EDS: Energy-dispersive X-ray spectroscopy

EASA: Electrochemically active surface area

PAN: Polyacrylonitrile

DNR: Dorsal raphe nucleus

CSF: Cerebrospinal fluid

FBS: Fetal bovine serum

HBSS: Hanks' Balanced Salt Solution

AITC: Aryl isothiocyanate

CGM: Continuous glucose monitoring

I^2C: Inter-integrated controller

SPI: Serial peripheral interface

DAC: Digital-to-analog converter

LPDAC: low power digital-to-analog converter

PA: potentiostat amplifier

LPTIA: low power transimpedance amplifier

SE: Sense electrode

GUI: Graphical User Interface

UART: Universal asynchronous receiver-transmitter

PBS: Phosphate-buffered saline

DLW: Direct laser writing

SLA: Stereolithography

Chapter 1 Introduction

1.1 Motivation and Background

Serotonin (5-hydroxytryptamine, 5-HT) is a monoamine neurotransmitter that has been implicated in numerous behavioral and physiological processes [1]–[16]. It is synthesized by serotonergic neurons in the brain and used to transmit messages to other neurons to modulate virtually all human behavioral process, ranging from mood, memory, aggression, addiction to sexuality [1], [2], [9]–[12]. Outside of the central nervous system (CNS), 5-HT also regulates physiological functions in vascular biology, cardiac function, metabolism and gastrointestinal system [1], [3]–[8], [12]–[16]. Dysregulated serotonergic system and 5-HT signaling have been linked to psychiatric disorders, highlighting its potential as a biomarker for conditions like anxiety disorders, depression, Alzheimer's disease, and impulsive aggressiveness [9], [17]–[20].

Despite the significance of these conditions and disorders, the precise mechanism and 5-HT signaling underlying serotonergic modulation in their development remain largely unexplored and still need to be elucidated in more detail. One reason for the lack of knowledge can be attributed to the absence of available tools to measure the release of 5-HT with high temporal and spatial resolution. Until recently, the gold standard analytical tools for detecting 5-HT signaling in biological samples involve sample extraction, followed by high-performance liquid chromatography (HPLC) [14] or enzyme-linked immunosorbent assay (ELISA) [21]. However, these techniques are limited in low temporal and spatial resolution since samples must be collected for off-line analysis. Due to the rapid response time of neurotransmitters and their fast release and clearance from the extracellular space [22], there is a need to develop a rapid technique for detecting 5-HT concentration dynamics in real-time with high temporal and spatial resolution.

Current researchers have been focusing on developing alternative analytical methods for *in situ* quantification of 5-HT signaling in real time. Techniques using microdialysis probes [23]–[26], optical fibers [27]–[29], and electrochemical sensors [30]–[35] have been implemented for detecting neurotransmitters in the brain region and have been instrumental in advancing our understanding of neurobiology, psychopharmacology, and behavioral neuroscience, revealing new insights into phenomena such as the sleep-wake cycle [25] and reward-related responses [36]. However, during *in vivo* experiments, these methods often require guide cannulas, optical fibers, electrodes, and other components affixed to the animal's skull, allowing for the direct connection of electrical cables and fluid lines [37]–[39], which limit their capability in more complex behavioral studies. Behavioral assays usually involve confining a single animal within a box or cylinder with an open top. However, the cables used for the connection are intrusive and often restrain the animal, and animal movements may damage the wires or cause wires to coil around the animal. Furthermore, wires limit the animals' range and hinder experiments exploring interactions between multiple animals. While there is a strong desire to integrate neurotransmitter detection into wirelessly operated devices for living animals, this area remains underdeveloped in current research. An untethered sensing system is preferred to eliminate the impact on animal behavior during the measurement for a better understanding of serotonergic modulation.

1.2 Thesis Contribution

Based on the background and motivations discussed above, my dissertation focuses on developing electrochemical sensing systems for 5-HT detection with high spatiotemporal resolution, designed for investigating serotonergic modulations in animal models. This work involves (1) the development of novel surface-modified carbon fiber microelectrodes (CFMEs)

for sensitive, selective 5-HT sensing with minimal fouling, (2) the implementation of a customized printed circuit board (PCB) for electrochemical measurement with wireless communication, and (3) the systematic integration for a miniaturized implantable device for continuous 5-HT monitoring in freely moving animals (**Figure 1-1**). The developed microelectrodes were validated for 5-HT detection in both a modeled gut epithelial cell culture environment and a homogenized nerve cord sample, demonstrating their potential to study 5-HT molecular transportation and serotonergic modulation in complex biological environments. The customized PCB potentiostat module provided a small form-factor, low-cost, precision electrochemical sensing solution for electrochemical sensing. This device served as an intermediate step toward developing an implantable, miniaturized, low-cost, battery-operated electrochemical sensing system which can be operated without a tether. Together, an integrated untethered implantable system is developed for *in vivo* 5-HT monitoring and studying serotonergic modulation related to animal behaviors. Overall, this work presents engineered approaches detect 5-HT signaling and dynamics, therefore facilitates the study of serotonergic modulations.

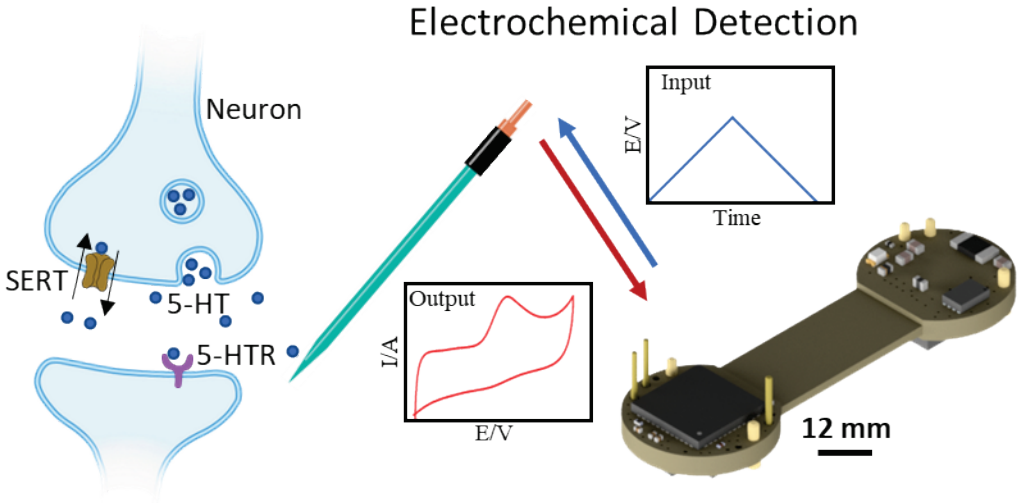

Figure 1-1 Developed CFME and PCB potentiostat can be used to monitor 5-HT signaling and dynamics with high spatiotemporal resolution to investigate serotonergic modulation. SERT: 5-HT transporter. 5-HTR: 5-HT receptor.

1.2.1 Novel Carbon Fiber Microelectrode Modification Methods

In this work, I developed novel surface treatment techniques for CFMEs to achieve sensitivity and selectivity in 5-HT detection. CFMEs were electrochemically treated to improve their sensitivity and coated with Nafion and carbon nanotubes (CNTs) to enhance their selectivity and fouling resistance. Two types of microelectrodes were developed based on their applications: (a) a microelectrode with a **single** carbon fiber to achieve a lower limit of detection (LOD) suitable for *in vitro* applications, and (b) a microelectrode with a **bundle** of carbon fibers to achieve higher sensitivity and mechanical strength for *in vivo* measurements.

Both microelectrodes were evaluated in a standard 5-HT solution to assess their sensitivity, selectivity, and fouling resistance. The single fiber microelectrode demonstrated a sensitivity of 84.6 nA/μM with a LOD of 17 nM for 5-HT detection, while the fiber bundle microelectrode exhibited a sensitivity of 129.9 nA/μM, with a LOD of 85.1 μM. For 5-HT detection, another challenge is the interference from 5-hydroxyindoleacetic acid (5-HIAA), uric acid (UA), dopamine (DA), norepinephrine (NE), and adenosine (ADN) [40]–[42]. These molecules are present in all biological fluids at high concentrations and, unfortunately, are electrochemically active, complicating its selective detection. Both microelectrodes showed high selectivity for 5-HT over these electroactive molecules. Additionally, both microelectrodes demonstrated good fouling resistance over multiple consecutive cycles.

Furthermore, the performance of the developed microelectrodes was tested in realistic biological samples, including *in vitro* gut cell culture, homogenized crayfish tissue, and *in vivo* crayfish hemolymph (i.e., blood), yielding promising results. *In vitro* gut cell culture and crayfish are common models for investigating 5-HT signaling and serotonergic effects [43], [44]. Overall,

the developed microelectrodes with the novel surface modification methods demonstrated feasibility and potential for reliable detection of 5-HT in complex biological environments.

1.2.2 Development of Miniaturized Electrochemical Sensing Module

In this section, a customized PCB potentiostat module was implemented for cyclic voltammetry (CV) measurements and utilized for 5-HT detection. One of the key components is an analog front-end (AFE), AD5941, which is a commercial-off-the-shelf component specifically designed for performing low-power and high-precision electrochemical measurements. This makes it an ideal component for portable and miniaturized applications. The AD5941 evaluation board was utilized to configure and evaluate the performance of AD5941 in electrochemical sensing, in comparison to a benchtop potentiostat.

By combining the surface-modified CFME with the AD5941-based sensing system, successful detection of 5-HT was achieved with a sensitivity of 73.7 nA/μM and a LOD of 140 nM. Although the system did not reach the sensitivity and LOD of the benchtop potentiostat, it is still sufficient for detecting 5-HT at physiological concentrations.

Non-invasive rapid tests usually require samples of body fluids, such as blood, urine, saliva, and nasal secretions. In the body, 5-HT is produced and released into the blood, transported to the kidneys through systemic circulation, and then excreted into the urine [45], [46]. Thus, urinary 5-HT is a potential biomarker of 5-HT syndrome [47], as well as other serotonergic imbalance associated physiological conditions such as depression [45] and carcinoid tumors [48]. The sensing platform demonstrated its ability to sense 5-HT in artificial urine samples, indicating its potential as a portable analytical tool for diagnosing 5-HT syndrome.

Moving forward, a miniaturized PCB based on the AD5941 and a Bluetooth Low Energy-Microcontroller Unit (BLE–MCU) was used to perform electrochemical measurements to detect 5-HT with the previously developed microelectrode using CV, demonstrating a sensitivity of 70.0 nA/μM, which is very similar to the result obtained from the AD5941 evaluation board. This showcased the successful adoption of cyclic voltammetry functionalities on the customized board. The performance of the PCB and the developed CFMEs were tested for *in vivo* 5-HT detection through wired connections. The sensing system successfully achieved 5-HT monitoring in crayfish hemolymph 30 minutes after 5-HT injection.

1.2.3 System Integration for an Untethered Implantable Electrochemical Sensing Device

Upon the development and characterization of two key components, the surface-modified CFME and customized PCB potentiostat, I have successfully integrated them into a fully integrated electrochemical sensing device with wireless transmission capability (**Figure 1-2**). To ensure a compact design that minimizes its impact on animal behavior, the device was prototyped using 3D printing technology, resulting in dimensions of 2.8 × 2.3 × 2.1 cm. For *in vivo* CV measurement in crayfish, the device was further protected with an additional epoxy layer to ensure water resistance, as crayfish prefer an underwater environment, which aligns with their natural habitat. Moreover, the device capability has been expanded for simultaneous co-detection of 5-HT and DA, allowing the study of their *in vivo* interactions.

The cyclic voltammetry waveform was optimized to achieve simultaneous detection of DA and 5-HT using the portable device for beaker level testing, yielding sensitivities of 51.6 nA/μM and 133.0 nA/μM, respectively, within the sub-micromolar range. With the 3D printed customized package, the device can be easily attached to the dorsal carapace of a crayfish, facilitating electrode

implantation into the crayfish's heart to monitor the dynamics of DA and 5-HT before and after drug injections. Notably, the implantable biosensor system exhibited a significant increase in oxidation peak currents (Ipas) following DA and 5-HT injections. This successful demonstration of the device establishes its application for simultaneous *in vivo* monitoring of DA and 5-HT in the hemolymph of freely behaving crayfish underwater. Consequently, the device serves as a valuable experimental tool to enhance our understanding of the co-modulation of DA and 5-HT. The potential applications of this device extend to monitoring the dynamic interactions of neurotransmitters in correlation with real-time animal behaviors.

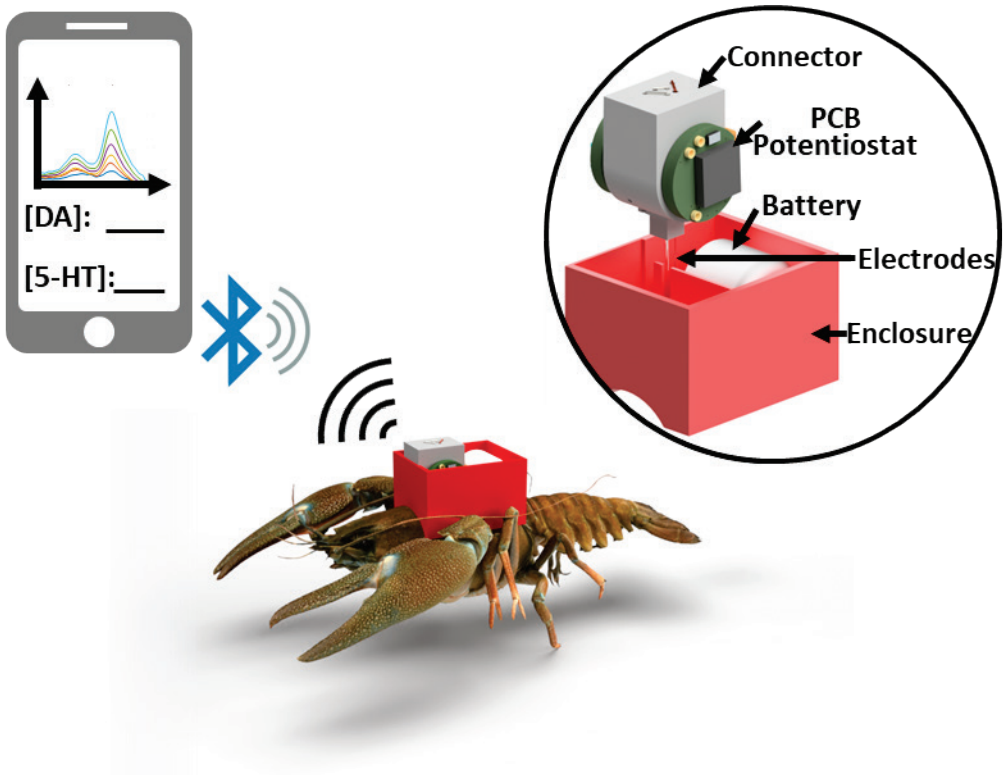

Figure 1-2 Schematic illustrations depict the electrochemical sensing device and its capabilities for wireless simultaneous detection of DA and 5-HT in freely moving crayfish.

1.3 Literature Review

1.3.1 Serotonergic Modulation and Animal Behaviors

Serotonin Physiological Functions

5-HT plays a crucial role as a monoamine neurotransmitter in regulating various behavioral and physiological functions within the brain and peripheral systems (**Figure 1-3**). As the neurotransmitter in the brain, 5-HT is synthesized mainly in the brainstem by 5-HT neurons located in the raphe nuclei. These neurons project to various regions of the brain, including the prefrontal cortex, hippocampus, amygdala, and basal ganglia, as well as to the spinal cord and peripheral organs. The amount of 5-HT in these neurons can regulate cognition, such as memory and learning [49], as well as several social behaviors, such as sexual preference [50]. In clinical settings, lower levels of 5-HT also lead to higher possibility of depression, suicide and violence [18], [51]–[53].

On the other hand, 5-HT also regulates hormonal functions in the human body, which is maily produced in the gastrointestinal tract. The gut-derived 5-HT is mostly produced by enterochromaffin cells, and locally activates afferent nerve endings that are connected directly to the CNS [8]. Gut 5-HT can also be transported into plasma, and blood 5-HT is stored in platelets. This systemic 5-HT cannot reach the brain since it cannot cross the “blood-brain barrier” and does not directly impact brain functions. However, there are a considerable number of 5-HT receptors expressed in various peripheral organs, suggesting 5-HT functions in regulating vascular biology, cardiac function, metabolism and gastrointestinal motility [1], [3]–[8], [12]–[16].

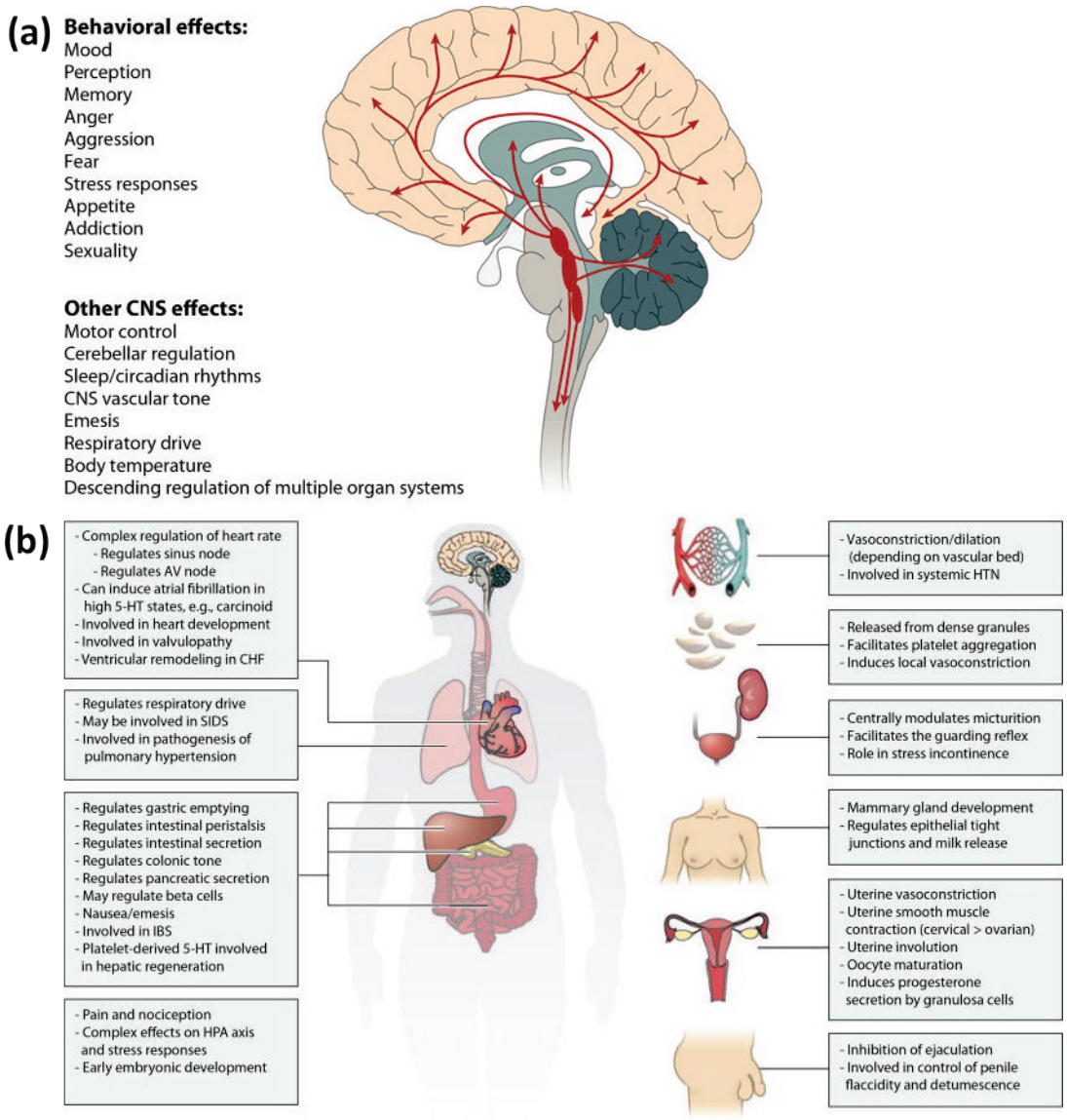

Figure 1-3 Serotonergic modulations in human. (a) Central serotonergic pathways, effects. (b) Systemic serotonergic modulations outside the CNS [1].

Serotonergic neurons in the CNS and enterochromaffin cells in the mucosa of the gastrointestinal tract synthesize 5-HT through a two-step metabolic pathway. Tryptophan is first hydroxylated to 5-hydroxytryptophan (5-HTP) by tryptophan hydroxylase (TPH), followed by the decarboxylation of 5-HTP by aromatic l-acid decarboxylase to finally form 5-HT [16]. Once synthesized, 5-HT is released from the presynaptic neuron or enterochromaffin cell into the

synaptic cleft, where it binds to and activates 5-HT receptors (5-HTRs) on the postsynaptic neuron or other target cells. Upon activation, they produce either excitatory or inhibitory response based on the different receptor families. Although the signaling pathways to which these receptors are coupled are known, it is has not been possible to link direct clinical effects systematically to their stimulation [54].

Another mechanism for the regulation of 5-HT signaling is the serotonin transporter (SERT), which is responsible for the reuptake of 5-HT from the synaptic cleft back into the presynaptic neuron. Drugs that inhibit SERT, such as selective serotonin reuptake inhibitors (SSRIs), have been used clinically to increase the concentration of 5-HT in the synaptic cleft and enhance 5-HT signaling. Monoamine oxidase (MAO) is also involved in the regulation of 5-HT signaling by breaking down 5-HT into inactive metabolites. The subtype MAO-A preferentially metabolizes 5-HT, while MAO-B preferentially metabolizes DA. Drugs that inhibit MAO, such as monoamine oxidase inhibitors (MAOIs), increase the concentration of 5-HT in the synaptic cleft and enhance 5-HT signaling.

The neural circuitry responsible for each of behavioral and physiological processes modulated by 5-HT still needs to be elucidated. Current research simplifies the question of how 5-HT modulates each process in terms of how specific 5-HTRs modulate the specific brain regions or organs involved in producing the behavioral and physiological output. A complicated interplay of numerous 5-HTRs, which are expressed in different brain regions and organs, influences a variety of behavioral and physiological functions. For instance, the 5-HT_{1A} and 5-HT_{2C} receptors are principally involved in the control of anxiety-like behavior [55], [56]. Interestingly, in addition to anxiety, the 5-HT_{2C} receptor also regulates food, energy balance, movement, reward processing,

and more [57]. This basic idea clarifies why medications that target particular 5-HTR may have an impact on a variety of behavioral processes [57].

In summary, serotonergic modulation is a highly complex system, with multiple mechanisms involved in the regulation of serotonin signaling. Understanding the serotonergic pathways and mechanisms is crucial for the development of new drugs and treatments for various psychiatric and neurological disorders.

Serotonergic Modulation in Crayfish Behaviors

Both invertebrates and vertebrates have been used to investigate serotonergic modulations. Although there is a huge structural difference between invertebrates and vertebrates, the influences of 5-HT on behavior and cognition are evolutionary conserved [9]. Both invertebrates and vertebrates have shown similar serotonergic modulations in motor activities [58], [59], sleep cycles [60], [61], feeding [62], social interaction [63], [64], aggressiveness, anxiety [65], mood [66], and learning [9], [67] (**Figure 1-4**).

Crayfish have been used extensively for studying serotonergic modulation for several reasons. The nervous system of crayfish is relatively simple, making it easier to study the effects of neurotransmitters such as 5-HT on behavior. The crayfish nervous system is composed of about 100,000 neurons, compared to the billions of neurons found in mammals [68], [69]. This simplicity allows researchers to investigate the effects of 5-HT on specific neuronal circuits and behaviors more easily.

Crayfish exhibit robust behavioral responses to changes in 5-HT levels, making it easier to study the effects of 5-HT on behavior. Changes in 5-HT levels can lead to changes in aggression [63], escape behavior [66], [70], and circadian rhythms [71] in crayfish, providing clear and measurable behaviors to study. For example, citalopram, a common SSRI, exposed crayfish exhibit

increased boldness and spend more time orienting to food resources [72]. Similarly, 5-HTR agonists exposure also alters aggression and escape behavior in crayfish [73]. Furthermore, altered 5-HT levels in crayfish by direct 5-HT injections also led to altered aggression and boldness [74], [75]. These findings demonstrate the importance of the serotonergic system in regulating a variety of behaviors in crayfish.

Crayfish are relatively easy to obtain and maintain in the laboratory, making them a convenient model organism for studying serotonergic modulation. They can be easily obtained from local waterways or from commercial suppliers, and they can be maintained in relatively simple aquarium systems. The serotonergic system is highly conserved across species, meaning that the basic principles of serotonergic modulation that are discovered in crayfish can be applied to other organisms, including humans. Overall, the simple nervous system, robust behavioral responses, accessibility, and evolutionary conservation of crayfish make them an excellent model organism for studying serotonergic modulation and its effects on behavior which can provide insights into the role of 5-HT in the modulation of behavior in other animals, including humans.

(a)

Species	Function modulated
Motors activities	
C. elegans	• locomotion mode selection • speed of crawling • induction and maintenance of swimming • direction locomotor behavior
***Drosophila* larvae**	• body wall contractions • turning behaviors
Drosophila adult	• locomotor activities
Networks activities	
leech	• network activities
***Drosophila* larvae**	• MNs activities
crayfish	• locomotor network activities • giant fibers network
rodents	• network activities
xenopus	• maturation locomotor network • network activities

(b)

Species	Function modulated
Sleep and circadian rhythms	
Drosophila	• degradation of clock protein timeless • circadian activity • sleep regulation
crayfish	• dark/light phase
mammals	• sleep-wake states • wakefulness • sleep phase with REM
pigeon	• synchronization cycle • circadian activity rhythm

(c)

Species	Function modulated
Feeding	
C. elegans	• pumping behavior
Rhodnius proxilus	• urine production by Malpighian tubules
Drosophila larvae	• feeding behavior
chinese mitten crab	• regulation of hepatopancreas and intestines
mammals	• anorectic effect • feeding behavior • food appetence (interact with DA system)

(d)

Species	Function modulated
Social interactions, social status and aggressiveness	
crayfish	• social status • duration of fight • fight initiation • escape behavior • decision making • risk assessment
Drosophila	• aggressiveness
Anolis carolinensis	• reverse social status
crickets	• escape behavior • aggression
Drosophila	• aggressiveness
O. bimaculoides	• prosocial behavior
client reef fish	• cooperative behavior
mammals	• aggressiveness

(e)

Species	Function modulated
Anxiety	
Drosophila	• anxiety like behavior
crayfish	• anxiety like behavior
rodents	• anxiety like behavior

(f)

Species	Function modulated
Mood	
Drosophila	• depressive like behavior (chronic stress)
crayfish	• depressive like behavior (social defeat)
mammals	• depressive syndrome

(g)

Species	Function modulated
Learning and memory	
Aplysia	• persistant facilitation of the withdrawal reflex
Drosophila	• short and long-term plasticities
A.mellifera	• short and long-term plasticities
mammals	• long-term plasticities in memory

Figure 1-4 Functions related to (a) motor activities and locomotion, (b) sleep and circadian rhythms, (c) feeding, (d) social interactions, (e) anxiety, (f) mood, and (g) learning that are modulated by 5-HT in different species [9].

1.3.2 Electrochemical Sensors for Serotonin Sensing

Electrochemical Techniques for Serotonin Sensing

Detection of 5-HT from biological samples has been achieved via different benchtop and *in vivo* methods, including HPLC [76] and ELISA [45]. Despite the advantages of these methods, they have extremely low spatiotemporal resolution and require many analysis steps, labeling and treatment with reagents, and significant technique training. In recent years, electrochemical techniques have emerged as sensitive and reliable methods for detecting 5-HT levels in biological fluids, as 5-HT is an electroactive redox molecule that can be electrochemically detected directly. Electrochemical detection techniques, particularly CV, fast-scan cyclic voltammetry (FSCV), differential pulse voltammetry (DPV), and chronoamperometry (CA) attract more attention for their simplicity, sensitivity, selectivity, low cost, ease of use, and fast response times [40], [77], [78]. This section reviews the electrode materials, working principles, advantages, and disadvantages of electrochemical techniques for 5-HT sensing.

Materials for Electrochemical Serotonin Sensors

Carbon-based electrodes have been commonly used for neurotransmitter detection, including glassy carbon electrodes (GCEs), carbon paste electrodes (CPEs), and screen-printed carbon electrodes (SPCEs) [79]. The most popular electrodes for neurotransmitter detections are CFMEs because of their small dimension, low-cost, chemical stability, biocompatibility, and wide potential range, making them desirable for *in vivo* analysis [80]. However, CFMEs have disadvantages such as poor chemical selectivity and biofouling during measurement. Electrode fouling is caused by non-specific binding of macromolecules from the environment, which blocks the electrode surface over time. Thus, surface modification methods are used to enhance selectivity and anti-fouling property (e.g., conductive polymers, charged films, and nanomaterials).

Conductive polymers have been used extensively as surface coating materials for detecting various compounds [81]–[83]. Dip-coating is the most common surface coating method. However, a more uniform polymer layer thickness can be coated on the electrode via electrodeposition. Charged polymeric film coatings are useful for neurotransmitter detection because of their ability to repel molecular contaminants by electrostatic force. Multiple examples of using conductive polymers for neurotransmitter detection are reported in the literature, for instance, aniline [84]–[86], hydroxybenzoic acid [87], 3-hydroxyphenylacetic acid [88], xanthurenic acid [89], gallic acid [90], pyrrole [91], pyrene [92], methylene blue [93], among others [94].

Nafion is a commonly used polymeric electrode coating for neurotransmitter detection. Nafion is a negatively-charged, perfluorinated ion-exchange membrane [40]. Multiple studies have shown that Nafion coated electrodes serve to enhance cationic neurotransmitter selectivity such as 5-HT and DA by eliminating interferences from anionic contaminants such as ascorbic acid (AA) and UA [95].

Poly(3,4-ethylenedioxythiophene) (PEDOT) is one of the most popular conducting polymers used for electrochemical sensors. PEDOT can be electropolymerized on a microelectrode chip, and showed good peak resolution for 5-HT, DA, AA, and UA detection [96]–[98]. However, unlike Nafion, PEDOT is a conjugated polymer and carries positive charges which is not desirable for 5-HT detection.

Nanomaterials for electrode modification provide improved sensitivity and selectivity of electrochemical measurements due to their unique catalytic properties. Nanomaterials are characterized by nanometric dimensions (1-100 nm) [40]. The nanoscale dimension results in different physical, chemical, magnetic, and optical properties than their macroscale counterparts. Carbon-based nanomaterials, such as CNTs, have been widely used for electrode modification due

to their unique structures for high conductivity, high surface area, and fast heterogeneous electron transfer properties [99], [100], heightening electrocatalytic activity with minimal surface fouling [101]. CNTs are cylindrical graphite sheets with sub-nanometer dimensions, giving them a large surface-to-volume ratio and high strength. They have been used for numerous biosensing applications due to their chemical and thermal stability [102]. CNT-based electrochemical sensors have been used for detection of NAD+, nitric acid, cytochrome c, morphine, cysteine, glucose, indole acetic acid, cholesterol and DNA [103]–[105].

CNT has poor solubility in most of the common solvents due to their hydrophobicity [106]. Nafion has been used as a solvent for CNT due to its hydrophobic molecular structure [107]. Nafion-CNT modified electrode was introduced by Wang et. al. and used for hydrogen peroxide detection [108]. Since then, Nafion-CNT has been used as an electrode modification material for glucose [109], [110], ions [109], [111], and especially neurotransmitters like DA [112], [113], and 5-HT [114]. It has been reported that Nafion-CNT coated CFMEs show enhanced selectivity and sensitivity to neurotransmitter detection comparing to bare CFMEs [114]. Nafion-CNT coating provides fast response times and biocompatibility, which are ideal electrode materials for real-time *in vivo* neurotransmitter monitoring [115].

Electrochemical Techniques

Cyclic voltammetry: In CV, a triangular voltage waveform is applied at the working electrode wherein any electroactive redox molecules that contact the working electrode surface may undergo oxidation or reduction at given voltages. Current is produced due to the electron transfer between the redox molecules and the electrode in response to the cyclic excitation signal, and is measured by an amperemeter. A peak in current indicates whether a given substance has been involved in a

redox reaction in that potential range, and the peak height is proportional to the molecular concentration.

CV is a common electroanalytical technique and can be used to characterize a new system because the current-voltage curves produced indicate features of the reaction mechanism and kinetics, such as identifying oxidative and reductive potentials for given species. The CV is capable of simultaneous multimodal detection of neurotransmitters if they have different oxidation potentials. A gabapentin modified carbon paste electrode was reported for DA detection with a detection limit of 0.35 μM [116].

Fast-scan cyclic voltammetry: In FSCV, similarly to CV, a triangular waveform is applied to the working electrode, but at a higher scan rate (>100 V/s) to rapidly oxidize and reduce electroactive species at the electrode surface. Various performance aspects (i.e., sensitivity, selectivity, and temporal resolution) can be optimized by altering the potential limits, scan rate, and application frequency of the waveform. For instance, a commonly used DA waveform scans from −0.4 to +1.3 V at 400 V/s, repeated at 100-ms intervals showing reducing [79]. In the resulting cyclic voltammogram, the peak potentials provide a chemical signature to identify the species detected. Peak currents are usually converted into concentrations using calibration factors obtained from standards of known concentration. Given its chemical selectivity and sub-second time-resolution, FSCV has been widely employed *in vitro* and *in vivo* to detect a number of electroactive species including but not limited to DA [30], [117]–[119], NE [119], [120] and 5-HT [121], [122]. Puthongkham et al. has reported carbon nanohorn-modified CFMEs for DA detection using FSCV at 400 V/s with a limited of detection of 15 nM and a linear range up to 10 μM [30]. Although FSCV is considered as one of the most sensitive electrochemical techniques for neurotransmitter detection, the sophisticated equipment required for employing FSCV is difficult to miniaturize.

Differential pulse voltammetry: In DPV, a series of voltage pulses are superimposed on the potential linear sweep or stairsteps. The resulting current is sampled immediately before and after each pulse signal. The output signal is the current difference between two current values. DPV is a sensitive technique based on elimination of background currents and allows for the simultaneous direct analysis of multiple neurotransmitters. Wu et al. employed the DPV technique for the determination of DA and 5-HT using a CNT-coated GCE. It was observed that DA and 5-HT have two oxidation peaks at 0.18 V and 0.36 V, respectively. The CNT surface coating enhanced the sensing sensitivity compared to bare electrode. With a scan rate of 20 mV/s, the DA measurements showed a linear range of 0.05 μM – 5 μM with a detection limit of 0.011 μM, and the 5-HT measurements showed a linear range from 0.02 μM to 5 μM with a detection limit of 5 nM [123]. The DPV provides better sensitivity but on a slower time scale.

Chronoamperometry: In CA, a square-wave potential is applied to the working electrode and a steady state current is measured at the working electrode as a function of time. Alterations in current arise due to instantaneous fluctuations in redox molecule concentrations near the electrode surface. CA has been applied to real-time measurements of 5-HT concentrations in the guinea-pig ileum [124] and kinetics of DA uptake in the cerebral fluid of the brain [125], [126]. Prater et al. reported a CFM based sensor using CA for DA detection with the limit of detection of 0.2 μM [127]. CA suffers from limited chemical selectivity since multiple species that react cannot be distinguished, as they would be in CV, FSCV, and DPV. However, CA is the simplest and lowest power technique discussed here that can still provide real-time molecular dynamic detections.

1.3.3 Wearable System for Physiological Analytes Detection

Miniaturized Potentiostat Electronics Module

With rapid development in the past 40 years, electrochemical biosensing devices are now common analytical tools and have been applied in a variety of applications due to their rapid and reliable detection capabilities. With the development of microelectronics, miniaturized electrochemical sensing electronics have become popular for medical and clinical applications due to the capability of non-invasive monitoring of chemical markers in real-time. Various miniaturized electronics have been reported using customized application-specific integrated circuit (ASIC) design and PCB technology. Both implementation approaches require a stable bias potential between the functional working electrode (WE) and reference electrode (RE), utilizing a circuit known as a potentiostat, to perform electrochemical measurements. The electrochemical sensor produces an output current signal proportional to the analyte concentration. However, this current must be converted to a readable voltage. This is accomplished using a transimpedance amplifier (TIA) with a resistor placed in a negative feedback configuration, which both amplifies the small currents from the electrochemical cell and converts them into a scaled voltage depending on the resistor value. An analog-to-digital converter (ADC) then samples the output of the TIA and produces a digital representation (in bits) of the voltage level. Further, a microprocessor is required to process the digital reading and determine actual analyte concentration. Several ASIC-based and PCB-based potentiostats have been reported for electrochemical measurements [128]–[131]. The potentiostat circuit parameters such as dimensions and power consumptions are summarized in **Table 1-1**. The ASIC-based potentiostat circuits have advantages in space and energy, but require additional external control unit. The PCB-based potentiostats are larger in size and consume more power. However, their dimension and power consumption can be further minimized by design

optimization. Moreover, the commercial off-the-shelf (COTS) components used in PCB-based designs are more stable, better characterized by manufacturers, and more compatible with further integration.

Table 1-1 Comparison of reported ASIC-based and PCB-based potentiostat circuit designs.

Electronics	Techniques	Dimension	Voltage	Power	Ref
ASIC	CA	1.4 × 4.3 mm	1.2 V	30 μW	[128]
ASIC	CA, CV	3.8 × 3.1 mm	3.3 V	188 μW	[129]
PCB	CA	18 × 23 mm	3.3 V	1.5 mW	[130]
PCB	CV	45 × 50 mm	3.3 V	N/A	[131]

Wireless Electrochemical Device for *In Vivo* Detections

Electrochemical biosensing devices have garnered significant attention from researchers and industries worldwide. These devices offer portable, sensitive, selective, and rapid detection methods for biochemical analysis [32], [132]–[136]. Thus, they possess the capacity to address numerous analytical problems and challenges, making them potential ubiquitous tools for disease diagnosis, monitoring, treatment, and health management. In recent years, the field has witnessed a surge of interest in the advancement of miniaturized wireless electrochemical sensing devices, notably wearable, ingestible, and implantable devices, which hold great promise for fulfilling these objectives (**Figure 1-5**) [31], [137]–[142]. This section presents an overview of the ongoing research and development in this field.

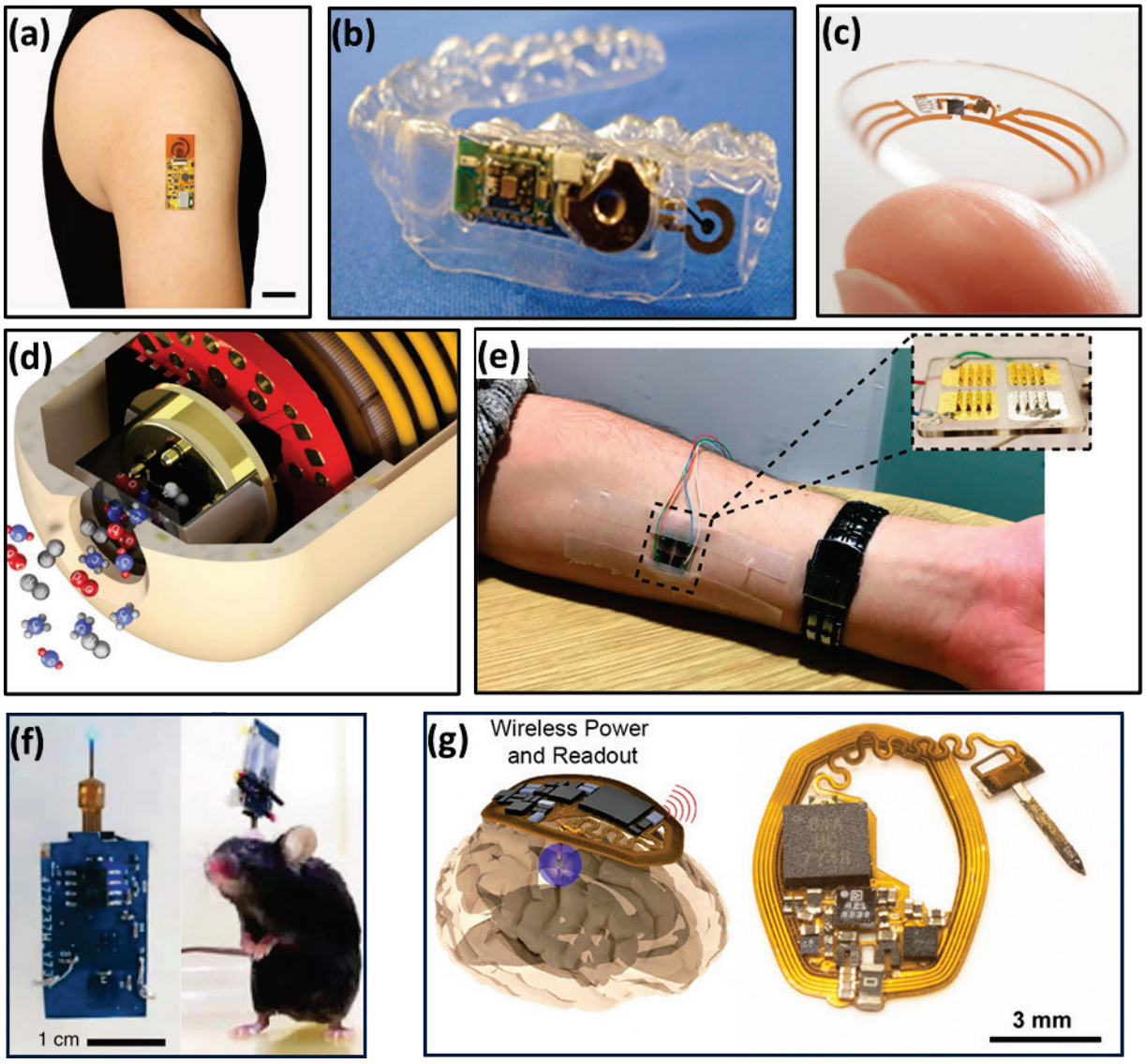

Figure 1-5 Wireless electrochemical sensing device for in vivo detection. (a) Tattoo-like wearable sensor for multimodal sensing amino acids in sweat [137]. *(b) Sensor integrated mouthguard for in vivo glucose measurement in saliva* [138]. *(c) Smart lens for tear glucose measurement* [139]. *(d) Ingestible capsule device for gastrointestinal fluidic sensing* [140]. *(e) Microneedle based sensor for epidermis β-Lactam monitoring* [141]. *(f) Implantable probe based device for DA sensing in the brain of mice [31]. (g) Fully implantable device for DA sensing in the brain* [142].

Wearable devices such as wristbands, smartwatches, smart lens and mouthguard can use biosensors to detect biochemicals mainly in body fluids such as sweat, tear, and saliva. Sweat harbors an abundance of biomarkers, including electrolytes (such as sodium, potassium, chloride,

ammonium, and calcium), metabolites (such as glucose, lactate, and alcohol), trace elements (like iron, zinc, and copper), small molecules (such as cortisol, urea, and tyrosine), neuropeptides, and cytokines [132], [136], [137], [143], [144]. Given the wealth of physiological information present in sweat, wearable sweat sensors hold immense potential for various applications. These sensors offer promising prospects in fields like fitness tracking and health monitoring for athletes engaged in high-performance sports, as well as disease diagnosis and medical monitoring.

Mouthguards with biosensors can non-invasively detect physiological details of saliva. Several types of smart mouthguards have been created to detect analytes include glucose, UA, sodium, and alcohol [138], [145]–[150]. These devices offer the pump-free collection of fluid, user-friendly, continuous monitoring of multiple markers, control of dietary food intake, and pain-free analysis.

Similarly, smart contact lenses have been developed to non-invasively detect physiological information from both the eyes and tears. These innovative lenses utilize optical and electrical techniques to track the chemistry of tear fluid, including glucose and lactate levels, as well as the electrical conductivity and transcutaneous gases present in the eye's mucous membrane. For instance, Thomas et al. developed an electronic enzyme-based L-lactate sensor that utilizes contact lenses for the non-invasive detection of L-lactate in tear fluid [151]. The sensor incorporates a functional platinum structure coated with glutaraldehyde, lactate oxidase, and bovine serum albumin cross-linking, all enclosed within a medical polyurethane coating, achieving an average sensitivity of around 53 $\mu A/mM/cm^2$. Senior also demonstrated glucose sensing in tear using Google smart lens [139].

Other than wearable devices, ingestible devices, also known as ingestible capsules, have been also under the development of in vivo sensing in the digestive tract. These devices are designed to traverse the gastrointestinal tract and reach organs within the abdominal region. As a result, this

sensor not only captures intrinsic contents and luminal fluid but also collects and delivers biometric data regarding enzymes, hormones, electrolytes, microbial communities, and metabolites in close proximity to the organs [140], [152]–[156]. Utilizing an ingestible sensor to obtain the desired fluid for detection purposes offers a safe and non-invasive option [152]. Over the past decade, significant advancements have been made in the development of such pills, rendering them useful for a wide range of applications. For instance, a gut microbiome redox sensor has been created to monitor the gut's oxidation state by evaluating oxidation redox potential. Although *in vivo* results of this device are currently awaited as it undergoes trials, it has already been tested in rats [140].

Implantable devices are equipped with probes that can be inserted into the body, enabling access to biofluids or tissues that are inaccessible to wearable and ingestible devices. This provides opportunities to detect biomarkers that are not easily measurable using other devices. For instance, a novel microneedle-based biosensor has been developed for the continuous and real-time detection of β-lactam antibiotic levels in a minimally invasive manner [141]. The dimensions of the microneedle arrays are carefully designed to allow a significant portion to penetrate the viable epidermis without going deeper. This biosensor utilizes an iridium oxide pH-sensing layer to accurately detect local pH changes resulting from the hydrolysis of β-lactam antibiotics by β-lactamase enzymes. The penetrative ability enables the implantable devices to be an ideal approach for neurotransmitter detection, as most neurotransmitters mainly exist in the brain or blood. **Table 1-2** summarizes the existing wireless electrochemical device for *in vivo* neurotransmitter detection. Liu et al. developed an implantable probe constructed using PEDOT: polystyrene sulfonate (PSS)-coated diamond films as electrochemical sensors [31]. The probe possesses the capability for real-time dopamine detection in the ventral tegmental area (VTA) in the freely behaving mice. With a customized lightweight circuit module, untethered remote signal control

and data acquisition can be incorporated. With a mini-LED for optogenetic simulation, the device clearly demonstrates the multifunctional opto-electrochemical microprobe system's effectiveness in interfering with place preferences through optogenetics and detecting dopamine release. Similarly, Stuart et al. developed a lightweight, wireless, battery free implants for electrochemical DA sensing [142]. With a CNT-based sensor, this device achieved sensitive DA concentration detection and demonstrated its capabilities in freely moving, untethered subjects. Implantable devices therefore have the potential to provide highly selective and sensitive detection of biomarkers, such as neurotransmitters, enabling a more comprehensive analysis of physiological and biochemical conditions.

Table 1-2 Comparative table of in vivo neurotransmitter sensing device.

Analytes	Technique	Wireless	Weigh	LOD	Ref
DA	CA	Yes, RF	2 g	100 nM	[31]
DA	CA	Yes, IR	49 mg	300 nM	[142]
DA	FSCV	Yes, RF	35 g	50 nM	[157]

1.4 Structure of Dissertation

Chapter 1 of this dissertation has focus on the background, motivation, and key contributions of this work, introducing serotonergic modulation involved in animal physiology and behavior as well as summarizing related electrochemical devices. Chapter 2 describes the development and characterization of novel surface-modified CFMEs for sensitive, selective 5-HT detection. Chapter 3 demonstrates the development of miniaturized PCB potentiostat module, including a portable development and customized PCB board. Chapter 4 includes the integration of microelectrode

with miniaturized PCB using 3D printing technology for rapid prototyping of implantable device of 5-HT monitoring in freely moving crayfish. Finally, the key contributions of my dissertation and the future direction of this work are summarized in Chapter 5.

This **thesis accomplishments which will be detailed explained throughout this research include:** (1) the development of novel surface-modified CFMEs for sensitive, selective 5-HT sensing with minimal fouling, (2) the implementation of a customized PCB potentiostat for electrochemical measurement with wireless communication, and (3) the systematic integration for a miniaturized implantable device for continuous 5-HT monitoring in freely moving animals. The developed microelectrodes were validated for 5-HT detection in both a modeled gut epithelial cell culture environment and a homogenized nerve cord sample, demonstrating their potential to study 5-HT molecular transportation and serotonergic modulation in complex biological environments. The customized PCB potentiostat module provides a small form-factor, low-cost, precision electrochemical sensing solution for electrochemical sensing. This device is a first step in developing an implanted, miniaturized, low-cost, battery-operated electrochemical sensing system which can be operated without a tether. Together, an integrated untethered implantable system is developed for *in vivo* 5-HT monitoring and studying serotonergic modulation related to animal behaviors. Overall, this work presents engineered approaches detect 5-HT signaling and dynamics, therefore facilitates the study of serotonergic modulations.

Chapter 2 Neurotransmitter Detection Based on Surface-Modified Carbon Fiber Microelectrodes

Surface-modified CFMEs have been commonly used for electrochemical measurements of neurotransmitters [8], [34], [97], [114], [122], [158]–[164]. However, while research mainly focuses on the detection of DA, sensitive and selective detection of 5-HT remains challenging due to the low concentration of 5-HT in the body and the reduced sensor sensitivity caused by 5-HT fouling. Here, I present a novel surface modification approach that combines electrochemical treatment with Nafion-CNT coating to achieve the synergistic effect for sensitive and selective detection of 5-HT with minimal surface fouling. In this chapter, I demonstrate that the electrochemical treatment greatly increases the surface area, resulting in an increased signal response, while the Nafion-CNT coating improves the sensor selectivity and antifouling property. The developed sensor's performance for 5-HT detection was validated by 5-HT detection in standard solution as well as real biological samples, including cell-secreted 5-HT in cell culture media and 5-HT from homogenized tissue.

I give credit to Dr. Ashley Chapin and Dr. Pradeep Rajasekaran for their significant contributions to this work. They first characterized the electrochemical properties of 5-HT and developed a planner Au-CNT electrode for 5-HT detection, which inspired the development of CFMEs. Dr. Ashley Chapin also contributed to Section 2.3, in which the surface-modified CFMEs were used to detect cell-released 5-HT from a cell culture medium. Furthermore, Ta-wen Ho and his advisor Dr. Jens Herberholz also made significant contributions to the work in Section 2.3, where the surface-modified CFMEs were tested for 5-HT detection in the homogenized crayfish nerve cord.

2.1 Surface-Modified Carbon Fiber Microelectrode

Carbon-based materials, such as CFMEs, have commonly been used for electrochemical measurements due to their excellent properties, such as high electrical and thermal conductivities, and adequate corrosion resistance [165]–[167]. However, the limited sensitivity of bare CFMEs prevents direct detection of 5-HT at a physiologically relevant level directly [162]. Surface modifications are required for CFMEs to achieve fast, precise, selective, and sensitive detection of 5-HT in biological samples. Recently, improved electrochemical sensitivity has been demonstrated in CFMEs with deposited CNTs dispersed in Nafion (Nafion-CNT CFMEs). These modified CFMEs have been used to detect biochemicals such as ADN [168], DA [113], [114], and 5-HT [114] in biological samples using a benchtop potentiostat with ultra-fast scan rates. Nafion is a negatively charged, perfluorinated ion-exchange film [40] and Nafion-coated CFMEs show improved selectivity for cationic amines, such as 5-HT, over negatively charged interference molecules like UA and AA during electrostatic interaction [40]–[42]. CNTs, cylindrical graphite sheets with nanometer dimensions, provide a large surface-to-volume ratio and surface area. Due to their unique structures, they offer increased sensitivity, electron transfer kinetics, and electrocatalytic activity with minimal surface fouling [101], [169], [170]. Sensitive and selective electrochemical detection can be achieved by combining Nafion and CNT coatings on CFMEs. However, such measurements often necessitate the use of FSCV systems to achieve ultra-high scan rates (~400 V/s), which can be costly and challenging to further miniaturize for portable and point of care (POC) applications. Portable or miniaturized potentiostat devices can only perform regular CV with a scan rate below 1 V/s, thus further electrode surface enhancement is necessary to realize a more sensitive electrode for 5-HT detection with miniaturized devices. Therefore, in addition to surface coatings, surface activations such as thermal activation, mechanical polishing, and

electrochemical activation have been applied to carbonaceous electrodes to improve their electrochemical performance and sensing sensitivity. These activations lead to the generation of electrochemically active oxygen-rich groups [171] and nanostructures that increase the electroactive surface area [172], [173]. Considering the fragility of CFMEs, electrochemical treatment is preferable over other activation techniques due to its cost-effectiveness and mild process.

Here, I present the development of a novel surface modification approach combining Nafion-CNT coating and electrochemical treatment to modify CFMEs, and assessment of their synergistic effect for 5-HT detection using CV. I found that electrochemically treated CFMEs had significantly increased 5-HT sensitivity due to the production of oxygen-rich functional groups and increased surface area achieved through the surface etching effect. Also, Nafion-CNT coated CFMEs showed improved 5-HT fouling resistance and selectivity in the presence of interfering molecules. By combining Nafion-CNT coating and electrochemical treatment, Nafion-CNT/EC CFMEs showed overall improved sensitivity, selectivity, and 5-HT fouling resistance. This electrode was also used to detect cell-released 5-HT in an *in vitro* culture, and homogenize crayfish nerve cord, indicating its ability to perform in biological samples. Ultimately, the developed novel surface modification technique for CFMEs enables 5-HT detection using portable and miniaturized potentiostat electronics, which will be covered in Chapter 3 and Chapter 4.

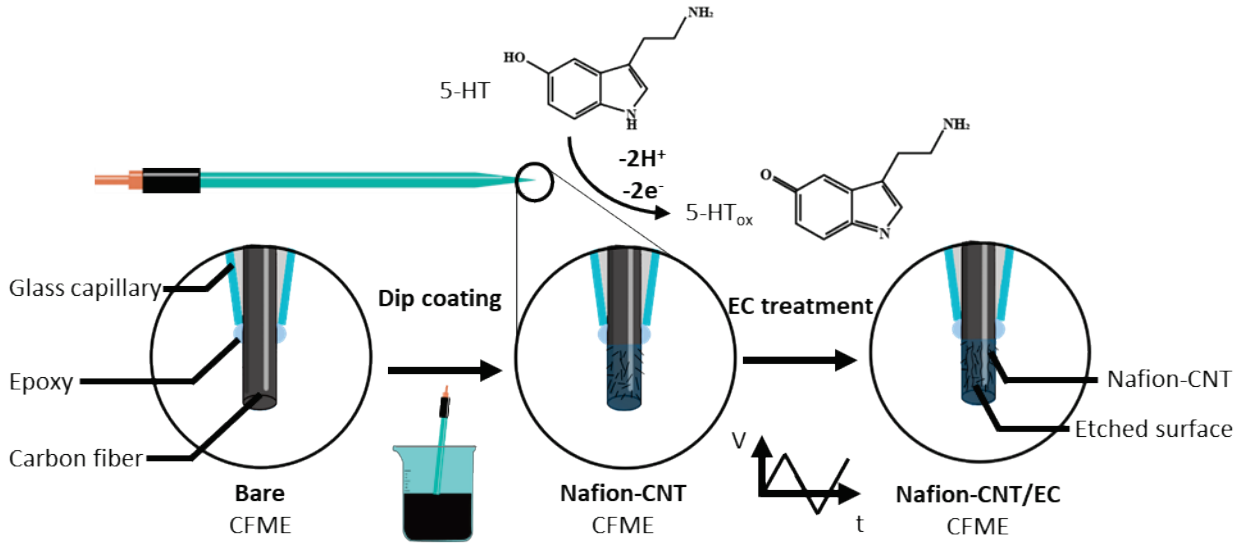

Figure 2-1 Process flow of the fabrication a surface-modified CFME. The Nafion-CNT/EC CFME is first dip coating in Nafion-CNT solution and then treated electrochemically.

2.1.1 Materials and Methods

Carbon Fiber Microelectrode and Surface Modifications

The surface of T-650 carbon fiber (Solvay, TX) was modified with Nafion-CNT and electrochemical treatment to improve its sensitivity and selectivity. A single fiber was inserted into a glass capillary with an inner diameter of 0.4 mm (A-M Systems, WA). The carbon fiber was sealed using 5 minute epoxy (J-B Weld, TX) and cut down to a 5 mm tip. Copper wire (30 AWG) was inserted into the glass capillary from the backside. A 0.5 mg/mL Nafion-CNT solution was sonicated for 30 min before each use to re-suspend the nanotubes. CFMEs were coated with the Nafion-CNT film by dip-coating and were air-dried for 30 minutes before use. Electrochemical treatment consisted of applying two repeated CV waveforms of 0 to +2.5 V and 0 to -1.5 V at a scan rate of 100 mV/s. The Nafion-CNT CFMEs were only modified with dip-coated Nafion-CNT and the Nafion-CNT/EC CFMEs were modified with dip-coating Nafion-CNT, followed by electrochemical treatments.

Microscopic Surface Characterization

All scanning electron microscopy (SEM) images and energy-dispersive X-ray spectroscopy (EDS) analysis were acquired in the University of Maryland Nanocenter AIM Lab using Tescan GAIA (Czech Republic). The CFME samples were prepared and attached to a clean Si wafer using carbon tape for surface characterizations. The SEM images were recorded with an accelerating voltage of 10.0 kV and a working distance of approximately 5 mm.

Electrochemical Surface Characterization

The surface-modified CFMEs were first characterized for electrochemically active surface area (EASA) using a benchtop potentiostat (VSP-300, BioLogic, France) with a standard Ag/AgCl (3M KCl) RE and a Pt CE (CH Instruments, TX). The EASAs of Nafion-CNT, Nafion-CNT/EC, EC, and EC/Nafion-CNT CFMEs were estimated by measuring the CV response to ferrocyanide and ferricyanide pair at various scan rates from 50 mV/s to 1000mV/s, applying a waveform from -0.5 to +1 V. All collected data is analyzed using MATLAB.

2.1.2 Surface Morphology Analysis

The surface morphology of bare, Nafion-CNT, and Nafion-CNT/EC CFMEs were characterized using SEM. As shown in **Figure 2-2a-c**, the bare CFME (**Figure 2-2a**) shows a smooth surface with striation, which is typical of the polyacrylonitrile (PAN) manufacturing process used to create carbon fibers. The Nafion-CNT modified CMFE (**Figure 2-2b**) shows a thin, dense coating of CNT on the electrode surface. With further electrochemical treatment, the Nafion-CNT/EC CFME (**Figure 2-2c**) shows even rougher surface striations as a result of the electrochemical etching effect, while still retaining some of the Nafion-CNT film. The SEM

images suggest that the increased surface area and nanostructures are due to the Nafion-CNT dip coating and further electrochemical treatment.

EDS analysis was used to obtain detailed information on the elemental composition of modified electrodes (**Figure 2-2d-f**). The bare CFME shows carbon exists in the sample with a small amount of oxygen (**Figure 2-2d**). The presence of oxygen may be from a thin epoxy protective layer that resides on the surface during the fiber sizing process. Dip-coating the CFME in Nafion-CNT increases oxygen in the sample (**Figure 2-2e**), likely due to the carboxylic acid functional groups on the CNTs and the oxygens from the $-SO_3$ groups in the Nafion structure. Electrochemical treatment further increases the oxygen content in the sample (**Figure 2-2f**), which may indicate the addition of oxygen functional groups to the surface during electrochemical process [171], [174]. Silicon appears across samples due to the use of a Silicon substrate holder for EDS analysis and is not from the sample itself.

The SEM images and EDS analysis verify my hypothesis that the Nafion-CNT coating followed by electrochemical treatment increase the surface nanostructure, EASA, and oxygen groups to the surface, which improve electrochemical performance.

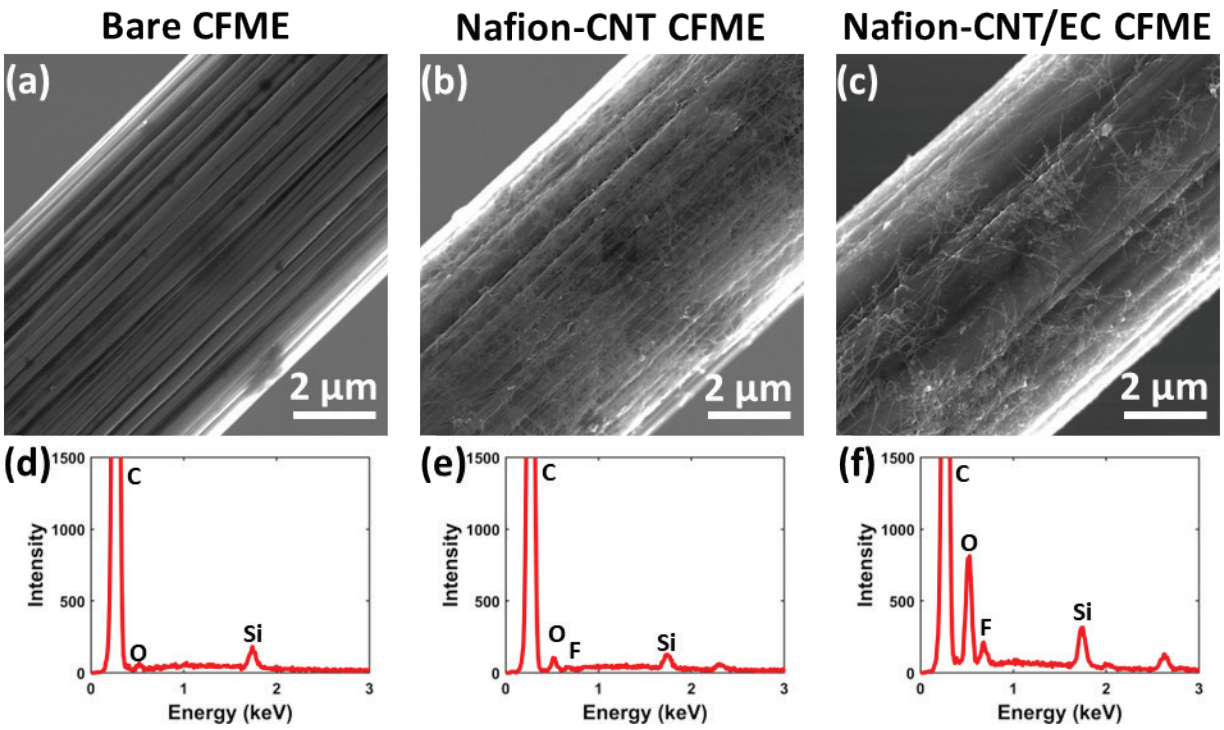

Figure 2-2 (a-c) SEM images and (d-f) EDS analysis of bare, Nafion-CNT and Nafion-CNT/EC CFME.

2.1.3 Electrochemically Active Surface Area of Surface-Modified Microelectrodes

To estimate the EASA of surface-modified CFMEs, equimolar 10mM potassium ferrocyanide ($K_4[Fe(CN)_6]$) and potassium ferricyanide ($K_3[Fe(CN)_6]$) were used because their electrochemical sensitivity is highly relevant to the defects/edge plane site [175]. CV was performed at various scan rates from 50 mV/s to 250 mV/s, and the resulting currents were plotted against the square root of scan rates (**Figure 2-3**). Visible changes in the shape of the cyclic voltammograms are apparent after each step of surface modification. In **Figure 2-3a**, before surface modification, the bare CFME shows a poorly defined CV current plateau with high linear background and almost no peak current to measure. After Nafion-CNT coating, the Nafion-CNT CFME also shows a poorly defined plateau with linear background, but the peak is more distinguishable than the bare

electrode (**Figure 2-3b**). After further electrochemical treatment, the Nafion-CNT/EC CFME shows a well-defined steady-state plateau with measurable peaks, shown in **Figure 2-3c**.

An alternative surface modification method is to apply electrochemical treatment first, followed by Nafion-CNT coating. Taking a new bare CFME, after the electrochemical treatment, the EC CFME shows a well-defined steady-state plateau with measurable peaks (**Figure 2-3d**). However, further Nafion-CNT coating after the electrochemical treatment results in a decreased but sharper current peak than electrochemical treatment alone (**Figure 2-3e**). The changes in the shape of cyclic voltammograms of ferricyanide/ferrocyanide at CFMEs after surface modifications are direct indications of changes in the surface electrochemical properties as a result of Nafion-CNT coating and electrochemical treatment.

The plot of Ipa versus the square root of the scan rate ($\nu^{1/2}$) is shown in **Figure 2-4f**. The linear relationship between Ipa and $\nu^{1/2}$ suggests a diffusion-controlled detection of ferricyanide/ferrocyanide on the CFMEs' surface. For a diffusion-controlled electrochemical reaction, the EASA can be estimated using the Randles–Ševčik equation:

$$i_{pa} = 0.4463nFAC\left(\frac{nFvD}{RT}\right)^{1/2}$$

where n is the number of electrons appearing in the half-reaction for the redox couple, A is the EASA (cm^2), D is the analyte's diffusion coefficient (cm^2/s), ν is the scan rate (V/s), F is the Faraday constant (C/mol), C is the analyte concentration (mol/cm^3), R is the gas constant (J/(K·mol)), and T is the temperature (K). It is worthwhile to highlight that the shape of the CV does not resemble the one expected for a microelectrode, where the reverse sweep of the voltammogram exactly overlaps the forward one. On the contrary, the curve represents a transition between microelectrode and macroelectrode behavior, possibly due to the high surface roughness,

large surface area, and fast scan rates. Compton *et al* have shown that at fast scans rates, regardless of the geometry of the electrodes, the Ipa can be estimated by the Randles– Ševčik equation [176].

EASA can be estimated based on the slope calculated from **Figure 2-3f**, the EASA for Nafion-CNT, Nafion-CNT/EC, EC, and EC/Nafion-CNT CFME are 3.855×10^{-5} cm^2, 9.208×10^{-5} cm^2, 17.18×10^{-5} cm^2, and 5.436×10^{-5} cm^2, respectively. The bare electrode is not electrochemically responsive to ferricyanide/ferrocyanide. This may be attributed to the thin epoxy layer (1% UC.309 epoxy) coated during carbon fiber fabrication, which blocks electron transfer. The initial Nafion-CNT coating on the bare electrode increases the EASA, which is further increased by the electrochemical treatment (from 3.855×10^{-5} cm^2 to 9.208×10^{-5} cm^2). The increased EASA may be attributed to the electrochemical etching effect, which can remove the epoxy layer as well as generate nanostructured surface texture on the carbon fiber and Nafion-CNT film [172], [173]. In the EC/Nafion-CNT CFME, the initial electrochemical treatment increases surface area, which then decreases after surface coating with Nafion-CNT (from 17.18×10^{-5} cm^2 to 5.436×10^{-5} cm^2). The EASA for EC/Nafion-CNT is close to the EASA for Nafion-CNT, which may suggest that the Nafion-CNT coating after electrochemical treatment covers the nanostructure generated by electrochemical treatment and results in decreased EASA. Both Nafion-CNT coating and electrochemical treatment enhance electrochemical properties, including improving the shape of the CV curve and increasing the Ipa, which increases the sensitivity to electrochemically active species. Overall, the electrochemical treatment results in a more significant increase of EASA than Nafion-CNT coating.

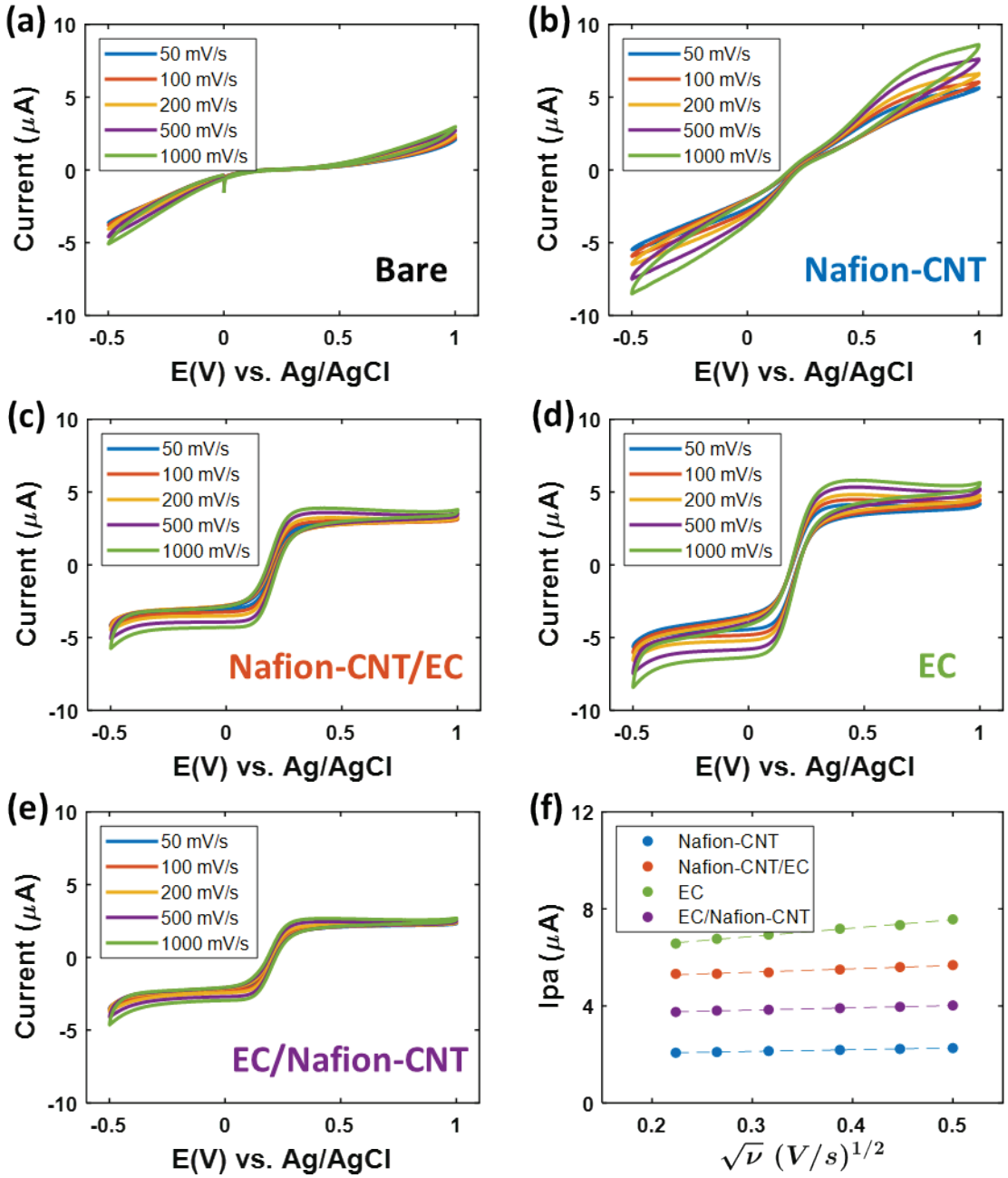

Figure 2-3 CV scan rate variation to estimate electroactive surface area. Cyclic voltammograms of 10 mM ferricyanide/ferrocyanide at (a) bare, (b) Nafion-CNT, (c) Nafion-CNT/EC, (d) EC, and (e) EC/Nafion-CNT CFMEs. (f) Linear regression of Ipa vs. the square root of scan rates (50, 70, 100, 150, 200, 250 mV/s). R^2=0.9982, 0.9947, 0.9719, 0.9959 for Nafion-CNT, EC, Nafion-CNT/EC, and EC/Nafion-CNT CFMEs, respectively. (n = 1).

2.2 Evaluation of Surface-Modified Carbon Fiber Microelectrodes for Serotonin Detection

The ultimate goal for the development of surface-modified CFMEs was to detect 5-HT in biological environments. Considering the low concentration and complex environments, the surface-modified carbon fiber microelectrode required to be sensitive and selective to 5-HT. Another challenge in 5-HT detection is electrode fouling. 5-HT is known to foul the electrode during measurements, and form a membrane cause reduced sensitivity. Here, in this chapter, the sensitivity, selectivity, and 5-HT fouling resistance of developed CFMEs are evaluated.

Sensitivity: 5-HT is synthesized in different regions of the body. It is abundant in enterochromaffin cells of the gastrointestinal tract, in platelets, and as a neurotransmitter in the CNS [177]–[179]. Of the approximately total amount of 10 mg 5-HT in the human body [180]. The 5-HT concentrations vary significantly depending on the species and region of interest. For animals, Bertrand et al. showed a 5-HT release from rat ileum of 12 ± 6 μM through a mucosa compression stimulation [181]. Hata et al. showed a 5-HT concentration of 500 nM in colon lumen, and 25 μM in the colon tissue from germ-free mice [182]. Gross and Sturkie showed a 5-HT concentration of 61 μM from female chicken intestine tissue [183]. Ren et al. showed a 1700 μM of 5-HT in the mice brainstems [184]. Atkinson et al. showed 5-HT concentration in platelet-depleted plasma is roughly around 50 nM [185]. For human samples, Qasem et al. showed a 5-HT concentration of 2.4 μM from health clinical serum [186]. The blood 5-HT test suggests the normal 5-HT range is 262 to 1550 nM in blood [187], [188]. Khoshnevisan et al. suggested a normal urinary 5-HT level ranges from 300 to 1650 nM [158]. The supporting information suggests the 5-HT concentrations in the body are at micromolar range, so that the developed sensor needs to be capable of 5-HT detection at micromolar and sub-micromolar ranges.

Selectivity: Detecting 5-HT in physiological samples can be impacted by other electroactive metabolites, such as DA, AA, UA, ADN, and 5-HIAA, with concentrations higher than 5-HT and oxidation potentials close to 5-HT at bare conventional electrodes [189]. In this chapter, the selectivity of developed sensor for 5-HT detection will be evaluated in comparison to other interference molecules discussed above, including DA, UA, AA, ADN, and 5-HIAA.

DA is a neurotransmitter in the brain, while the 5-HT is mainly synthesized in the dorsal raphe nucleus (DNR), DA is produced in the dopaminergic neuron in VTA. Since DA and 5-HT are produced in different regions in the brain, DA will not interfere with 5-HT detection for sensors with high spatial resolution. However, DA is a potential interference molecule for 5-HT detection in homogenized tissue or blood, although the normal range for blood dopamine is 0 to 30 pg/mL (195.8 pmol/L), which is much lower than blood 5-HT concentration.

UA is a waste product that is formed when purines are broken down in the body. Most UA dissolves in the blood, passes through the kidneys and leaves the body in urine. The reference range of UA in the blood is 160 to 510 μmol/L.

AA, also known as Vitamin C, is a water-soluble vitamin that is essential for many biological processes in the body. It plays a crucial role in the synthesis of collagen, a protein that is found in skin, bones, and connective tissues, as well as in wound healing, immune function, and the metabolism of certain amino acids. The total body content of AA ranges from 0.3 g to about 2 g [190]. High levels of AA (millimolar concentrations) are maintained in cells and tissues, and are highest in leukocytes (white blood cells), eyes, adrenal glands, pituitary gland, and brain.

ADN is one of the four nucleoside building blocks of RNA, and is used thoroughly throughout the entire body in general metabolism [191]. Nafion-CNT coated CFMEs have been used to detect ADN in rat brain slices [168]; therefore the selectivity between ADN and 5-HT must be determined.

5-HIAA is the primary metabolite of 5-HT. While most 5-HIAA is produced in the liver by breaking down 5-HT, it is collected in the urine. The reference level of urinary 5-HIAA concentration is 40 μmol/24h, which is approximately 20 μM considering 2 L urine is collected per 24 hours. 5-HIAA can also be found in blood and cerebrospinal fluid (CSF). Considering the high level of 5-HIAA which always co-exists with 5-HT, the selectivity between 5-HIAA and 5-HT must be determined.

5-HT Fouling: 5-HT fouling is a key challenge in 5-HT detection electrochemically. The electrochemical reaction involves a multi-step two-electron, two-proton transfer oxidation process with by-products formed in reactions. These reactive by-products are formed during the oxidation process and polymerized to form an insoluble film on the surface of electrodes [192], [193]. The polymer-like film hinders electron transfer and causes electrode fouling, which decreases sensitivity for repeated measurements. The novel surface treatment is intended to reduce 5-HT fouling during the measurements. The antifouling property will be evaluated in this section.

2.2.1 Materials and Methods

Sensitivity Characterization of Surface-Modified Carbon Fiber Microelectrodes

Electrochemical measurements for 5-HT detection were done using CV with a VSP-300 potentiostat (BioLogic, France) and a standard Ag/AgCl (3M KCl) RE (CH Instruments, TX) and a Pt CE (CH Instruments, TX). To compare the 5-HT signal response between CFMEs with different surface modifications, the bare, Nafion-CNT, Nafion-CNT/EC, EC, and EC/Nafion-CNT CFMEs were used for 5-HT detection in 10 μM 5-HT containing phosphate buffered saline (1X PBS, containing 8g/L NaCl, 0.2 g/L KCl, 1.44 g/L Na_2HPO_4, and 0.24 g/L NaH_2PO_4, pH 7.4, Research Product International, IL) solution with applying a CV waveform from -0.1 to +0.8 V

and back at a scan rate of 1 V/s. All electrodes underwent identical CV measurement protocols, including: (1) background signal measurement in PBS, (2) 5-HT measurement after a constant accumulation time, and (3) 3 cycles to fully oxidize any remaining 5-HT molecules attached to the surface to "clean" the surface before the next measurement. This sensing protocol was used to minimize the variations of different accumulation time for 5-HT adsorption to the surface, which may cause variations in the Ipa signal. All collected data is analyzed using EC-Lab and visualized in MATLAB.

Selectivity Characterization of Surface-Modified Carbon Fiber Microelectrodes

The sensor selectivity is compared between EC and EC/Nafion-CNT CFMEs using 1 μM 5-HT and 10 μM UA as a benchmark. VSP-300 potentiostat (BioLogic, France) and a standard Ag/AgCl (3M KCl) RE and a Pt CE (CH Instruments, Austin) were used in all measurements. A CV waveform from -0.1 to +0.8 V and back at a scan rate of 1 V/s. The accumulation time between each measurement is 1 minute.

The oxidation potential for 10 μM DA, UA, NE, 5-HIAA, and ADN were determined in their PBS solution using Nafion-CNT/EC CFMEs. VSP-300 potentiostat and a standard Ag/AgCl (3M KCl) RE and a Pt CE were used in all measurements. A CV waveform from -0.1 to +0.6 V and back at a scan rate of 200 mV/s. The accumulation time between each measurement is 1 minute.

The selectivity to 5-HT over 5-HIAA, UA, DA, NE, and ADN was evaluated by calculating the ratio of Ipa for 1 μM 5-HT and Ipa for 1 μM 5-HT with additional 10 μM 5-HIAA, 10 μM UA, 20 μM DA, 10 μM NE, and 10 μM AND, respectively. A CV waveform from -0.1 to +0.6 V and back at a scan rate of 200 mV/s. The accumulation time between each measurement is 1 minute.

5-HT Fouling Characterization of Surface-Modified Carbon Fiber Microelectrodes

The antifouling property of surface-modified CFMEs (Nafion-CNT, Nafion-CNT/EC, EC, and EC/Nafion-CNT) were compared by continuous measurements of 1 μM 5-HT for 20 cycles using the same electrode. A CV waveform is applied from -0.1 to +0.8 V and back at a scan rate of 1 V/s. The accumulation time between each measurement is 1 minute. The 5-HT fouling is evaluated by taking the ratio of the Ipa after 30 cycles and the maximum Ipa using the fresh electrode.

A modified CV was developed to minimize 5-HT fouling. The modified CV waveform is applied from -0.1 to +0.6V and back at a scan rate of 200 mV/s. The antifouling property of developed Nafion-CNT/EC CFMEs with modified CV waveform was evaluated by continuous measurements of 1 μM 5-HT for 30 cycles using a same electrode. The accumulation time between each cycle is 1 minute. The 5-HT fouling is evaluated by taking the ratio of the Ipa after 30 cycles and the maximum Ipa using the fresh electrode.

2.2.2 Improved Signal Response with Electrochemical Treatment

To evaluate the electrochemical performance of surface-modified CFMEs in 5-HT detection, I first compared CFMEs with different surface modifications using CV (**Figure 2-4**). The Nafion-CNT CFMEs showed an increased background current in PBS, with further electrochemical treatment, the Nafion-CNT/EC CFMEs showed dramatically increased background current (**Figure 2-4a)**. Similarly, Nafion-CNT coating and electrochemical treatment also showed increased Ipa in the detection of 5-HT (**Figure 2-4b**).

The effect of reversed modification processes was also investigated. While the EC CFMEs showed a dramatically increased background current in PBS, the additional Nafion-CNT coating showed a decreased background current (**Figure 2-4c**). Similarly, the EC CFMEs showed a large

Ipa in the detection of 5-HT, but with additional Nafion-CNT coating, the EC/Nafion-CNT CFMEs showed a slightly decreased Ipa in 5-HT detection than EC CFMEs (**Figure 2-4d**).

The increased background signal after Nafion-CNT coating and electrochemical treatment suggests increased double-layer capacitance, indicating higher EASA. All surface-modified CFMEs showed similar oxidation peak potential (Epa = 0.43 V) to 5-HT.

The Ipas are compared between CFMEs with various surface modification methods. The averaged Ipas are 0±0.001, 0.012±0.0012, 0.139±0.03, 0.676±0.029, 0.638±0.067, and 0.527±0.040 μA for bare, Nafion, Nafion-CNT, Nafion-CNT/EC, EC, and EC/Nafion-CNT CFMEs, respectively (**Figure 2-4e**). The surface coatings (Nafion and Nafion-CNT) increase Ipas to 5-HT compared to the bare CFMEs, which are not electrochemically active. The additional electrochemical treatment after Nafion-CNT coating results in a 4.9-fold increase in Ipa. Similarly, both EC and EC/Nafion-CNT CFMEs showed significantly increased Ipas to 5-HT compared to CFMEs without EC treatment. Interestingly, with additional Nafion-CNT coating, the EC/Nafion-CNT CFMEs showed a slightly reduced Ipas compared to EC CFMEs.

Overall, all CFMEs with electrochemical treatments (Nafion-CNT/EC, EC, and EC/Nafion-CNT/EC) showed significant increased signal response to CFMEs without electrochemical treatment (Bare, Nafion, Nafion-CNT). There is no significant difference between Nafion-CNT/EC and EC CFME. However, there are significant differences between Nafion-CNT/EC and EC/Nafion-CNT ($p<0.05$), as well as EC and EC/Nafion-CNT ($p<0.05$). The variations in Ipa captured by the error bars are expected to be caused by variations in the dip-coating and electrochemical treatment processes.

These surface modifications may enhance 5-HT detection performance in the following ways: (1) increased surface charges, (2) increased surface area and defects/edge plane sites, and (3)

increased oxygen functional groups generated on the surface. Coating CFMEs with Nafion and carboxylic acid-functionalized CNT increases the negative charges, availability of edge plane active sites for adsorption, and the conductivity and electron transfer by adding oxygen atoms with open π orbital [194], [195]. Similarly, the electrochemical treatment also creates negative charges, defects/edge plane sites, and adds oxygen-containing functional groups to the surface [174]. Both treatments enhance 5-HT detection, but electrochemical treatment causes a significantly higher signal, which may suggest larger quantities of surface charges, defects/edge plane sites, and oxygen functional groups generated by electrochemical treatment than Nafion-CNT coating.

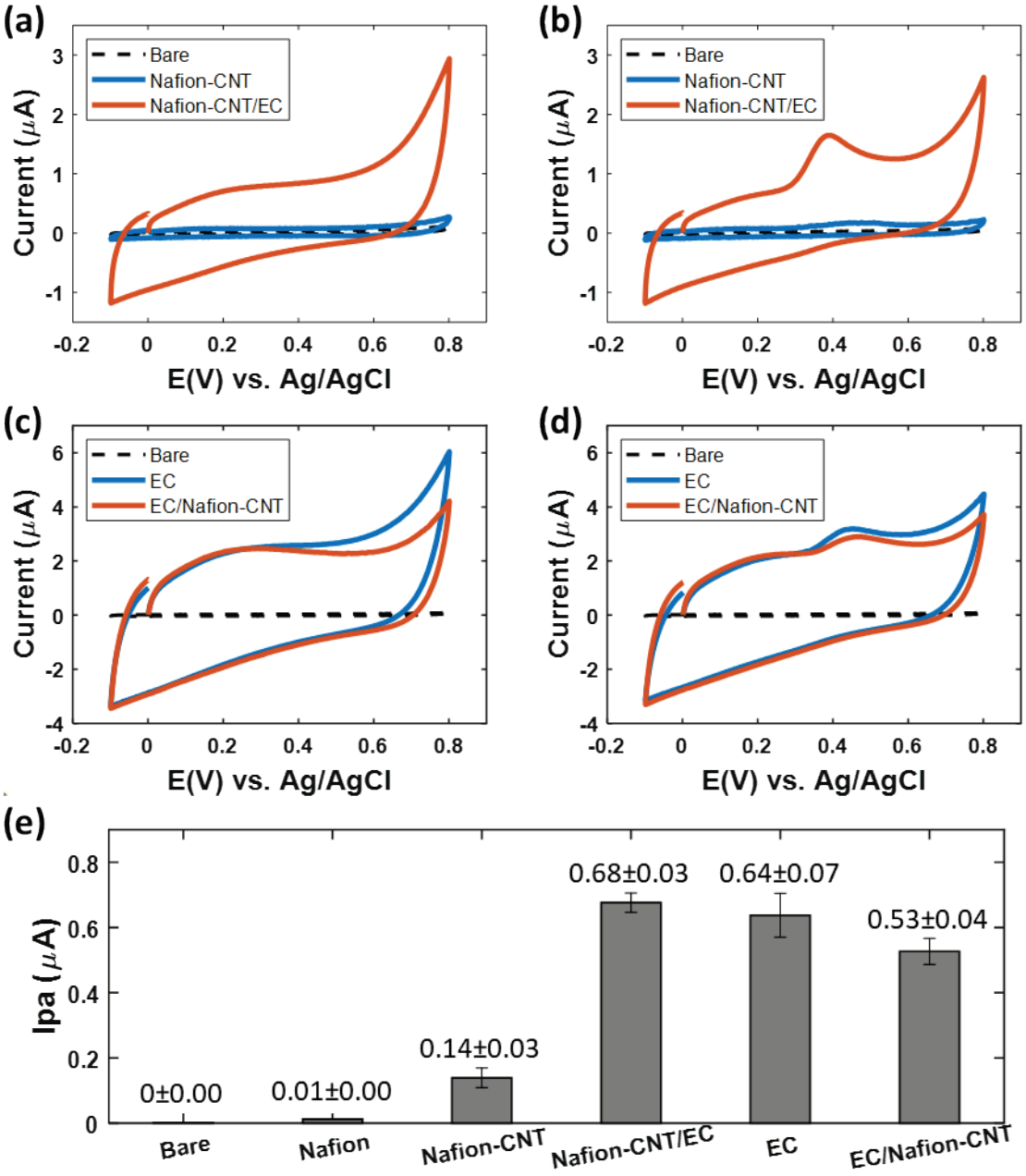

Figure 2-4 CV response of modified CFMEs in PBS and 5-HT. (a) Non-faradaic current in PBS with bare, Nafion-CNT, and Nafion-CNT/EC CFMEs. (b) Faradaic current response to 10 μM 5-HT in PBS with bare, Nafion-CNT, and Nafion-CNT/EC CFMEs. (c) Non-faradaic current in PBS with bare, EC, EC/Nafion-CNT CFMEs. (b) Faradaic current response to 10 μM 5-HT in PBS with bare, EC, EC/Nafion-CNT CFMEs. (e) Average Ipas in the detection of 10 μM 5-HT using bare (n=6), Nafion (n=3), Nafion-CNT (n=6), Nafion-CNT/EC (n=6), EC (n=4), and EC/Nafion-CNT (n=4) modified CFMEs. Error bars denote standard error. All experiments were performed at the scan rate of 1 V/s.

2.2.3 Improved Serotonin Resistance with Nafion-CNT Coating

In the process of 5-HT electrochemical detection, 5-HT molecules adhere to an electroactive surface and undergo oxidation, resulting in the generation of a detectable electrical current. However, this oxidation reaction leads to downstream electrode fouling as 5-HT spontaneous polymerization results in the formation of polymeric by-products [196]. These byproducts accumulate on the electrode, progressively reducing the available electroactive surface area with each successive measurement [164], [197]–[199]. Based on my hypothesis, applying a Nafion-CNT coating not only increases the sensitivity but also improves fouling resistance and selectivity of CFMEs, which is a well-known property of Nafion [41] and CNT [164].

The fouling resistance of CFMEs with or without Nafion-CNT coating were compared (**Figure 2-8**). CFMEs were immersed in 1 μM 5-HT and subjected to 30 consecutive cycles of 5-HT sensing. The current values were normalized to the first cycle. A 10% loss of signal at the 30th cycle is observed at Nafion-CNT/EC, while a 34% loss of signal at the 30th cycle is observed at EC CFMEs. The results indicate the antifouling property of Nafion-CNT coating, while the EC CFME shows a limited fouling resistance.

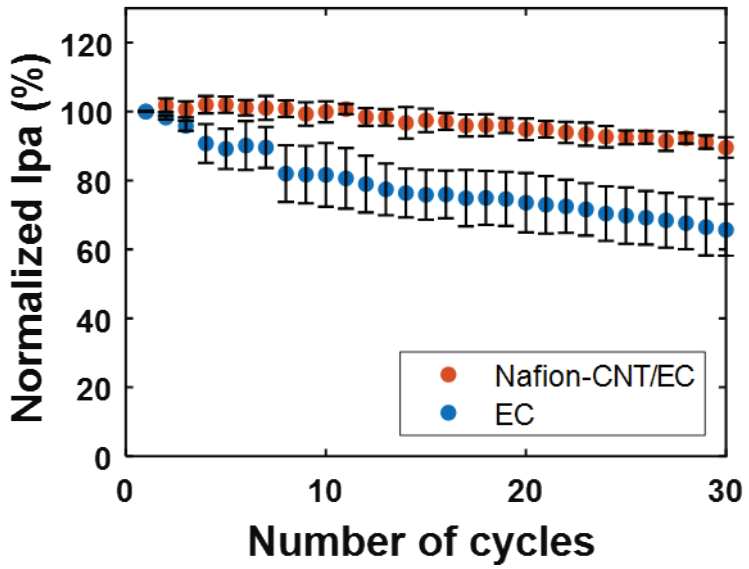

Figure 2-5 5-HT fouling at Nafion-CNT/EC (orange) and EC (blue) CFMEs in 1 μM 5-HT solution for 30 consecutive cycles. The Ipas are normalized to the initial cycles. Error bars denote standard error (n=3).

2.2.4 Improved Selectivity with Nafion-CNT Coating

The primary reason for using CFMEs is to achieve minimally invasive 5-HT detection for *in vivo* applications. For an *in vivo* environment, 5-HT detection is likely to face interferences from other electrochemically active biomolecules, including DA, UA, AA, ADN, and 5-HIAA [32]. To evaluate the improved selectivity of developed surface-modified CFMEs with Nafion-CNT coating, UA was used as a benchmark.

Two types of CFMEs (EC vs. Nafion-CNT/EC) were tested in 10 μM 5-HT and 1 mM UA. A representative Nafion-CNT/EC CFME shows an Ipa of 0.65 μA for 10 μM 5-HT and 0.67 μA for 1 mM UA. The signal ratio of 10 μM 5-HT to 1 mM UA is calculated to be 1.51 (**Figure 2-6a**). A representative EC CFME showed an Ipa of 0.72 μA for 10 μM 5-HT and 1.03 μA for 1 mM UA. The signal ratio of 10 μM 5-HT to 1 mM UA is calculated to be 1.72 (**Figure 2-6b**), which is less than Nafion-CNT/EC CFME. On average, the signal ratios of 10 μM 5-HT over 1 mM UA are

1.51 for Nafion-CNT CFME and 0.73 for EC CFME, respectively (**Figure 2-6c**). The results indicate that Nafion-CNT coating improves CFME selectivity to 5-HT. The large error bar is cause by electrode variation in the fabrication and modification process.

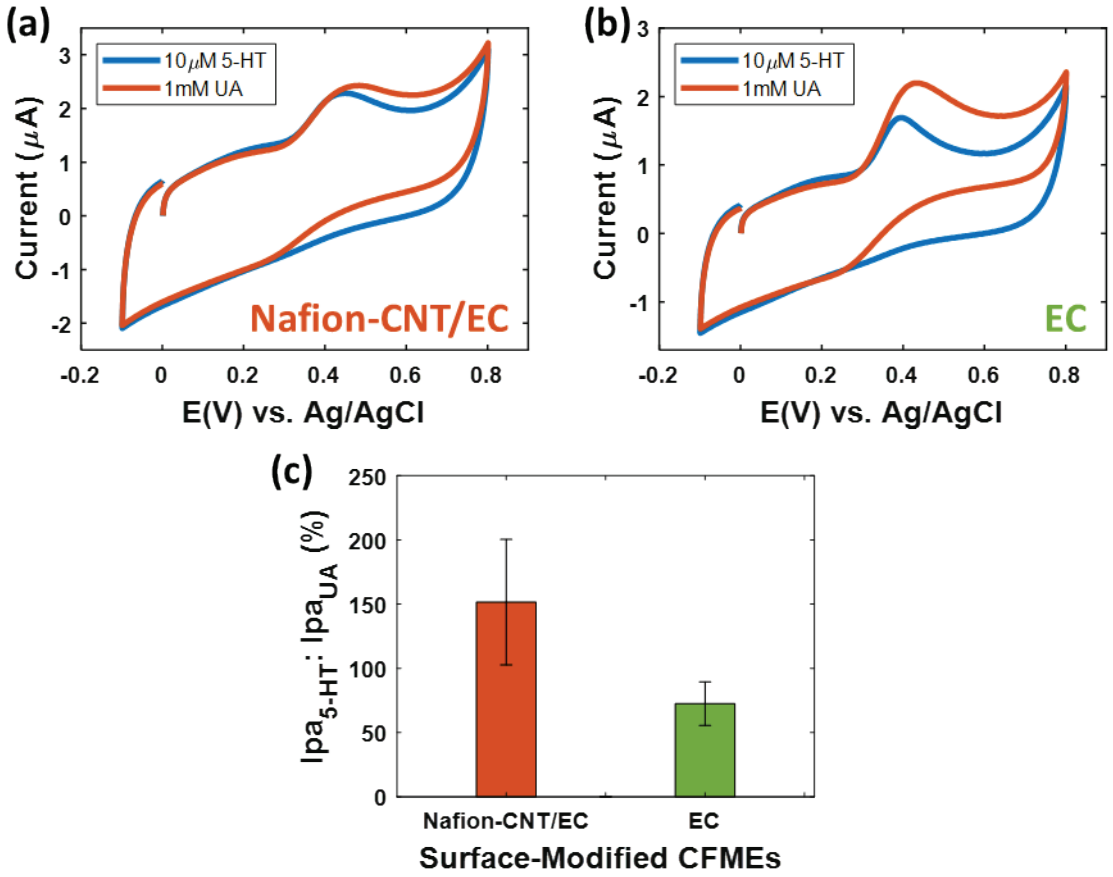

Figure 2-6 CV response of modified CFMEs in 10 μM 5-HT and 1mM UA with an (a) Nafion-CNT/EC, and (b) EC. (c) Signal ratio of 10 μM 5-HT over 1mM UA using surface-modified CFMEs. All experiments were performed at the scan rate of 1 V/s.

Based on the sensitivity, fouling, and selectivity characterizations above, Nafion-CNT/EC CFME is an ideal candidate for sensitive and reliable 5-HT sensing in complex environments. Once the microelectrode is selected, the selectivity characterization was expanded for other molecules, including DA, UA, NE, 5-HIAA, and ADN. Their Epa was first characterized using

CV with Nafion-CNT/EC CFMEs. The Epa for DA was found to be 0.18 V, which has no interference with 5-HT (Epa = 0.37 V, **Figure 2-7a**). The Epas for UA, NE, 5-HIAA, and ADN are 0.25 V, 0.20 V, 0.35 V, and 0.19 V (**Figure 2-7b-e**). The results suggest that, based on the Epa, UA and 5-HIAA may interfere with 5-HT signal, whereas DA, NE, and ADN will not.

These interfering molecules (10 μM for UA, NE, 5-HIAA, ADN; and 20 μM for DA) were also mixed with 1 μM 5-HT and the Ipas of CV responses were recorded on Nafion-CNT/EC CFMEs to explore the selectivity of this electrode. **Figure 2-7f** illustrates that a 10-fold concentration of 5-HIAA, UA, NE, ADN, and a 20-fold concentration of DA had little influence over the detection of 1 μM 5-HT, where the differences in Ipas were within 7%.

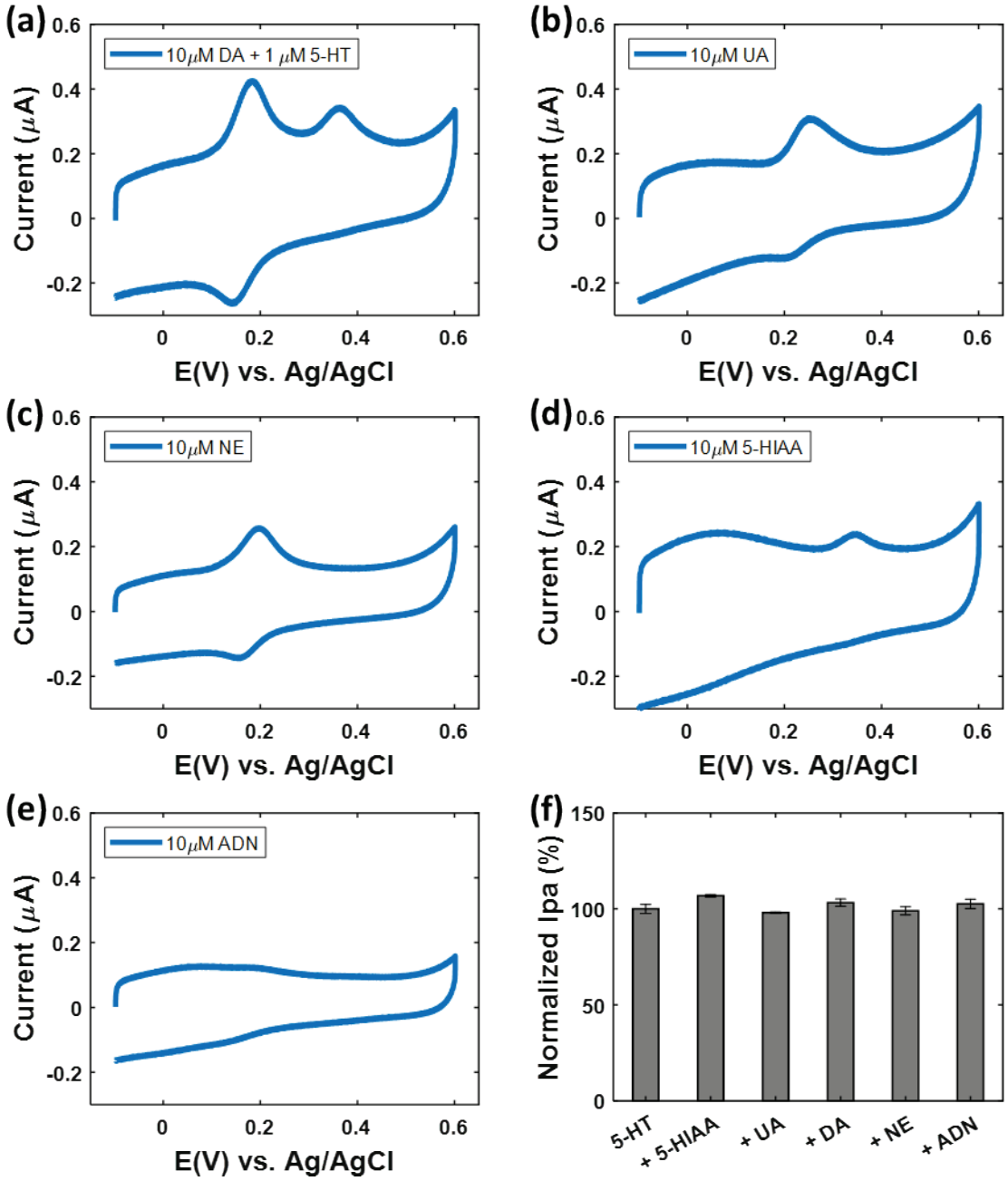

Figure 2-7 CV response of Nafion-CNT/EC CFMEs in (a) 10 μM DA and 1 μM 5-HT, (b) 10 μM UA, (c) 10 μM NE, (d) 10 μM 5-HIAA, and (e) 10 μM ADN. (f) Average normalized Ipas of 5-HT coexisted with different interfering substances: 1 μM 5-HT (100%); 1 μM 5-HT + 10 μM 5-HIAA (107%); 1 μM 5-HT + 10 μM UA (98%); 1 μM 5-HT + 20 μM DA (103%); 1 μM 5-HT + 10 μM NE (99%); 1 μM 5-HT + 10 μM ADN (103%). Ipas are normalized to 1 μM 5-HT. Potential range: -0.1 to 0.6 V. Scan rate: 200 mV/s for all experiments.

2.2.5 Determine Sensitivity for Nafion-CNT/EC Carbon Fiber Microelectrodes

Applying time for molecular accumulation before each measurement can improve the amount of adsorption of 5-HT at the electrode, thereby improving the signal. Therefore, the effect of accumulation on the oxidation signals of 0.5 μM 5-HT was investigated for various accumulation times (30 s to 30 min) before each CV cycle. As shown in Figure **2-8a**, Ipa increases with the increase of accumulation time for surface-modified CFMEs (Nafion-CNT, EC, Nafion-CNT/EC and EC/Nafion-CNT), thereby suggesting that increasing accumulation time increases 5-HT sensitivity until saturation is achieved. The saturation time for all CFMEs with electrochemical treatments is longer than it for CFME with only Nafion-CNT coating (< 10 min). This result also indicates more available edge plane active sites for 5-HT adsorption using electrochemical treatment rather than Nafion-CNT coating. Using longer accumulation time to improve 5-HT detection has a trade-off of losing time resolution. To balance the time resolution and sensitivity, the accumulation time of 1 min was used to determine the sensitivity.

To determine the improvement in 5-HT sensitivity due to electrochemical treatment, 5-HT sensitivity was compared between Nafion-CNT and Nafion-CNT/EC CFMEs (**Figure 2-8b-d**). In **Figure 2-8c**, the voltammograms of the Nafion-CNT show an increasing signal response for increasing 5-HT concentrations. A similar trend is observed for Nafion-CNT/EC voltammograms (**Figure 2-8d**). Their calibration is obtained to determine the linear range, sensitivity, LOD, and limit of quantification (LOQ) (**Figure 2-8b**). The Nafion-CNT electrodes showed a linear range in the 200 to 800 nM range, while the Nafion-CNT/EC electrodes showed a linear range in the 100 to 800 nM range. The slope of this linear region denotes 5-HT sensitivity, for which the Nafion-CNT/EC CFME is calculated as 84.6 nA/μM (R^2 = 0.9911). The LOD is obtained as 3 × resolution/sensitivity = (3 × 0.52 nA) / (84.6 nA/μM) = 17 nM, and the LOQ is calculated to be 56

nM. The Nafion-CNT CFME shows a sensitivity of 7.23 nA/µM (R^2 = 0.8880). The LOD is obtained with the same calculation (3 × 1.51 nA) / (7.23 nA/µM) = 626.5 nM, with a LOQ of 2.07 µM. Overall, the Nafion-CNT/EC electrode shows significantly improved sensitivity (11.7x) and LOD (36.9x) of 5-HT detection than the Nafion-CNT CFME. Based on our hypothesis, this improved performance after electrochemical treatments is due to the increased EASA, the creation of charged molecules and edge plane sites for 5-HT binding.

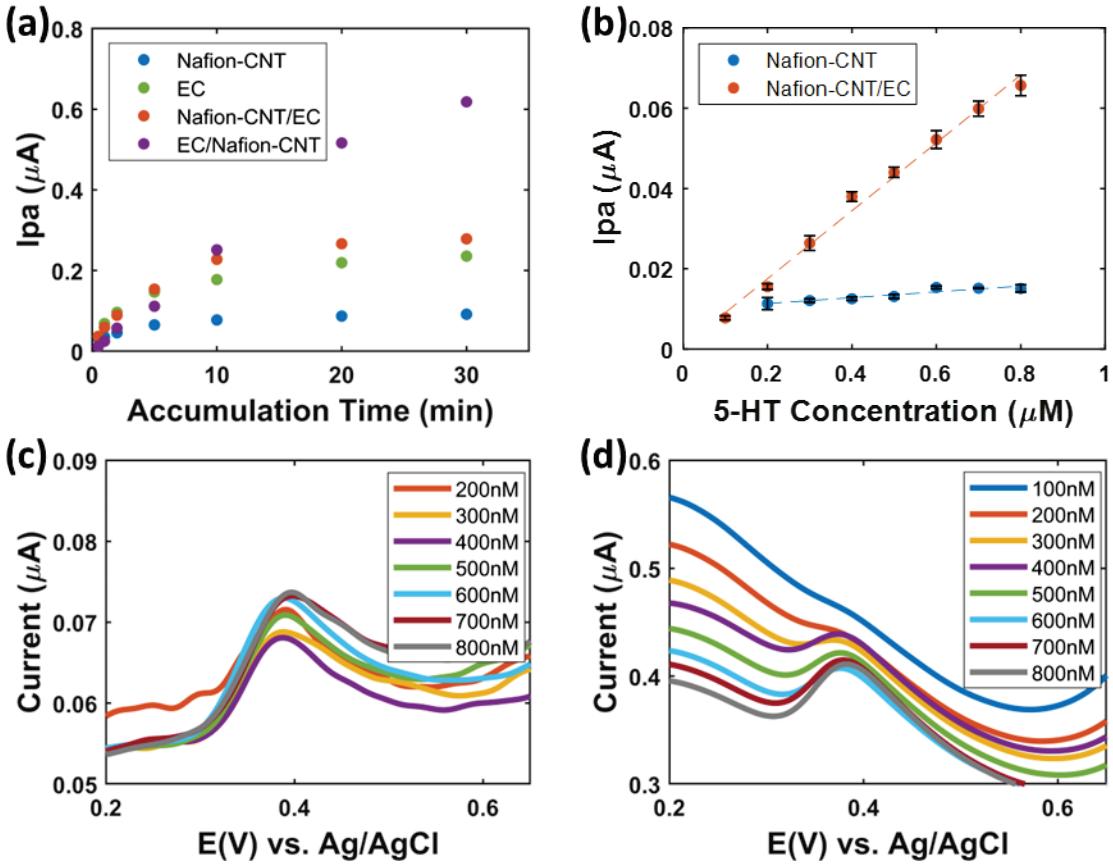

Figure 2-8 Accumulation time-dependent 5-HT sensitivity at surface-modified CMFEs. (a) Effect of accumulation time on 5-HT detection using modified CFMEs. (n=1). (b) Calibration curves of 5-HT for Nafion-CNT (200 nM – 800 nM) and Nafion-CNT/EC (100 nM – 800nM) with 1 min accumulation time. (n=3). Error bars denote standard error. (c) Representative Nafion-CNT CV curves within the linear range (200 nM – 800 nM). (d) Representative Nafion-CNT/EC CV curves within the linear range (100 nM – 800 nM). All experiments were performed at the scan rate of 1 V/s, with potential range from -0.1 to 0.8V.

2.3 Serotonin Detection in Biological Samples

Based on the beaker characterizations in standard 5-HT solution, Nafion-CNT/EC CFMEs exhibits high sensitivity, high selectivity, and fouling resistance in the detection of 5-HT. To further verify the performance of developed Nafion-CNT/EC CFMEs for 5-HT detection in complex environments, electrodes were tested in real biological samples, including (a) cultured RIN14B cells, and (b) crayfish nerve cord.

As most 5-HT is synthesized in the enterochromaffin cell from the mucosa in gastrointestinal tract, RIN14B cells have been used as a modeled enterochromaffin cell line to experiment with 5-HT release pathway. The RIN14B cell line was obtained from a rat delta islet tumor, like enterochromaffin cells, RIN14B was found to be capable of releasing 5-HT in response to TRPA1 agonists. When TRPA1 is activated, in both ECCs and RIN14B cells, Ca^{2+} influx is triggered through voltage-gated Ca^{2+} channels [200], [201], which stimulates release of 5-HT [43]. In addition to its 5-HT-releasing ability, RIN14B also expressed both endocrine (chromogranin A, synaptophysin, and VMAT1) and EC cell markers (TPH1). These results indicate that the RIN14B cell line could be a useful model for studying the physiological and pharmacological nature of enterochromaffin cells.

Sensing 5-HT concentrations and transmission is important to learn about the role of 5-HT in modulating neuronal circuit development and activities. As a neurotransmitter throughout the body, 5-HT regulates multiple brain and peripheral functions. In local neurotransmission, 5-HT is synthesized in serotonergic neurons or enterochromaffin cells, packed in vesicles to be released into the synapse and interact with its receptors. The interaction causes the receptors to open either inhibitory channel to negatively charged ions, or excitatory channel to positively charged ions. The post-synaptic neuron is either inhibited or excited.

2.3.1 Materials and Methods

Customized Ag/AgCl Reference Electrode and Pt Counter Electrode

Customized RE and CE were fabricated to perform electrochemical measurements in biological with small sample volume. The Ag/AgCl RE was fabricated by coating AgCl on a bare Ag wire (32 AWG, A-M Systems, WA). An Ag wire and Pt wire (36 AWG, A-M Systems, WA) were partially immersed (~1 cm) in KCl (1M) solution and connected to the WE and RE/CE of the benchtop VSP-300 potentiostat (BioLogic, France), respectively. A 0.15 mA current was applied to the Ag wire to chloride the surface until a uniform AgCl coating was formed. Both Ag/AgCl RE and Pt CE were inserted into glass capillaries with a 1 cm tip extended.

Cell Released 5-HT Detection

The RIN14B rat islet cell line (ATCC® CRL2059™, VA) was used as a surrogate for 5-HT-secreting enterochromaffin cells in the mammalian gut epithelium. Standard cell culture was performed in T25 polystyrene flasks from Thermo Fisher Scientific with incubation at 37°C and 5% CO_2. Cells were cultured in RPMI 1640 media with 10% Fetal Bovine Serum (FBS) (Thermo Fisher Scientific, MA). Cell passaging was performed every 3-5 days with 2.5% trypsin-EDTA (Sigma-Aldrich, MO). When cells reached 100% confluency (cell count ~ 9×10^6), 5-HT release experiments were performed. Cells were first washed with 37°C PBS, and then 5-HT release was stimulated with 300 μM aryl isothiocyanate (AITC) in 1 mL Hanks' Balanced Salt Solution (HBSS) with 4.5 g/L D-glucose and 2 μM fluoxetine to prevent 5-HT reuptake over the 20 min incubation. The supernatant was taken for 5-HT detection using a Nafion-CNT/EC CFME. Cell-released 5-HT concentration was quantified against 5-HT standards in HBSS. The CV waveform from -0.1 to 0.8V with a scan rate of 1 V/s was applied for electrochemical measurements. Customized RE and CE were used.

5-HT Detection in Homogenized Crayfish Nerve Cord

In the *in vitro* 5-HT detection experiment, crayfish (Procambarus clarkii) with weight of 20 g was selected. These crayfish were estimated to be 6 to 8 months old. Upon receipt from our supplier (Atchafalaya Co., LA), the animals were housed in dechlorinated tap water at a temperature of 21°C. They were fed twice a week diet with formula one pellets (Ocean Nuitrition, CA). Prior to the surgical procedure, crayfish received an injection of 0.5 mL of 3 mM 5-HT into their ventral sinus cavity. 30 minutes after the 5-HT injection, the abdominal nerve cords were extracted. To facilitate this, the abdomen was placed ventral side up in a petri dish lined with Sylgard and filled with crayfish saline. The integument was meticulously removed, revealing the intact abdominal nerve cord comprising six ganglia. Great care was taken to ensure that only the targeted samples were collected, excluding any extraneous muscle tissue. For the CV measurement, each nerve cord was manually homogenized in 200 µL of 1X crayfish saline (202 mM NaCl, 5.37 mM KCl, 13.53 mM $CaCl_2 \cdot 2H_2O$, 2.6 mM $MgCl_2 \cdot 6H_2O$, and 2.4 mM HEPES). The CV waveform from -0.1 to 0.6V with a scan rate of 100 mV/s was applied for electrochemical measurements. Customized RE and CE were used.

2.3.2 Customized Reference Electrode and Counter Electrode

In order to perform electrochemical measurement in biological samples with small volume, a customized three-electrode configuration was developed, which consists of a Nafion-CNT/EC CFME, a fabricated Ag/AgCl wire, and a Pt wire (**Figure 2-9a**). The performance of customized RE/CE is compared with their commercially available standards. Cyclic voltammograms of 10 µM 5-HT were recorded with a benchtop potentiostat to compare a standard commercial Ag/AgCl (3M KCl) RE and Pt wire CE with a fabricated Ag/AgCl wire RE and Pt wire CE **(Figure 2-9b**). The

customized electrodes showed identical Ipas and a 29 mV potential shift to the left compared to the standard electrodes. This result infers that the customized electrodes perform similarly to the standard RE/CE, except for a slight peak shift likely due to the difference in potential of the REs.

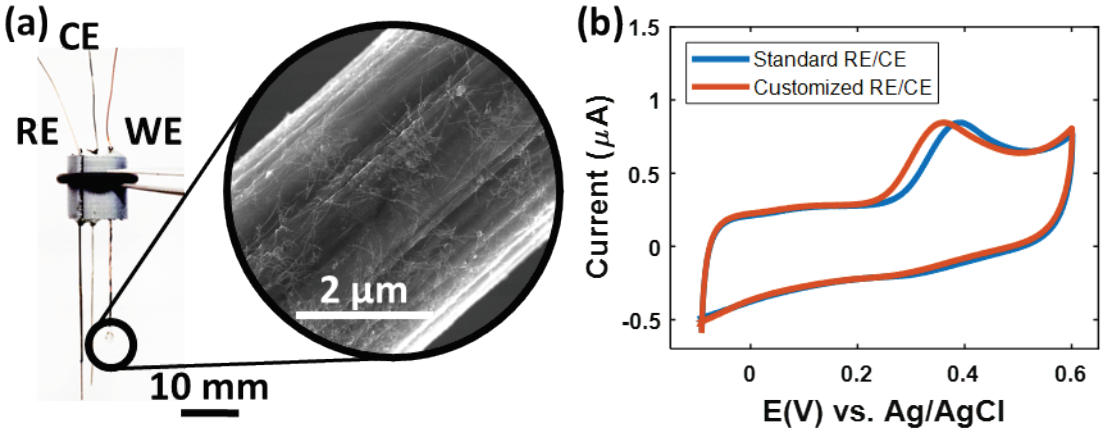

Figure 2-9 (a) Photograph of customized three-electrode configuration arranged in a 3D-printed holder and an SEM image (50k×) of the Nafion-CNT/EC as WE. (b)Comparison between standard and customized RE/CE using 10 µM 5-HT, Nafion-CNT/EC working electrode. Potential range: -0.1 to 0.6V, scan rate: 200 mV/s.

2.3.3 Cell Culture Released Serotonin Detection

Considering the sensitivity, selectivity, and fouling resistance, the Nafion-CNT/EC CFME was used to detect cell-released 5-HT in the supernatant of RIN14B cells, a model enterochromaffin cell line, cultured in a T25 flask (**Figure 2-10**). **Figure 2-10b** shows a representative image of RIN14B cells plated on polystyrene T25 flasks at 95% confluency, imaged with brightfield microscopy. 300 µM AITC in HBSS with 4.5g/L D-glucose and 2 µM fluoxetine was used to trigger 5-HT release from cultured RIN14B cells (+AITC). This was compared to a negative control (vehicle, -AITC) condition, in which an equivalent volume of 30% DMSO without AITC was added to the above solution. AITC is a TRPA1 receptor agonist and triggers a Ca^{2+}-dependent 5-HT release pathway in RIN14B [43]. **Figure 2-10c** shows that the addition of AITC increased

5-HT secretion from RIN14B cells (Ipa = 19.04 nA) over vehicle (Ipa = 2.64 nA). The Nafion-CNT/EC CFME was then calibrated in 5-HT standards in HBSS, showing a linear range from 100 to 250 nM with R^2=0.9853 (**Figure 2-10d**). According to the calibration curve, the 5-HT concentration released from cells treated with AITC is 120.1 nM, while the 5-HT level in the vehicle sample is below the LOQ (< 56 nM). The results indicate that, on average, each cell released 8.04×10^6 5-HT molecules within the 20 minutes incubation time with AITC. This result is in the same order of magnitude as previously reported (5.40×10^6) [200]. This experiment demonstrates the feasibility of using Nafion-CNT/EC CFME to detect 5-HT from biological samples using CV.

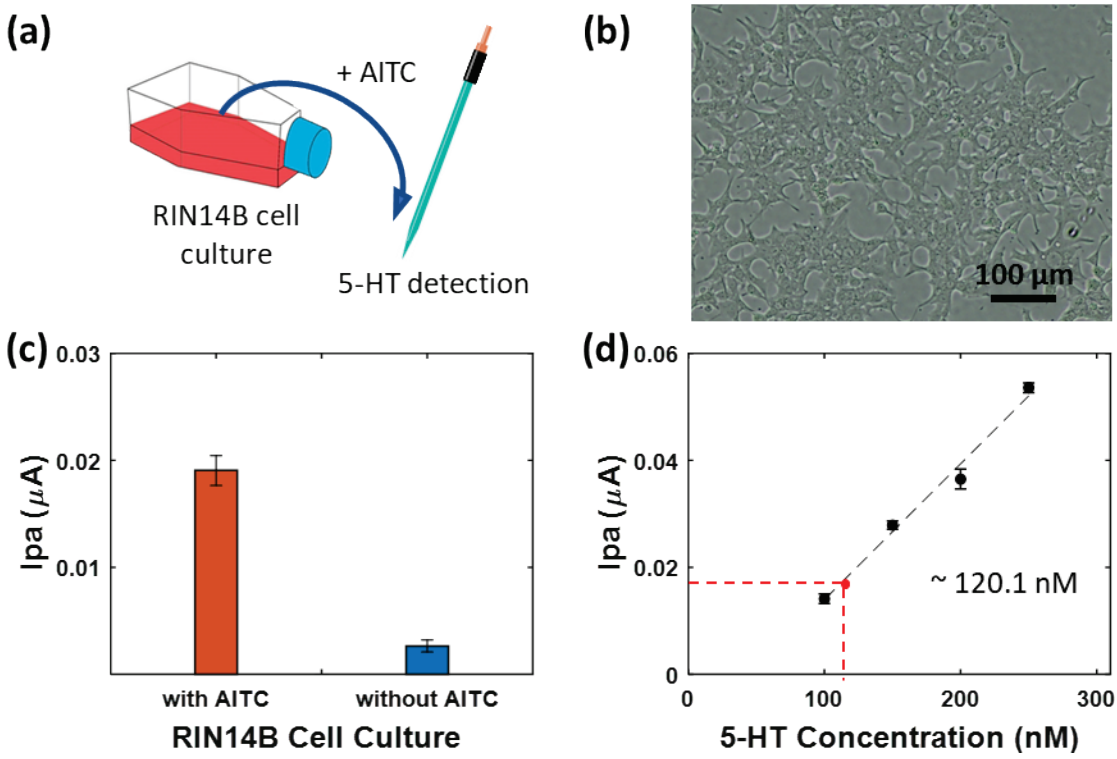

Figure 2-10 RIN14B cell-released 5-HT experiment using Nafion-CNT/EC CFMEs. (a) Illustration of cell-released 5-HT detection using Nafion-CNT/EC CFME in cell supernatant. (b) Brightfield image of RIN14B on a T25 polystyrene flask at 95% confluency. (c) Stimulated 5-HT release was chemically evoked using HBSS ± 300 µM AITC. (n=3). (d) Calibration curve of 5-HT standards (100 to 250 nM) using Nafion-CNT/EC CFME. Sensitivity: 254.0 nA/µM, LOD: 18.3 nM, R^2 = 0.9853 (n=3). Error bars denote standard error.

2.3.4 Serotonin Detection in Crayfish Nerve Cord

The Nafion-CNT/EC CFMEs with customized RE and CE were used to detect 5-HT in the crayfish nerve cord. As an invertebrate, crayfish have relatively simple and well-characterized nervous system, with a small number of neurons that can be easily studied and manipulated, making crayfish an ideal model for investigating the neural mechanisms underlying and 5-HT signaling. Crayfish possess an open circulatory system, where their blood and extracellular tissue fluid, known as hemolymph, are pumped throughout their body by the heart. Within this open circulatory system, neurotransmitters are released into the hemolymph and subsequently transported back to the heart for circulation. During the circulation, chemicals in the hemolymph can be uptake by the nervous system that may impact brain functions [202]. In the experiment, crayfish were injected with 0.5 mL of 3 mM 5-HT into the hemolymph through the ventral sinus cavity, and the hemolymph was expected to circulate though the crayfish and uptake by the nerve cord. The crayfish nerve cord was dissected and homogenized in crayfish saline for analysis (**Figure 2-11a**). This was compared to a negative control (-5-HT), in which the nerve cord was taken from a similar sized animal with no 5-HT injection. **Figure 2-11b** shows the signal response of crayfish saline as a baseline, the nerve cord with no 5-HT treatment, and the nerve cord with 5-HT treatment. No peak was observed from the cyclic voltammogram for crayfish saline baseline, which is expected as chemicals in the crayfish saline are not electrochemically reactive species. A small peak was observed for non-treated crayfish nerve cord, which has an Ipa of 4.9 nA. A clear peak was observed for the nerve cord pretreated with 5-HT, showing an Ipa of 20.7 nA. The results demonstrate the capability of using customized electrochemical electrode system for 5-HT measurement in crayfish nerve cord with a small volume. The results also demonstrate the injected

5-HT into crayfish hemolymph was being uptaken by the crayfish nerve cord and may cause downstream signaling to the serotonergic modulation circuit.

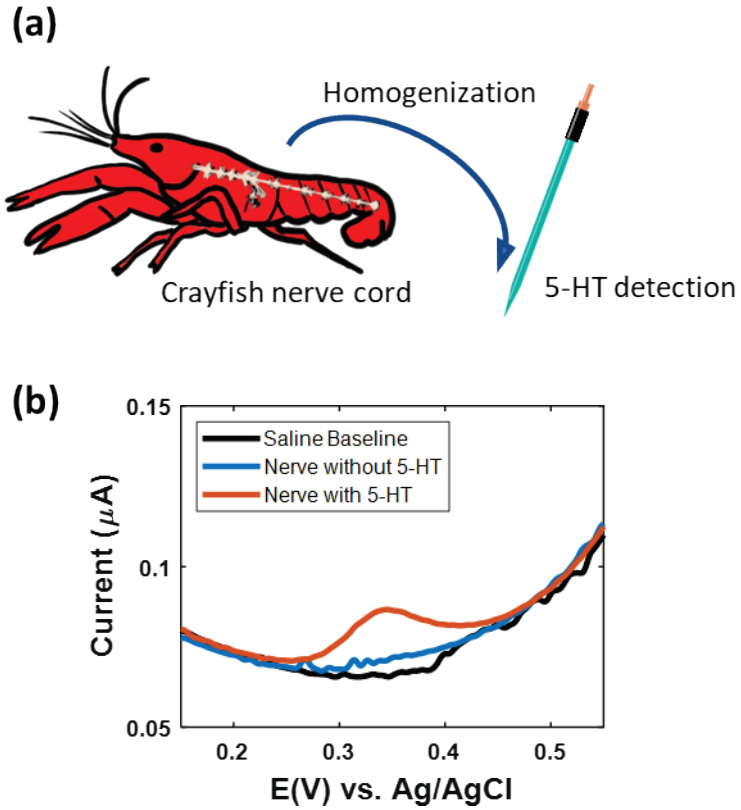

Figure 2-11 5-HT detection in homogenized crayfish nerve cord using a Nafion-CNT/EC CFME. (a) Illustration of 5-HT detection in homogenized crayfish nerve cord. (b) The cyclic voltammogram of the crayfish saline as baseline, the nerve cord with no 5-HT pretreatment, and the nerve cord with 5-HT pretreatment. The Ipa for treated nerve cord is 20.7 nA, and the Ipa for non-treated nerve cord is 4.9 nA. Potential range: -0.1 to 0.6 V. Scan rate: 100 mV/s.

2.4 Chapter Summary

This chapter demonstrated the fabrication and characterization of surface-modified CFMEs. Section 2.1 described the surface characterization of Nafion-CNT coating and electrochemical treatment from SEM, EDS, and electrochemical characterizations. The results showed increased surface area by surface coating and electrochemical treatment. Section 2.2 demonstrated the electrochemical characterization of surface-modified CFMEs for 5-HT detection, mainly focused

on sensitivity, selectivity, and 5-HT fouling. The results suggested EC treatment significantly increased electrode sensitivity to 5-HT due to increased surface area. Nafion-CNT coating showed improved selectivity and anti-fouling property compared to non-coated counter parts. Section 2.3 demonstrated the application of developed CFMEs, mainly Nafion-CNT/EC, for 5-HT detection in cell culture media and crayfish nerve cord. Due to the novel surface modification method, the cell-released 5-HT in cell culture media and 5-HT in the crayfish nerve cord have been successfully measured.

One of the key advantages of using a microelectrode is the ability to be placed in close proximity to serotonergic neurons or 5-HT-releasing cells to obtain 5-HT release dynamics with high spatial resolution, which was not demonstrated in this work. The nervous system of crayfish is a well-studied, and serotonergic neuron in the CNS are mapped out. One of the key challenges is to improve the mechanical strength to enhance the penetration ability of the microelectrode, allowing it to penetrate into the tissue around the nerve cord. An improved modification protocol using multi-carbon fiber microelectrodes is described in Chapter 4, which demonstrates improved mechanical strength. The future work will involve using the improved microelectrode to detect 5-HT release from intact *ex vivo* crayfish nerve cord to better understand serotonergic modulation in the CNS.

Overall, these novel surface-modified Nafion-CNT/EC CFMEs provide a 4.9-fold increased signal response, 11.7-fold increased sensitivity, and 36.9-fold increased LOD compared to Nafion-CNT CFMEs that were previously reported in the literature [114]. The novel CFME also exhibits excellent selectivity among other potential interfering molecules, including 5-HIAA, UA, NE, ADN, and DA, where less than 7% signal changes were observed with 10 times more concentrated interferant molecules. The novel electrodes also showed less than 10% signaling changes over 30

consecutive cycles, indicating excellent fouling resistance. The excellent performance enables the electrode to detect cell-released 5-HT at sub-micromolar concentrations and the ability to detect 5-HT from nervous tissue environments, which exhibits great potential for studying 5-HT signaling in the CNS and gastrointestinal environment and investigating serotonergic modulations.

Chapter 3 Miniaturized Potentiostat for Serotonin Detection

Portable analytical devices offer valuable insights for early-stage disease detection and physiological monitoring at the POC. By utilizing these devices personalized health diagnostics can be achieved, leading to more effective treatment strategies and improved patient outcomes [203]–[209]. Traditional diagnostic systems are limited to laboratory settings, and are not suitable for POC applications due to their high costs, need for trained personnel, lack of portability, and long wait times to obtain results [210], [211]. Today, POC devices are continuously undergoing development to provide accurate, rapid, and selective quantification of biomarkers, while also tracking important health informatics, such as time, age, and gender, to guide advanced treatment strategies. Miniaturization of these novel systems can potentially allow for direct interact with biological samples in real-time, collecting unprecedented information regarding a patient's metabolism, enabling precise monitoring of physiological parameters, and facilitating rapid diagnostic analyses [206], [212].

Electrochemical biosensors have emerged as a promising approach for selective, specific, and rapid detection of biomarkers within physiological ranges. By integrating laboratory biosensing with miniaturized electronics, there is great potential for mass production and commercialization. To achieve a POC electrochemical sensor for a specific target, it is necessary to utilize an immobilization matrix compatible with the target analyte, and develop an electrical platform that enables measurement control, data recording, correlation, storage, and display [213], [214]. A crucial component of this platform is a potentiostat, an electrical circuit that controls electrical signals during electrochemistry, enabling users to observe various electrochemical signals and monitor health status phenomena. Conventional potentiostat systems are expensive, bulky, and

impractical for POC applications, though advancements in miniaturized electronics have enabled portable potentiostat systems suitable for electrochemical devices and POC applications.

One of the most well-known commercial electrochemical sensing POC devices is the blood glucose meter. Over the past 40 years, it has evolved from an initial proof-of-concept to a mainstay POC medical device facilitating diabetes management [215]. Glucose meters provide fast analysis of blood glucose levels and allow management of diabetes disorders [216]. A glucose meter consists of two core components: an enzymatic reaction strip (biosensor) and a detector. When a patient's blood sample comes into contact with the enzymatic strip, it undergoes rehydration and triggers a redox reaction, leading to the production of a detectable signal by the potentiostat detector corresponding to the concentration of glucose. Recently, with the miniaturization of potentiostat systems, handheld blood glucose meters have transitioned into wearable devices featuring implantable electrodes for continuous glucose monitoring (CGM). The most advanced CGM system can be used to measure blood glucose levels continuously every 5 minutes using a transcutaneous sensor inserted just under the skin, with a device lifetime of up to 10 days [217]. Data is recorded in real-time, providing continuous feedback on the estimated glucose values and illustrating dynamic glucose trends over time, with little patient involvement. This advancement is mainly attributed to miniaturized electronics; however, this device is limited to CA measurements.

In this chapter, the process of miniaturizing a potentiostat circuit is introduced. The working principle, hardware design, and software implementation are introduced in Section 3.1. The miniaturized potentiostat electronics are based on the analog front-end (AFE) AD5941. To this end, an AD5941 evaluation board was first utilized to test the electrochemical sensing functionality for 5-HT measurements using CV (Section 3.2). Further, a customized potentiostat PCB equipped

with the AD5941 IC was developed for electrochemical measurement, and performance is characterized in both beaker and *in vivo* environmental settings (Section 3.3).

I thank Dr. Justin Stine for this significant contribution to this work, for originally designing the PCB potentiostat and assisting with the software implementation of CV measurements. Furthermore, Dr. Jens Herberholz contributed significantly to the discussion of *in vivo* 5-HT measurement in crayfish (Section 3.3). Ta-wen Ho also contributed to this section by performing crayfish surgery and assisting with the design of crayfish backpack sensing system.

3.1 Miniaturization of Potentiostat Electronics

A diagram of a simple potentiostat circuit is shown in **Figure 3-1**, and consists of two operational amplifiers, or OpAmps (OP1 and OP2). The fundamental function of this circuit is to (1) regulate the potential between WE and RE, (2) convert current flowing through the WE to a measurable voltage, and (3) supply sufficient current flow from the CE to facilitate the electrochemical reaction. To operate the potentiostat, a bias potential (Vin) is applied to the positive terminal of OP1. The RE is connected independently to the negative terminal of OP1. OP1 is configured as a voltage follower, whose output voltage follows the input voltage, to buffer Vin to be applied to the RE. The potential at the WE is typically grounded at 0 V or fixed at a virtual ground to facilitate single-sided operation of the OpAmp. That is, the potential difference between the RE and the WE is defined by the potential applied to Vin, which can be regulated by an external voltage reference circuit. OP2 is configured as a TIA, where current flows into the circuit from the WE and passes across a feedback resistor (R), resulting in an output voltage signal at Vout. The input-output relationship of the TIA is expressed as $Vout = -I \times R$. By recording Vout, the current flowing through the WE can be determined. The input impedance of an OpAmp is extremely large, no current flows through the RE, which is ideal to potentiostat operation to avoid voltage drop at

RE. In order to achieve high accuracy with this circuit, all of the OpAmps need to have high gain and high input impedance. OP2 should have very low input noise.

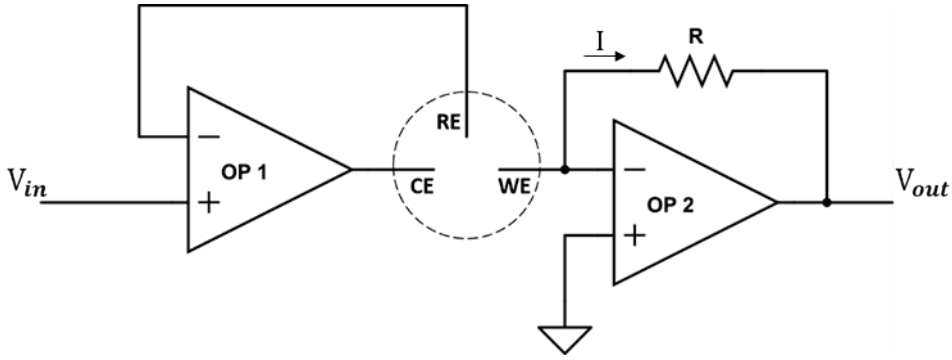

Figure 3-1 Potentiostat circuit implementation using electronic components. Vin – input voltage, Vout – output voltage.

Although a portable potentiostat can be implemented with discrete solutions using multiple OpAmps, this approach poses limitations and requires multiple ICs. Recent advancement in microelectronics provides a simple, effective solution of using an AFE, which integrates multiple functional modules, to incorporate potentiostat functionality in a single chip with similar performance. With software-configurability, the AFE can be used to rapidly implement ultra-low-power and miniaturized designs able to meet diverse requirements for accurate biological or electrochemical sensing.

The commercially available AFE chip, AD5941, is capable of electrochemical measurement with high precision and low power consumption, which makes it an ideal candidate for portable, wearable, and miniaturized applications. The AFE can be controlled by a MCU with communication interface, such as inter-integrated controller (I2C), serial peripheral interface (SPI), to achieved sensing applications. In this section, I first tested the functionality of the AD5941 with its evaluation board EVAL-AD5940ELCZ. Then a customized AD5941-based PCB potentiostat circuit was developed and implemented for CV measurements.

3.1.1 General Hardware Working Principle and Design

The core components of the potentiostat module consisted of an AFE and an MCU. The MCU controls the device functionalities and drives the digital-to-analog converter (DAC) in the AFE to generate a triangular excitation waveform to the electrode for CV measurements. The electrode started to generate a response current related to the 5-HT concentration, which was converted into analog voltage signals by a TIA in the AFE. The ADC then converts the analog voltage signals to digital voltage values, which can be stored in the internal memory of AFE. When a full CV cycle was finished, the MCU receives the data via SPI and the BLE module transmits it to the external receiver.

3.1.2 Analog Front-End AD5941

The AD5941 is a programmable, low power AFE designed for portable applications that require high precision, electrochemical-based measurement techniques, such as amperometry, voltammetry, and bioimpedance. The AD5941 consists of internal reference voltage sources, a digital waveform generator, a 16-bit ADC, a voltage DAC, a TIA to measure sensor current output, and a SPI to facilitate inter board data transfer (**Figure 3-2**) [218]. With these functions, the CV technique, used for 5-HT sensing, can be executed. AD5941 provides a signal path between the sensor and the MCU by generating an output voltage proportional to the sensor current by the TIA, so that it can be interpreted by the internal ADC. The TIA has 19 programmable gain resistors that range from 1kΩ to 512 kΩ. This wide range makes it suitable for most electrochemical sensors.

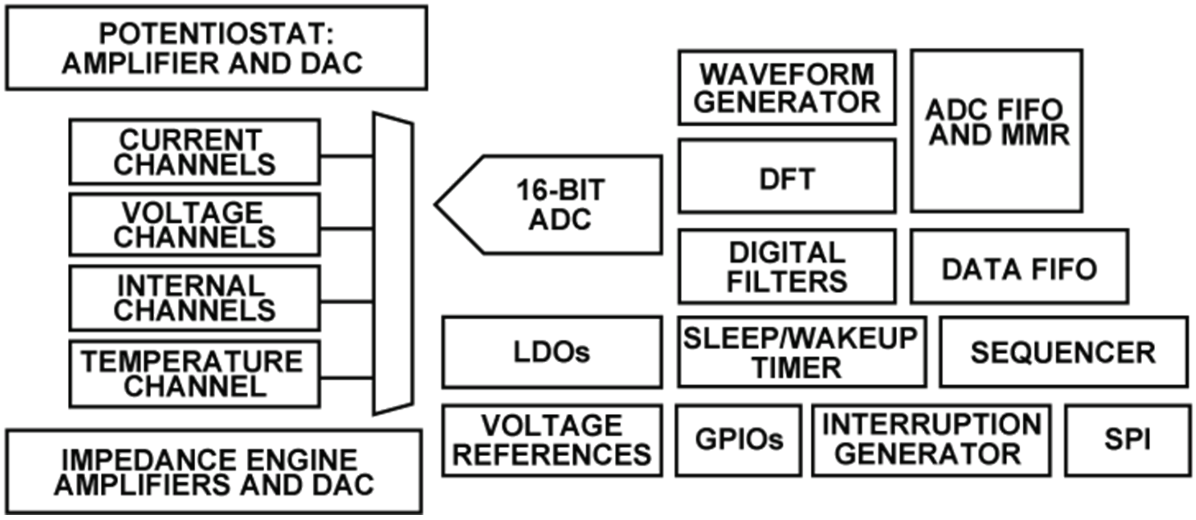

Figure 3-2 Simplified block diagram of AFE AD5941, which combines a complete set of subsystems required to generate excitation sources and measure current, voltage, and impedance [218].

For CV measurement, a triangular bias voltage waveform is applied to a sensor and the response current is monitored. The AD5941 uses its low power DAC (LPDAC), potentiostat amplifier (PA), and low power TIA (LPTIA) to set a voltage on the sensor and measure the current. The LPDAC is a dual output DAC with a 12-bit option and a 6-bit option. The 12-bit output, known as V_{BIAS}, sets the voltage on the CE and RE. The 6-bit output, known as V_{ZERO}, sets the voltage on the WE, also known as the sense electrode (SE). The bias voltage across the sensor is set by adjusting V_{BIAS} and V_{ZERO}. To carry out CV measurement on the AD5941, V_{ZERO} is set to output a voltage of 1.3 V. V_{BIAS} can sweep from 0.3 V to 2.3 V, giving a ±1 V sweep (maximum potential window). The response current at WE is measured using the LPTIA. A suitable R_{TIA} must be selected to maximize measurement accuracy and to ensure that the maximum input range of the ADC is not violated. The output signal is digitalized by a 16-bit ADC and output to MCU through SPI interface (**Figure 3-3**) [219].

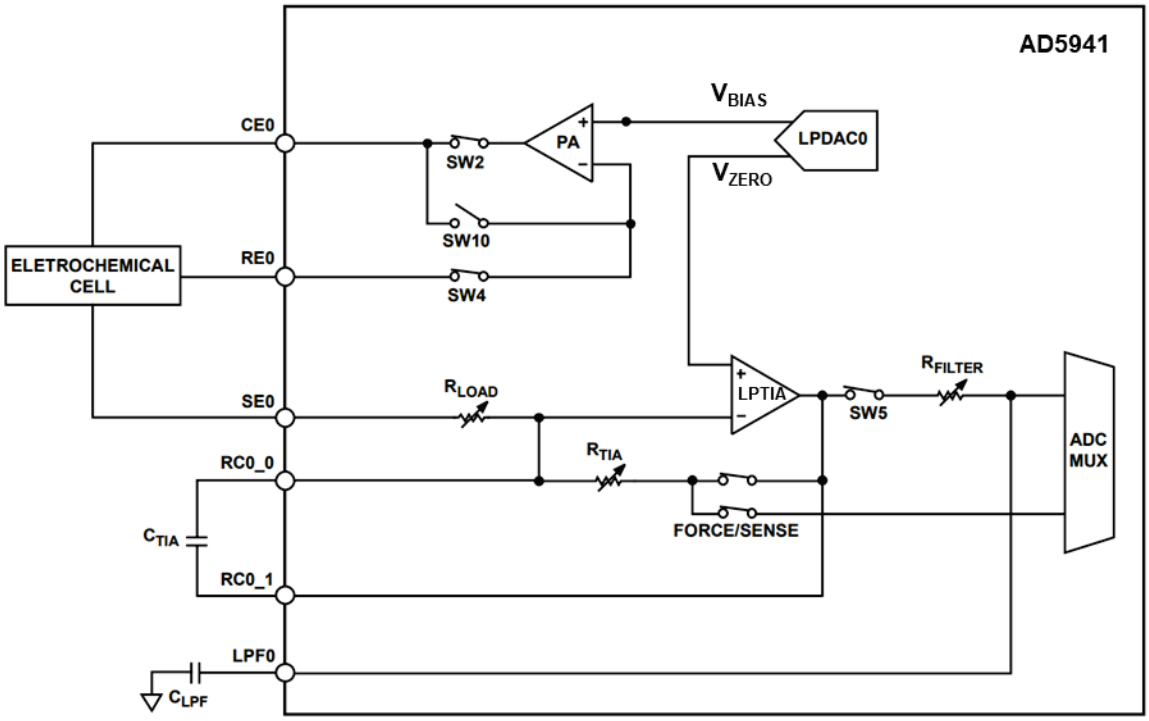

Figure 3-3 For three electrode configurations that require low-frequency excitation, the AD5941 low-bandwidth loop includes a PA whose output connects to the CE and whose input connects to the RE, while a LPTIA receives input from the SE and outputs to ADC [219].

3.1.3 Portable Potentiostat Electronics

The portable potentiostat system consists of EVAL-AD5940ELCZ evaluation board (Analog Devices, MA) and EVAL-ADICUP3029 evaluation board (Analog Devices, MA). An evaluation board is a basic system built around a specific part, along with all the other components needed to support its functionalities. The EVAL-AD5940ELCZ is built based on AFE AD5941, and the EVAL-ADICUP3029 board features the ADuCM3029, an ultra-low power ARM Cortex-M3 processor serving as its main device. This integrated mixed-signal microcontroller system excels in processing, control, and connectivity tasks (**Figure 3-4**). Together, the whole system was designed specifically for carrying out electrochemical measurements, which offers a wide range of sensing applications.

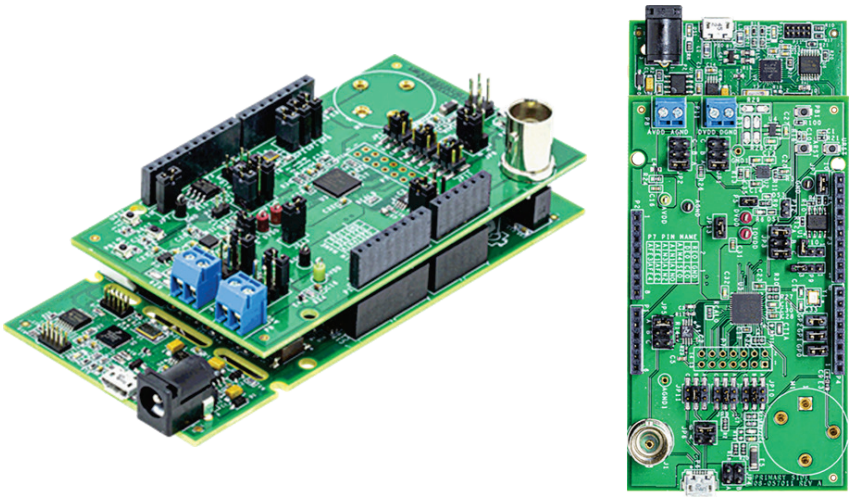

Figure 3-4 Image of EVAL-AD5940ELCZ evaluation board (top) plugged into the EVAL-ADICUP3029 evaluation board (bottom) as a portable potentiostat electronics [219].

Initially, a micro-USB cable was used to connect the EVAL-ADICUP3029 board to the PC for power supply, MCU programming, and data transfer. We utilized a free Graphical User Interface (GUI) tool called SensorPal (Analog Devices, MA), which provided graphing and data capture capabilities for making measurements. To connect the AD5940ELCZ board to the three-electrode system for electrochemical measurements, a micro-USB to crocodile chip cable was used. After testing the CV functionality of the evaluation board, I employed the arm µVision 5.0 IDE to program the MCU and further optimize the sensing parameters. Online resources provided example code and tutorials for developing MCU firmware. The portable platform utilized the universal asynchronous receiver-transmitter (UART) protocol for exchanging serial data between the device and PC. I used the terminal program RealTerm to view the measurement data. For proper connection and communication, it was necessary to set the Baud rate to 230,400 and connect to the relevant COM port, as illustrated in **Figure 3-5** [219].

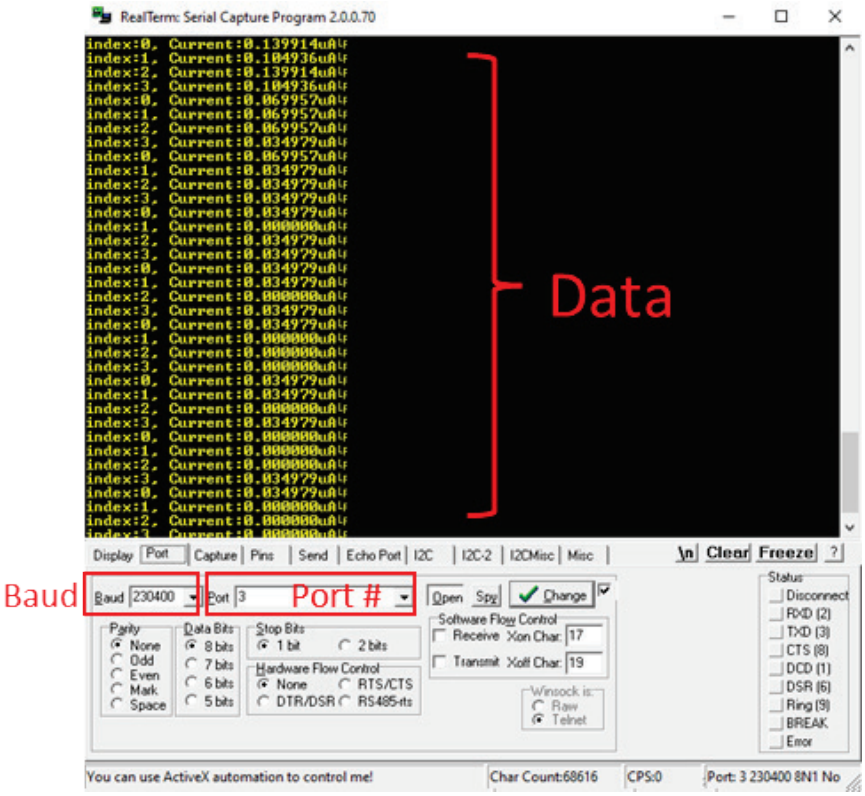

Figure 3-5 RealTerm program was used to communicate with evaluation board via UART for displaying results [219].

3.1.4 Customized Potentiostat Printed Circuit Board

A customized PCB potentiostat electronics based on AFE AD5941 (Analog Devices, MA) and MCU BGM13S (Silicon Labs, TX) is developed [220], [221]. The BGM13S is Silicon Labs' first SiP module solution designed for Bluetooth 5 connectivity. With the EFR32BG13 Blue Gecko SoC, the BGM13S is capable of wireless data communication through BLE with minimal energy consumption. With the advantages include small size, wireless capability, low power consumption and available open source code make it an ideal solution for miniaturized potentiostat circuit development [222].

The whole system was designed specifically for carrying out electrochemical measurements. The PCB is powered by a single 2L76 battery (Energizer, MO) with a regulator to provide 3.3V

for AD5941 and BGM13S. The 2L76 is a lithium battery with 3V output, 160mAh capacity, a weight of 3g, and a diameter of 11.6mm, which make it ideal for miniaturized device. To extend the operational lifetime of the miniaturized module, a magnetic reed switch was placed between the battery and voltage regulator such that, when idle, the presence of a magnetic field would power off the device. When powered, the BLE-MCU polls to establish a connection, and once paired with a smartphone, via the EFR Connect Mobile App (Silicon Labs, TX), enters low-power mode and waits for a command. External commands are sent to the BLE-MCU to control the device's function. The MCU periodically samples the AFE (rate: 100 ms) using SPI to determine when data is available, then transmits the stored data via BLE to the external smartphone.

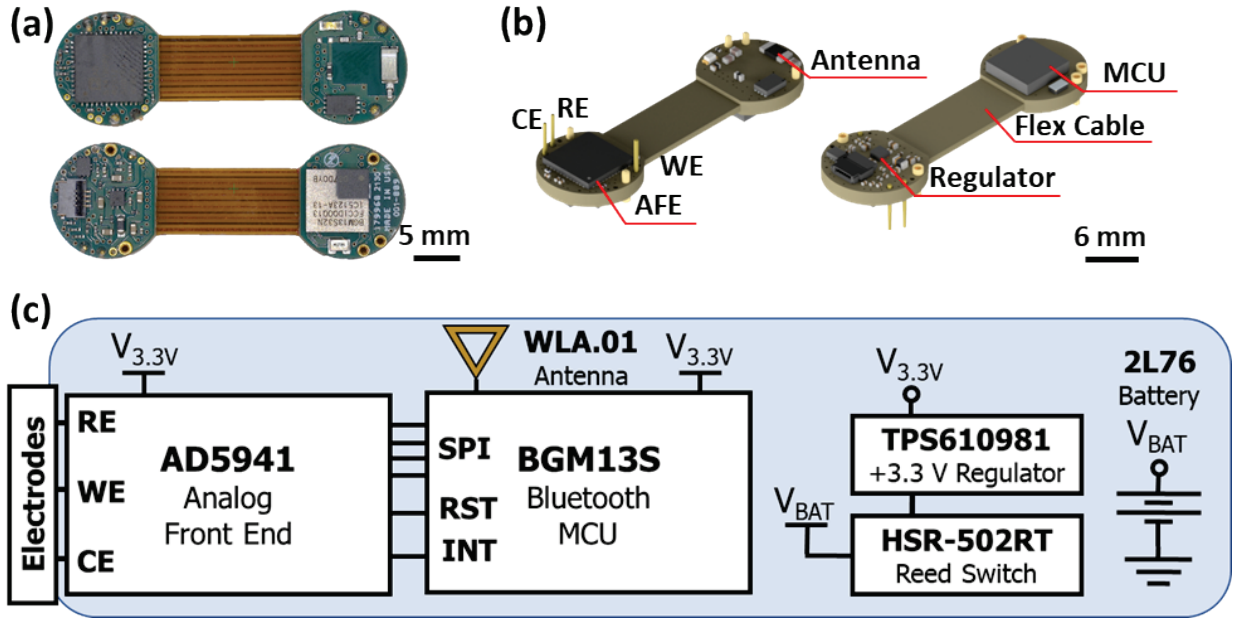

Figure 3-6 (a) Image, (b) schematic, and (c) block diagram of the customized potentiostat module.

3.2 Portable Potentiostat for Electrochemical Neurotransmitter Detection

The portable potentiostat system was first characterized for its functionality in CV measurements. Later, the evaluation board was used in combination with previously developed CFMEs and a customized RE/CE for 5-HT detection and applications (**Figure 3-7**). This commercially available system costs ~$300, serving as a low-cost portable potentiostat system. The price of a similarly functioning system can be further lowered using a customized PCB design only including components essential for operation, as a single AD5941 potentiostat IC costs $12, and ADuCM3029 IC costs $8. These commercially available ICs are particularly suitable for low-cost electrochemical sensing applications.

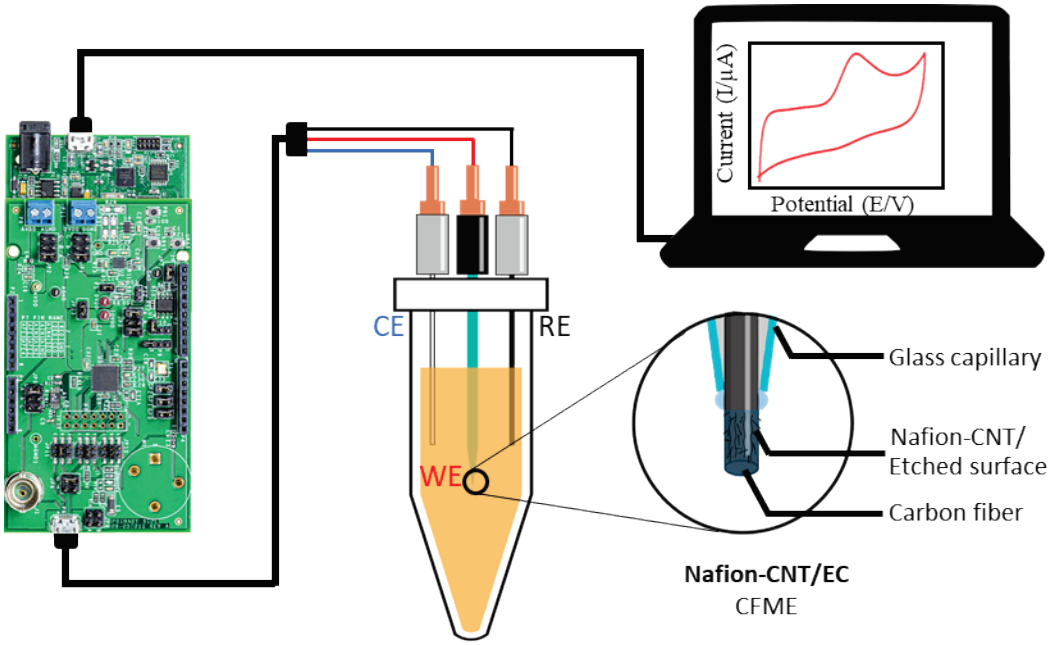

Figure 3-7 Schematic illustration of the Nafion-CNT/EC CFME-based portable 5-HT detection system: (a) the IC, (b) the sensing element, and (c) the PC with software interface.

3.2.1 Materials and Methods

Chemicals

Serotonin hydrochloride was purchased from Alfa Aesar (Haverhill, MA), and PBS powder was purchased from Research Products International (Mt Prospect, IL). 1X PBS (pH = 7.4) was

made by dissolving PBS powder in deionized (DI) water, which was used to prepare 5-HT solutions. Potassium ferricyanide (III) and potassium hexacyanoferrate (II) trihydrate were purchased from Sigma-Aldrich (St. Louis, MO). Single-walled CNTs functionalized with 1.0-3.0 atomic% carboxylic acid (P3-SWNT) were purchased from Carbon Solutions, Inc. (Riverside, CA). Nafion was purchased from Sigma-Aldrich (St. Louis, MO). A working Nafion solution was produced by diluting 5% stock solution in isopropanol. A 0.5 mg/mL Nafion-CNT solution was made with a suspension of CNT in 2.5% Nafion solution. Artificial urine (pH = 6.4) was made in DI water and the recipe [223] is listed below (**Table 3-1**).

Table 3-1 Composition of artificial urine for testing. Artificial urine was made in DI water.

Chemical Component	Concentration
Peptone	1 g/L
Yeast Extract	5 mg/L
Lactic Acid	100 mg/L
Citric Acid	400 mg/L
Sodium Bicarbonate	2.1 g/L
Urea	10 g/L
Uric Acid	70 mg/L
Creatinine Hydrochloride	900 mg/L
Calcium Chloride Dihydrate	370 mg/L
Sodium Chloride	5.2 g/L
Iron (II) Sulfate	1 mg/L
Magnesium Sulfate Anhydrous	240 mg/L
Sodium Sulfate Decahydrate	3.2 g/L
Potassium Phosphate Monobasic	950 mg/L
Potassium Phosphate Dibasic	1.2 g/L
Ammonium Chloride	1.3 g/L

Generation of CV Waveforms

CV waveforms were generated using the portable sensing system from user-provided measurement parameters, such as step size, step duration, number of data points, ramp duration,

and TIA resistance. Ideally in CV measurements, the WE potential is ramped linearly versus time. However, due to limited DAC capabilities, most measurements are performed in a staircase manner that closely resembles a linear sweep. The AFE initiates the internal DAC to generate and step the excitation voltage, while also recording the readout current between the WE and CE. The step size refers to the incremental change in amplitude of the applied voltage, and the step duration refers to the time delay prior to the next voltage increment, during which the current can be measured. For 5-HT detection, the CV waveform was varied from -0.1 to +0.6 V with other parameters optimized for improved measurement sensitivity. Considering the hardware limitations such as the minimum step size and duration of the portable sensing platform, a scan rate of 200 mV/s was used, resulting in a step size of 1.75 mV, step duration of 8.75 ms, 800 total recorded data points, and a ramp duration of 7 s. The peak current was estimated to be ~1 μA during 5-HT sensing, so the TIA resistance was set to 512 kΩ to maximize measurement accuracy. The generated waveform was confirmed by an oscilloscope (Tektronix, OR).

CFME Fabrication and Modifications

The surface of T-650 carbon fiber (Solvay, TX) was modified with Nafion-CNT and electrochemical treatment to improve its sensitivity and selectivity. A single fiber was inserted into a glass capillary with an inner diameter of 0.4 mm (A-M Systems, WA). The carbon fiber was sealed using epoxy and cut down to a 5 mm tip. Copper wire (30 AWG) was inserted into the glass capillary from the backside. A 0.5 mg/mL Nafion-CNT solution was sonicated for 30 min before each use to re-suspend the nanotubes. CFMEs were coated with the Nafion-CNT film by dip-coating and were air-dried for 30 minutes before use. Electrochemical treatment consisted of applying two repeated CV waveforms of 0 to +2.5 V and 0 to -1.5 V at a scan rate of 100 mV/s. The Nafion-CNT CFMEs were only modified with dip-coated Nafion-CNT and the Nafion-

CNT/EC CFMEs were modified with dip-coating Nafion-CNT, followed by electrochemical treatments.

Ag/AgCl Reference Electrode and Pt Counter Electrode Construction

The Ag/AgCl RE was fabricated by coating AgCl on a bare Ag wire (32 AWG, A-M Systems, WA). An Ag wire and Pt wire (36 AWG, A-M Systems, WA) were partially immersed (~1 cm) in 1 M KCl solution and connected to the WE and RE/CE of the benchtop VSP-300 potentiostat (BioLogic, France), respectively. A 0.15 mA current was applied to the WE to chloride the surface until a uniform AgCl coating was formed. Both Ag/AgCl RE and Pt CE were inserted into glass capillaries with a 1 cm tip extended.

Electrochemical Measurements

The portable potentiostat system was first compared to a VSP-300 benchtop potentiostat for CV sensing of 10 mM $K_3[Fe(CN)_6]$/ $K_4[Fe(CN)_6]$ with standard GCE as WE (CH Instruments, Austin, TX) , Ag/AgCl (3M KCl) as RE (CH Instruments, Austin, TX), and Pt as CE (CH Instruments, Austin, TX). The potential range was -1 to 1V with a scan rate of 100mV/s.

The portable potentiostat system was then compared to a VSP-300 benchtop potentiostat for CV sensing of 10 μM 5-HT with Nafion-CNT/EC CFMEs as WE, customized Ag/AgCl as RE, and Pt wire as CE. The potential range was -0.1 to 0.6 V with a scan rate of 200mV/s.

Finally, the portable potentiostat system with the customized three electrode system were tested in standard 5-HT solution for sensitivity, and then used to determine 5-HT in artificial urine samples. The potential range was -0.1 to 0.6 V with a scan rate of 200mV/s.

3.2.2 Comparing AD5941 Evaluation Board and Benchtop Potentiostat

The portable electrochemical sensing platform for 5-HT detection comprises a three-electrode system, an IC potentiostat, and a PC with software for data analysis (**Figure 3-8**). To evaluate its electrochemical performance, the potentiostat circuit and customized electrodes were compared to their standard counterparts, separately and integrated, to determine 5-HT sensitivity.

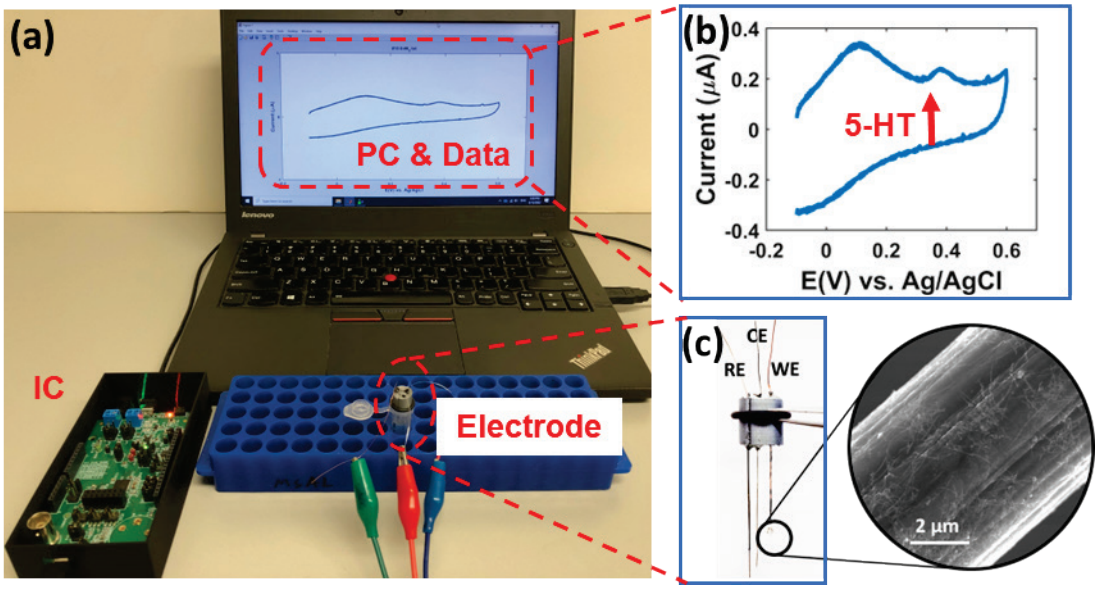

Figure 3-8 Photograph of the portable electrochemical 5-HT sensing platform, comprising PC, IC, and customized electrodes. (b) Software interface showing representative CV. (c) Customized three-electrode system, including Nafion-CNT/EC WE with SEM, Ag/AgCl RE, and Pt CE.

The portable AD5941 IC was first compared to a high-end VSP-300 benchtop potentiostat in 10 mM $K_3[Fe(CN)_6]/K_4[Fe(CN)_6]$ as a benchmark. **Figure 3-9a** compares the cyclic voltammograms that were recorded using a VSP-300 and AD5941 IC. The 5-HT Epas were observed to be 0.49 V for both instruments, while Ipas were 175 µA and 190 µA from the benchtop and portable potentiostats, respectively. Similar Epas and Ipas demonstrated the viability of using the portable IC for reliable CV measurements.

The surface-modified CFME with customized RE and CE were configured with portable electronics and used for 5-HT detection and their electrochemical performances were compared with a benchtop potentiostat (**Figure 3-9b**). Cyclic voltammograms of 10 µM 5-HT recorded by the benchtop and portable potentiostats had similar peak shapes, Epas (0.31 V for both), and Ipas (0.41 µA for the benchtop potentiostat, and 0.37 µA for the portable potentiostat) using customized electrodes.

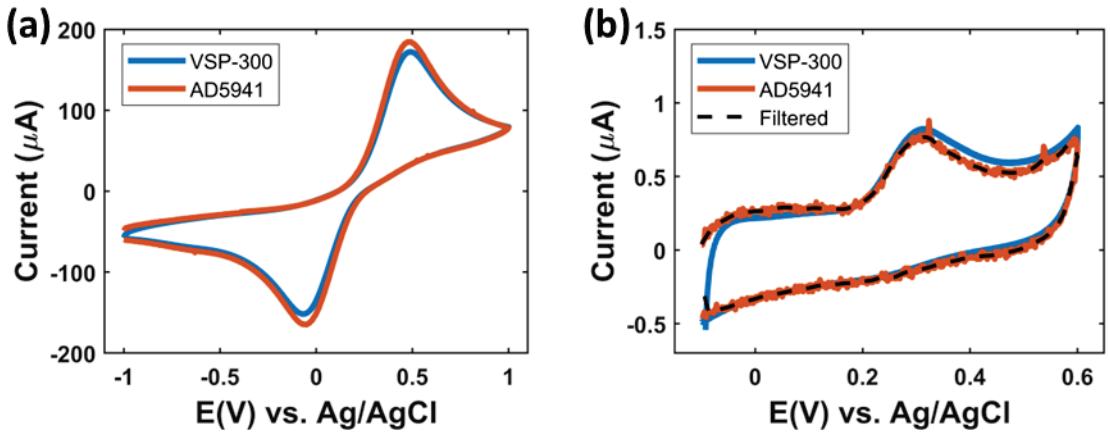

Figure 3-9 (a) Comparison of the AD5941 IC to a VSP-300 benchtop potentiostat for CV sensing of 10 mM $K_3[Fe(CN)_6]$/ $K_4[Fe(CN)_6]$. Potential range: -1 to 1 V. Scan rate: 100 mV/s. Standard glassy carbon as WE, Ag/AgCl (3M KCl) as RE, Pt as CE. (b) Cyclic voltammogram comparing the AD5941 and benchtop potentiostat in 10 µM 5-HT. Potential range: 0.1 to 0.6 V. Scan rate: 200 mV/s. Nafion-CNT/EC as WE, customized Ag/AgCl as RE, Pt as CE.

The sensitivity of the portable sensing platform system was also characterized. A calibration curve over 5-HT concentrations 0.1 – 10 µM (Figure 3-10) showed a linear range of 0.5 – 1.1 µM with a sensitivity of 0.074 µA/µM (R^2 = 0.9968), LOD of 140 nM, and LOQ of 420 nM. These results demonstrate the ability of the reported portable sensing system to reliably detect sub-micromolar 5-HT levels. The analytical characterization of this portable 5-HT sensing system in comparison with literature data is summarized in Table 3-1 [224]–[231]. Although other reports show superior performance with lower LODs, they require expensive (~ $10,000) and customized potentiostat hardware to generate faster scan rates and process large data sets to improve the LOD

[224]–[226]. This low-cost (~ $300), portable system shows an improved LOD compared to other portable systems for neurotransmitter detection, such as 5-HT and DA. Additionally, the performance of the proposed system is sufficient to detect 5-HT in urine samples (normal range between 0.27 and 1.65 µM) [232], thereby providing an alternative point-of-care solution.

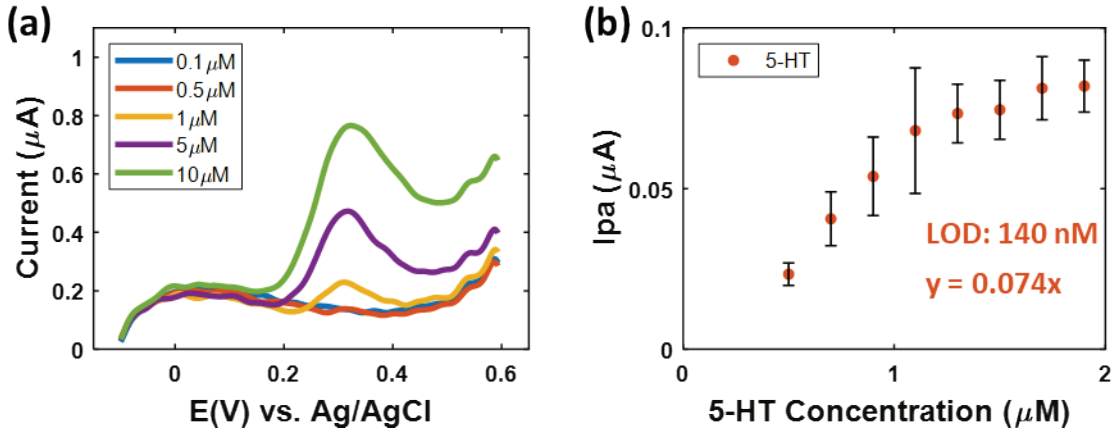

Figure 3-10 (a) Cyclic voltammograms of 5-HT concentrations (0.1 – 10 µM) using the portable system consisting of Nafion-CNT/EC and AD5941. [5-HT]: 0.1 µM (blue), 0.5 µM (orange), 1 µM (yellow), 5 µM (purple), and 10 µM (green). (b) Calibration curve of 5-HT with a linear range of 0.5 to 1.1 µM. Potential range: -0.1 to 0.6 V. Scan rate: 200 mV/s. Nafion-CNT/EC as WE, customized Ag/AgCl as RE, Pt as CE.

Table 3-2 Comparative table of benchtop and portable electrochemical equipment for 5-HT or dopamine detection.

Electrode Material	Target	Method	LOD	Run Time	Portable	Refs
Nafion CFME	5-HT	FSCV	2.4 nM	0.1 s	N	[224]
Nafion CFME	5-HT	FSCAV	1.6 nM	10 s	N	[225]
MWCNT-CS GCE	5-HT	DPV	50 nM	1 s	N	[226]
PEDOT:PSS/CS-G SPE	DA	DPV	290 nM	20 s	Y	[227]
Gr-AV	5-HT	CV	390 nM	60 s	Y	[228]
AuNPs/CNTs SPE	5-HT	CV, DPV	300 nM	70 s	Y	[229]
Nafion-CNT/EC CFME	5-HT	CV	140 nM	67 s	Y	This work

Abbreviations: MWCNT: multi-walled nanotube, CS: chitosan, GCE: glassy carbon electrode, PEDOT: poly(3,4-ethylenedioxythiophene), PSS: poly (styrene sulfonate), G: graphene, SPE: screen-printed electrode, Gr: graphite powder, AV: automotive varnish, AuNPs: gold nanoparticles.

3.2.3 Using AD5941 Evaluation Board for Urinary Serotonin Detection

5-HT is involved in a wide variety of physiological functions. The reference level for the urinary 5-HT test is 600 nM [233], and increased 5-HT levels in urine may confirm the diagnosis of 5-HT syndrome [47] or indicate the presence of a carcinoid tumor in the gastrointestinal tract [48]. This study investigated the applicability of the developed portable system for 5-HT detection in artificial urine, showcasing its application for point-of-care diagnostics.

The determination of 5-HT in artificial urine samples was investigated using CV on a Nafion-CNT/EC-based portable electrochemical sensing platform using the standard addition method. The CV responses to the direct addition of 5-HT (0.1 – 1 μM) in artificial urine were used to determine the recovery of 5-HT from artificial urine (**Figure 3-11**). While cyclic voltammograms recorded in artificial urine alone revealed no peak, when 5-HT was added, a well-defined anodic peak at +0.38 V was observed. The intensities of the peaks were correlated with 5-HT concentrations and increased with the successive addition of standard 5-HT solution into the artificial urine sample. 5-HT concentrations and their recovery rates were calculated based on the previously determined calibration curve. The spiked 5-HT concentrations were found to be between 0.3 μM to 1.0 μM, with recovery rates ranging from 74% to 105% (**Table 3-3**). The average recovery rate at low concentration exceeds 100%, which may be caused by variations between electrodes and interference molecules in the artificial urine samples, while the decrease in average recovery rate at higher concentrations may be caused by 5-HT fouling [170]. Overall, these recovery analysis results are similar to the recommended range (80% - 120%) [234], showing the proposed method

can be used efficiently for the determination of trace amounts of 5-HT directly from urine samples at low concentrations.

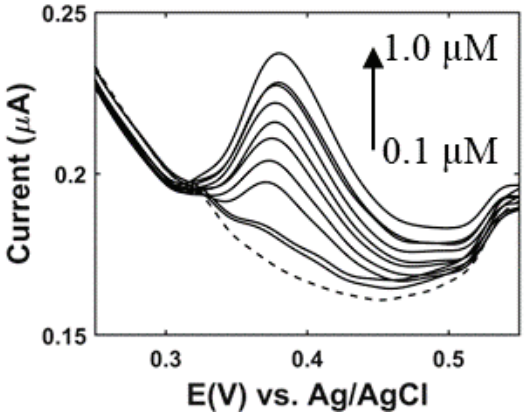

Figure 3-11 Cyclic voltammogram of 5-HT recorded at Nafion-CNT/EC-based portable sensing platform in artificial urine (dash line) with spiked 5-HT (solid line) at various concentrations (0.1 μM – 1.0 μM). Potential range: -0.1 to 0.6 V. Scan rate: 200 mV/s.

Table 3-3 Recovery rates and relative standard deviation (RSD) data obtained for 5-HT in artificial urine samples.

[5-HT] added (μM)	[5-HT] found (μM)	Average Recovery	RSD
0.30	0.30	100%	2.63%
0.40	0.42	105%	0.90%
0.50	0.48	96%	1.10%
0.60	0.57	95%	0.63%
0.70	0.62	89%	0.47%
0.80	0.67	84%	0.47%
0.90	0.68	76%	0.13%
1.00	0.74	74%	0.84%

3.3 Customized Potentiostat Circuit Board for Electrochemical Sensing

In this section, the functionality of the customized potentiostat system was characterized through CV measurements and 5-HT detection. The miniaturized potentiostat has compact dimensions, measuring only 12 mm wide and 36 mm long. Its flex-rigid PCB design allows for flexibility and adaptation to various designs. This compact electronic system holds great potential for applications in wearable systems for electrochemical sensing.

I developed an implantable biosensing system for 5-HT monitoring in freely moving crayfish. The sensor system features a previously fabricated CFME interfacing with the miniaturized potentiostat module with wired control and data acquisition. This biosensing system enables real-time monitoring of 5-HT dynamics *in vivo* and underwater through CV measurements in hemolymph without affecting crayfish behavior during its operation. By implanting electrodes into the crayfish heart, the device can be used to facilitate a better understanding of the relationship between 5-HT modulation and animal behavior (**Figure 3-12**).

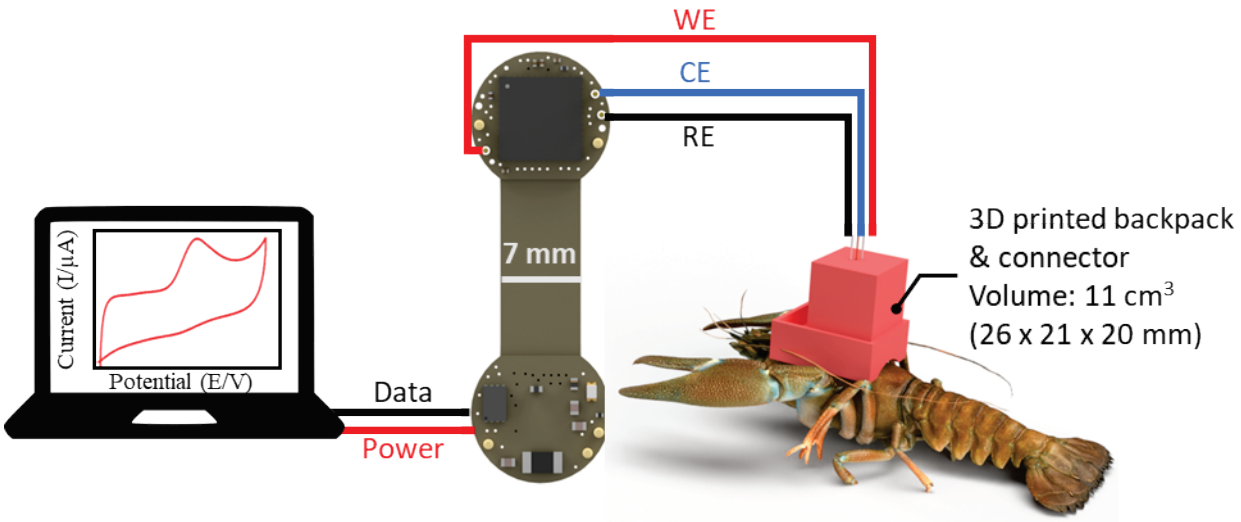

Figure 3-12 Schematic illustration of the implantable 5-HT sensing system on an adult crayfish, Electrode are implanted in the heart of crayfish for in vivo 5-HT measurements. Electrodes are connected to an external customized PCB potentiostat circuit for CV measurements which are analyzed by a PC.

3.3.1 Materials and Methods

Chemicals

Serotonin hydrochloride was purchased from Alfa Aesar (Haverhill, MA), and phosphate-buffered saline (PBS) powder was purchased from Research Products International (Mt Prospect, IL). 1X PBS (pH = 7.4) was made by dissolving PBS powder in DI water, which was used to prepare 5-HT solutions. Potassium ferricyanide (III) and potassium hexacyanoferrate (II) trihydrate were purchased from Sigma-Aldrich (St. Louis, MO). Single-walled CNTs functionalized with 1.0-3.0 atomic% carboxylic acid (P3-SWNT) were purchased from Carbon Solutions, Inc. (Riverside, CA). Nafion was purchased from Sigma-Aldrich (St. Louis, MO). A working Nafion solution was produced by diluting 5% stock solution in isopropanol. A 0.5 mg/mL Nafion-CNT solution was made with a suspension of CNT in 2.5% Nafion solution. Crayfish saline (202 mM NaCl, 5.37 mM KCl, 13.53 mM $CaCl_2 \cdot 2H_2O$, 2.6 mM $MgCl_2 \cdot 6H_2O$, and 2.4 mM HEPES) was prepared in DI water.

Electrode Fabrication

The three-electrode system consists of a surface-modified carbon fiber WE, Ag/AgCl RE, and Pt CE. The WE was assembled from T-650 carbon fibers (Solvay, TX) and modified using a Nafion-CNT solution and electrochemical activation to improve its sensitivity and selectivity. This procedure was previously reported in [235].

Generation of CV Waveforms

The customized potentiostat module was previously designed in [220], [236] and implemented with CV measurements in this work. The PCB pairs an AD5941 and BGM13S to control the sensor excitation voltages, capture and amplify the sensor signal, and transmit the data via a wired UART connection to a laptop. MATLAB was used for data processing and visualization.

CV waveforms were generated using this customized potentiostat module from user-provided measurement parameters, such as step size, step duration, number of data points, ramp duration, and TIA resistance. Due to limited DAC capabilities, most measurements are performed in a staircase manner that closely resembles a linear CV sweep. For 5-HT detection, the CV waveform was varied from −0.1 to +0.6 V with other parameters optimized for improved measurement sensitivity. Considering the hardware limitations such as the minimum step size and duration of the circuit, a scan rate of 100 mV/s was used, resulting in a step size of 3.5 mV, step duration of 35 ms, 400 total recorded data points, and a ramp duration of 14 s. The peak current was estimated to be below 1 μA during 5-HT sensing, so the TIA resistance was set to 512 kΩ to maximize measurement resolution. The generated waveform was confirmed using an oscilloscope (Tektronix, OR).

Electrochemical Measurements

The customized PCB potentiostat system was first compared to a VSP-300 benchtop potentiostat for CV sensing of 10 mM $K_3[Fe(CN)_6]$/ $K_4[Fe(CN)_6]$ with standard GCE as WE (CH Instruments, Austin, TX) , Ag/AgCl (3M KCl) as RE (CH Instruments, Austin, TX), and Pt as CE (CH Instruments, Austin, TX). The potential range was -1 to 1V with a scan rate of 100mV/s.

The customized PCB potentiostat system with the customized three-electrode system were tested in standard 5-HT solution for sensitivity, and then used to determine 5-HT in crayfish hemolymph *in vivo* with wired connection. The potential range was -0.1 to 0.6 V with a scan rate of 100mV/s.

Crayfish Experiment

In vivo experimentation was carried out on adult crayfish (Procambarus clarkii) purchased from commercial suppliers. Three electrodes were implanted in the crayfish heart under the dorsal

carapace to detect 5-HT levels in the hemolymph before the neurohormone is pumped into the arteries. Crayfish were anesthetized on ice for 15 min prior to surgery. Small incisions were then made through dorsal carapace of crayfish to expose the pericardial cavity. This opening provided access for the electrodes to be implanted directly into the heart. The backpack was glued onto the crayfish back above the surgery site. The alignment connector and electrodes were fixed onto the backpack and electrodes were implanted in the crayfish for CV measurements. For testing the performance of the system in vivo, the response currents of crayfish hemolymph were recorded at first as the baseline, then the internal 5-HT concentrations were changed by injecting 0.5 mL of 3 mM 5-HT into the crayfish ventral sinus cavity, and the variations of the response current were recorded continuously.

3.3.2 Comparing Customized Circuit Board and Benchtop Potentiostat

To compare the functionality of the customized PCB potentiostat with a benchtop potentiostat (VSP-300, BioLogic) as a benchmark, CV measurements were performed in 10 mM $K_3[Fe(CN)_6]/K_4[Fe(CN)_6]$ using standard GCE as WE, Ag/AgCl (3M KCl) as RE, and Pt as CE. CV measurements were performed in the potential range from -1 to 1 V at a scan rate of 100mV/s for both instruments (**Figure 3-13**). The Epas were observed to be +0.49 V for both instruments, while the Ipas were 175 μA and 190 μA from the benchtop and PCB potentiostat, respectively. By observing similar Epas and Ipas, the customized PCB potentiostat was validated for reliable CV measurements.

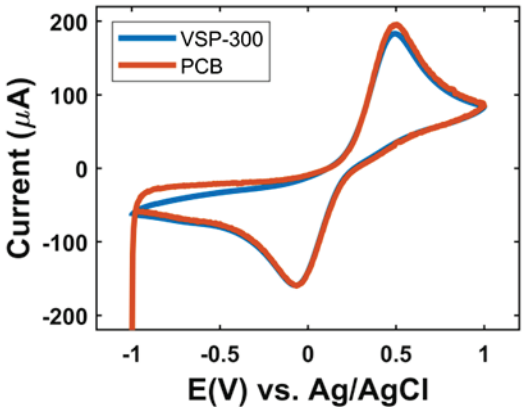

Figure 3-13 Comparison of the PCB to a VSP-300 benchtop potentiostat for CV sensing of 10 mM $K_3[Fe(CN)_6]$/ $K_4[Fe(CN)_6]$. Potential range: -1 to 1 V. Scan rate: 100 mV/s. Standard glassy carbon WE, Ag/AgCl (3M KCl) RE, and Pt CE were used.

3.3.3 Using Customized Circuit Board for Serotonin Detection

The fully assembled 5-HT sensing system underwent initial evaluation in a beaker containing known concentrations of 5-HT dissolved in a PBS solution. **Figure 3-14a** illustrates the voltammetric responses of the sensing system as the 5-HT concentrations increased from 0 µM to 2 µM. Notably, distinct oxidation peaks at 0.3 V were observed, indicating the oxidation of 5-HT on the electrode surface. The resulting Ipas values were measured, and a calibration curve was constructed to investigate the linearity between Ipas and 5-HT concentrations. **Figure 3-14b** demonstrates that the sensing system exhibited a linear response within the 0.4 to 1.2 µM range, with a sensitivity of 0.070 µA/µM (R^2=0.9735). It is worth mentioning that the microelectrode approaches its saturation when exposed to high 5-HT concentrations exceeding 1.6 µM.

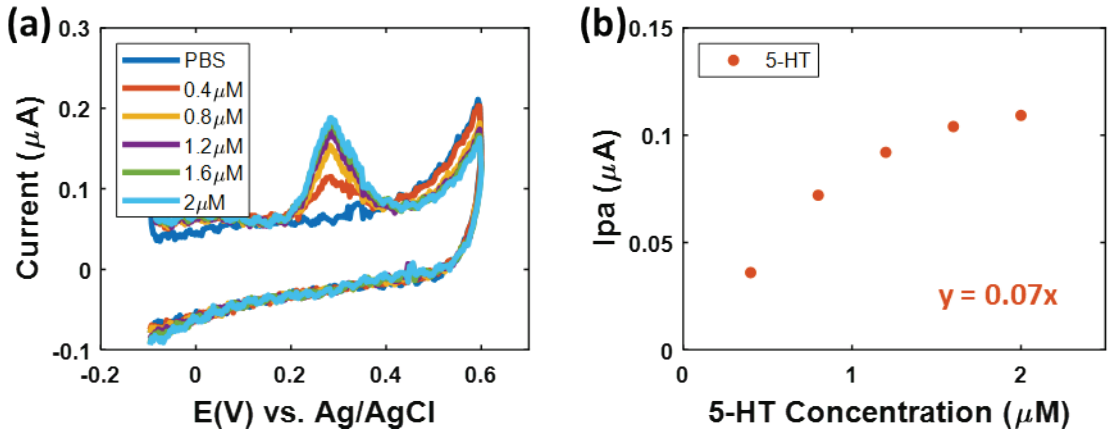

Figure 3-14 (a) Cyclic voltametric responses of the sensing system with 5-HT concentrations of 0 to 2 μM in 1X PBS. [5-HT]: 0 μM (blue), 0.4 μM (orange), 0.8 μM (yellow), 1.2 μM (purple), 1.6 μM (green), 2.0 μM (cyan). (b) The calibration curve of 5-HT. CV measurements were conducted with PCB potentiostat module and surface-modified CFME as WE, customized Ag/AgCl as RE, and Pt as CE. CVs were obtained in the potential range from -0.1 to 0.6 V at a scan rate of 100mV/s with 1 minute holding time between each measurement.

3.3.4 *In Vivo* Serotonin Detection with Customized Circuit Board

5-HT is a neurotransmitter that has been implicated in a wide range of physiological and behavioral processes in both vertebrates and invertebrates [237]. To better understand the role of 5-HT in modulating behavioral activation, studies have attempted to correlate 5-HT levels with specific behaviors. For this purpose, crayfish have traditionally been used as an animal model to investigate neuromodulation because of their well-characterized and quantifiable behaviors. Recent studies have implicated 5-HT in its regulation of stress and aggression in crayfish [65], [238]. For example, stressed crayfish exhibit increased levels of 5-HT in their nervous system. By injecting 5-HT into crayfish hemolymph, anxiety-like behavior can be induced [65] and an increase in aggression can be observed [239].

The standard techniques to determine 5-HT levels in biological samples include analytical methods such as micro-dialysis and high-performance liquid chromatography (HPLC) [26]. However, these offline techniques have limitations as they require repeated sample extraction from

animals, which can alter their behaviors, limit the temporal resolution of the target neurohormone, and make it difficult to correlate samples with related behaviors [240]. In crayfish, 5-HT is metabolized and/or uptaken by tissue, removing it from the hemolymph within a few minutes [241], highlighting the need for a real-time, *in vivo* neurochemical detection technique for monitoring of 5-HT signaling. Electrochemical detection is a simple, sensitive, and high-temporal resolution technique that has gained attention for detecting 5-HT and monitoring its dynamics in animals [242].

To evaluate the performance of integrated electrochemical sensing system *in vivo*, the device was attached to the crayfish carapace, and the electrodes were implanted directly into the heart (**Figure 3-15a**). To simulate an elevated 5-HT concentration near the electrode implantation site, injections of 0.5 mL crayfish saline (negative control) and 5-HT solution (0.5 mL of 3 mM), respectively, were administered through the ventral sinus cavity of the crayfish and circulated via the crayfish hemolymph [238]. During the experiment, CV cycles were recorded starting with the unaltered hemolymph (baseline), followed by four injection events that alternated between the crayfish saline and 5-HT solution. CV cycles were recorded after each injection event with a 1-minute holding time between injections.

Figure 3-15b compares the representative cyclic voltammograms before and after injection of 0.5 mL saline and 0.5 mL 3 mM 5-HT, respectively. The response current showed no peaks in unaltered hemolymph or the first saline injection in the crayfish, while a distinctive peak was observed at 0.3 V following 5-HT injection, which was in agreement with the beaker-level characterization.

Figure 3-15c summarizes the CV oxidation peaks resulting from continuous monitoring of crayfish hemolymph, depicting the dynamics of 5-HT levels before and after injection events.

Consistent with the findings described earlier, there was no observed increase in Ipa in hemolymph prior to any injections, and the administration of saline did not lead to an increase in Ipa. Immediately after the first 5-HT injection, the maximum measured Ipa was observed to be 82.9 nA and subsequently decreased until the next 5-HT injection event. The second 5-HT injection event also resulted in an increase in Ipa, with the maximum Ipa value occurring immediately after the injection (35.4 nA). A similar pattern showing a reduction of successive Ipa following the injection occurred, which was potentially due to 5-HT metabolism [241] and circulation through the heart [238]. However, the maximum Ipa value for the second 5-HT injection was noticeably diminished compared to the first injection, which is likely caused by reduced electrode sensitivity due to 5-HT fouling [33] and biofouling in hemolymph [243]. The saline injection administered between the two 5-HT injections overall did not elicit an increase in measured 5-HT signals. These findings demonstrate that the electrochemical sensing system can successfully monitor *in vivo* 5-HT dynamics in the hemolymph of freely-behaving crayfish.

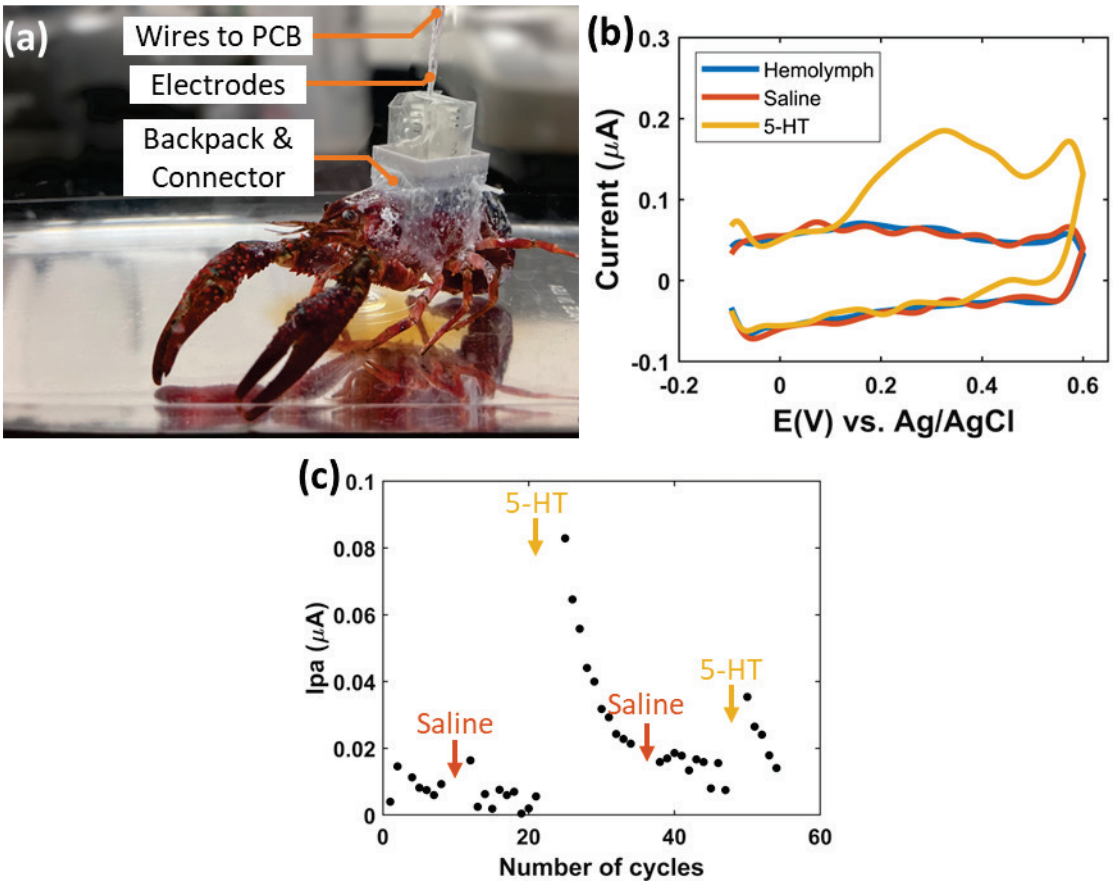

Figure 3-15 (a) Image of the implantable biosensing system on an adult crayfish. WE, CE, and RE are implanted into its heart and isolated using a 3D-printed backpack connector. (b) The cyclic voltammograms of in vivo hemolymph (blue), after separate injections of 0.5 mL saline (orange) and 0.5 mL 3 mM 5-HT (yellow). (c) Changes in oxidation peak current vs. time of multiple injection events: (1) 0.5 mL saline injection @9 min, (2) 0.5 mL 3 mM 5-HT injection @22 min, (3) 0.5 mL saline injection @35 min, and (4) 0.5 mL 3 mM 5-HT injection @48 min.

3.4 Chapter Summary

This chapter demonstrates the development of a miniaturized potentiostat circuit, from benchtop equipment, to a portable evaluation board, and finally to a PCB potentiostat. This work compares the CV functionality of each potentiostat in standard $Fe[(CN)_6]^{3-}$ and $Fe[(CN)_6]^{4-}$ electrochemical probes, as well as in standard 5-HT solution. The results suggest both the portable potentiostat and the PCB potentiostat exhibit similar performance compared to the benchtop device.

Section 3.2 describes the application of a portable electrochemical sensing platform for 5-HT detection in artificial biological fluid. Using previously developed CFMEs, the portable platform showed a LOD of 140 nM with a sensitivity of 74 nA/mM ($R^2 = 0.9968$) in the linear range of 0.5 to 1.1 μM, which is physiologically relevant. The applicability of the platform in artificial urine was investigated, revealing excellent recovery rates. The experimental results indicate that the portable 5-HT detection system, based on a Nafion–CNT/EC electrode, provides sensitive electrochemical 5-HT measurements as a low-cost, simple, rapid, and versatile POC solution to detect 5-HT.

Section 3.3 describes the application of an implantable biosensing system for continuous monitoring of injected 5-HT in circulated hemolymph in freely behaving crayfish. The system integrates the customized PCB potentiostat module and modified implantable microelectrodes with a 3D-printed package to enable electrochemical CV measurements. 5-HT detection capabilities were validated at the beaker-level with a sensitivity of 70 nA/μM in the linear range of 0.4 – 1.2 μM. This system also successfully achieved *in vivo* 5-HT detection in hemolymph through injections using the implantable device while the crayfish was unconstrained in an underwater environment.

Although *in vivo* monitoring of neurotransmitter dynamics has been achieved in this work, the sensing frequency was one measurement per minute. This sensing frequency is sufficient considering the half-life of increased 5-HT levels in the hemolymph, which is on the order of 10 minutes [244]. The transmission of neurotransmitters between neuron synapses occurs at the order of hundreds of milliseconds. Other electrochemical techniques can be implemented to improve the temporal resolution of 5-HT measurements. CA provides high temporal resolution but lacks selectivity, meaning that sensor modifications are needed to enhance selectivity. DPV can be used

as an alternative to CV. In DPV, short pulses of small amplitude are overlaid on a linear ramp. The current is measured before applying each pulse and at the end, enabling the calculation of the difference between the currents. The normal DPV process only requires a forward scan within the targeted potential window and takes only a few seconds, providing better time resolution. The DPV procedure effectively reduces the background current attributed to the DC ramp, resulting in a faradaic current that is mostly free from capacitive components. The major advantage of DPV lies in its low capacitive current, which leads to better sensitivity. Additionally, the use of small step sizes in DPV produces narrower voltammetric peaks, making it a preferred method for distinguishing analytes with similar oxidation potentials [245]. Consequently, DPV presents an effective approach for achieving improved time resolution, sensitivity, and selectivity compared to CV. The DPV function can be programmed and implemented using AD5941. The future work will involve implementing DPV measurements on the miniaturized potentiostat for 5-HT release event detection from intact *ex vivo* crayfish nerve cord to gain a better understanding of serotonergic modulation in the CNS.

Overall, both portable potentiostat and miniaturized potentiostat were implemented with CV measurements and exhibited similar electrochemical performance compared to the benchtop equipment. With previously developed CFMEs, the portable and miniaturized potentiostat circuits exhibited promising performance for the detection of 5-HT in different settings, including POC application for diagnosing 5-HT syndrome as well and monitoring 5-HT dynamics in animal models. Collectively, the portable and miniaturized potentiostat circuits offer a low-cost, sensitive, and rapid 5-HT sensing approach. These advancements have the potential for continuous 5-HT detection and monitoring, enabling further investigation into serotonergic modulation.

Chapter 4 Fully Integrated Wireless Device for Neurotransmitter Sensing in Freely Moving Animal

5-HT has been implicated in a wide range of physiological and behavioral process in both vertebrates and invertebrates [246], [247]. 5-HT is closely related to cognition, and more importantly, aggressive behaviors [247], [248]. Research also suggests the interaction between 5-HT and DA in regulating animal behaviors [249]. The current available analytical methods for quantifying detections of *in vivo* neurochemicals use tethered micro-dialysis probes [23], optical fibers [27], and electrochemical sensors [250], [251]. These techniques often require bulky and sophisticated equipment, and the wired connection limits their application for *in vivo* neurotransmitter detection in freely behaving animals. While there is a strong desire to integrate neurotransmitter detection into wirelessly operated devices for living animals, this area remains underdeveloped in current research. Quantifying and continuous monitoring of 5-HT dynamics and its interaction with DA in animals in real time would greatly benefit neuroscience research.

In this chapter, an untethered electrochemical sensing system for simultaneous monitoring of DA and 5-HT in freely moving crayfish was developed. The untethered wearable system features a CFME interfaced with a miniaturized potentiostat module with wireless control and data acquisition through Bluetooth connection. The device enables real-time monitoring of DA and 5-HT dynamics *in vivo* and underwater through CV measurements in hemolymph without affecting crayfish behavior during its operation. By implanting electrodes into the crayfish heart, the device can be used to facilitate a better understanding of the interaction between DA and 5-HT and their neuromodulation in animal behavior.

I give credit to Ta-wen Ho, who contributed significantly by performing the crayfish surgery. Dr. Jens Herberholz contributed to the discussion of 5-HT detection in crayfish.

4.1 Carbon Fiber Bundle Characterization

Previously, I have developed surface-modified CFMEs for sensitive and selective 5-HT measurements. However, because of the small size of the single fiber (7 μm diameter) being used as the substrate material, the microelectrodes are fragile, and suffered from mechanical failure during *in vivo* testing. In order to improve the mechanical reliability, multiple fiber bundles have been used as the substrate. The diameter of the fiber bundle is roughly 70 μm. The carbon fiber bundle microelectrodes were also treated electrochemically and coated by Nafion-CNT (EC/Nafion-CNT). The mechanical, optical, and electrochemical characterization results are demonstrated in this section. Specifically, mechanical properties, such as their resistance to bending and deformation, of the electrodes were evaluated. I also assessed their surface morphology using SEM and EDS analysis, and the electrochemical properties of the CFMEs were evaluated using electrochemical impedance spectroscopy (EIS) and CV. The results show that the EC/Nafion-CNT modification significantly improves the mechanical stability while still facilitating sensitive and selective sensing to 5-HT.

4.1.1 Materials and Methods

Carbon Fiber Bundle Electrode

The WE, referred to as Nafion-CNT/EC CFME, was constructed by utilizing T-650 carbon fibers from Solvay and modified with CNT containing Nafion solution. Additionally, electrochemical activation was employed to enhance the electrode's sensitivity. This procedure was slightly from a previously reported protocol [235]. Before processing, multiple fibers were inserted into a glass capillary with an inner diameter of 0.4 mm (A-M Systems, WA). The carbon fiber was sealed using epoxy by dipping in an 80 °C Epon 828 epoxy (Hexion, OH) and 14% m-

phenylenediamine hardener (Sigma Aldrich, MO) for 30 s to seal the fiber with the glass capillary, followed by dipping in acetone to remove excess epoxy on the tip area. Copper wire (30 AWG) was inserted into the glass capillary from the backside, providing electrical connections between the fiber strand and the electronics. The CFME was trimmed to a 5 mm tip and electrochemically treated via CV in phosphate buffered saline (1X PBS, containing 8g/L NaCl, 0.2 g/L KCl, 1.44 g/L Na_2HPO_4, and 0.24 g/L NaH_2PO_4, pH 7.4, Research Product International, IL) by applying a triangular wave from 0 to +2.5V and 0 to -1.5 V at a scan rate of 100 mV/s. The fibers were then dip-coated in 0.5 mg/mL of single-walled CNT (P3-SWNT, Carbon Solutions, CA) dispersed in a 2.5% Nafion solution and air-dried for 30 minutes before use. Standard Ag/AgCl (3M KCl) RE, and Pt CE were used in the modification process.

Optical and Electrochemical Surface Characterization

All SEM images and EDS analysis were acquired in the University of Maryland Nanocenter AIMlab using Tescan XEIA. The CFME samples were prepared and attached to a carbon tape for surface characterizations. The SEM images were recorded with an accelerating voltage of 2.0 kV and a working distance of approximately 5 mm.

The electrochemical characterization of the bare and EC/Nafion-CNT CFME was conducted using EIS and CV measurements performed by the VSP-300 benchtop potentiostat (BioLogic, France) in 10 mM $[Fe(CN)_6]^{3-}$/$[Fe(CN)_6]^{4-}$ in 0.1 M KCl solutions. The three-electrode system was used with a CFME as the WE, Ag/AgCl as RE (CH Instruments, Austin, TX) and Pt as CE (CH Instruments, Austin, TX). For the EIS measurements, the potential was set to 0 V and a frequency of 0.1 to 1 MHz. For the CV measurement, the potential ranges from -0.2 to 0.6 V with a scan rate of 100 mV/s.

Mechanical Strength Testing

Single fiber CFME (7 μm) and multifiber CFME (70 μm) were push down against a microbalance for deformation. The max force was recorded before break.

Electrochemical Testing for Serotonin and Dopamine Detection

DA (Sigma Aldrich, MO) and 5-HT (Alfa Aesar, MA) stock solutions were diluted to different concentrations with 1X PBS for detection in beaker. The electrochemical measurements were performed using either the benchtop potentiostat VSP-300 with standard RE/CE or miniaturized potentiostat described in Chapter 3 with customized RE/CE. CVs were obtained in the potential range from -0.1 to 0.6 V at a scan rate of 100 mV/s with a 1-minute holding time between each measurement.

4.1.2 Surface Morphology Characterization

The surface morphology of the surface-modified CFMEs was characterized using an SEM. As shown in **Figure 4-1a-b**, the bare carbon fibers have a smooth surface with striation, which is typical of the polyacrylonitrile (PAN) manufacturing process used to fabricate carbon fibers. After the surface modifications with electrochemical treatment followed by Nafion-CNT coating, the surface of the EC/Nafion-CNT becomes rougher with a dense coating of CNTs. The EDS analysis (**Figure 4-1c**) confirmed the presence of fluorine on the surface, which may be caused by the Nafion ($C_7HF_{13}O_5S \cdot C_2F_4$) coating.

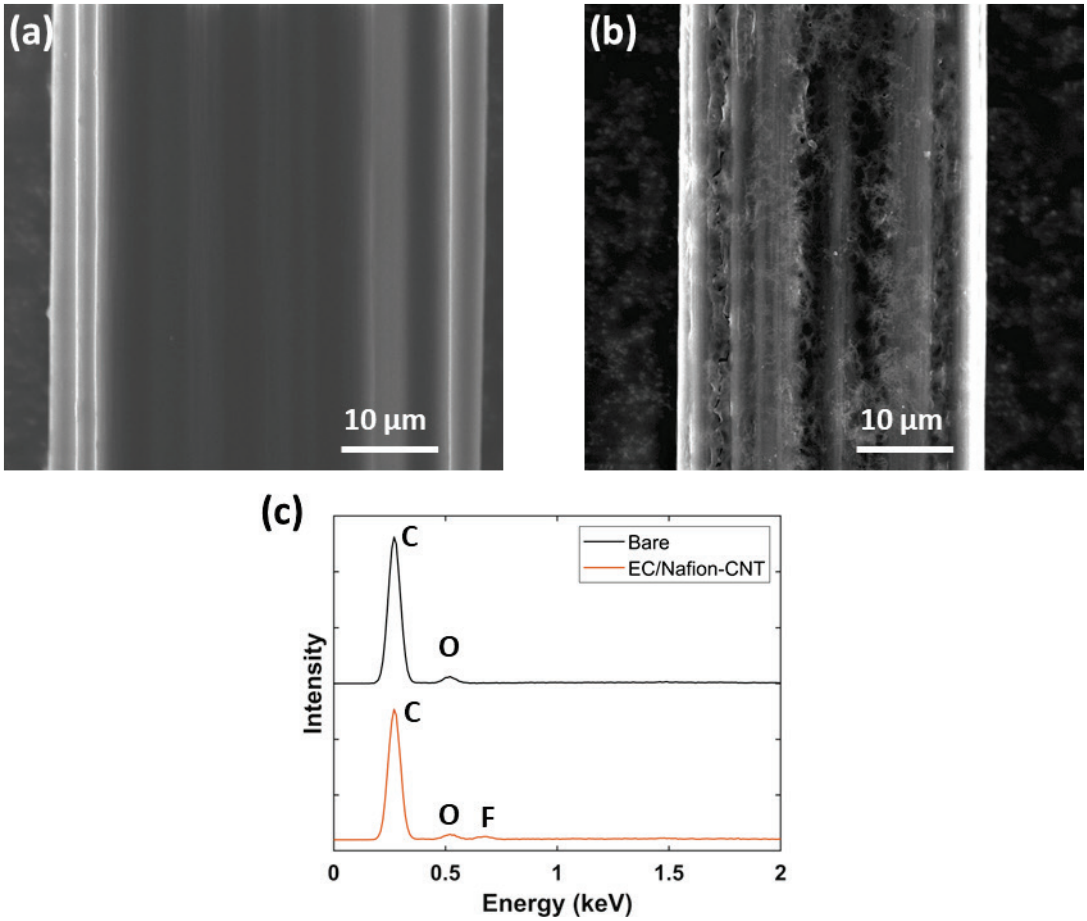

Figure 4-1 Surface characterization of CFMEs. SEM images of (a) bare and (b) EC/Nafion-CNT CFMEs. (c) EDS analysis of bare carbon fibers and EC/Nafion-CNT CFMEs.

The effect of electrochemical treatment and surface coating of Nafion-CNT thin film were investigated by EIS and CV for 10 mM $[Fe(CN)_6]^{3-}/[Fe(CN)_6]^{4-}$ in 0.1 M KCl solutions (**Figure 4-2**). **Figure 4-2a** shows the EIS spectra of the samples, by which the EC/Nafion-CNT electrode was confirmed to be more conductive than the bare electrode. This indicates that the treatment provides a better ionic transport between the electrolyte and active material, therefore promoting the progress of electrochemical redox activity. This is corroborated by the CV result, where no visible peaks were observed for bare electrode, proving that electrochemical oxidation and reduction of ferricyanide and ferrocyanide do not readily take place at bare CFME (**Figure 4-2b**).

Whereas the voltametric wave for the EC/Nafion-CNT electrode generated substantially larger current output, indicating faster electron-transfer reaction [252]. The Nafion-CNT thin film also has been shown to improve the selectivity [41] and fouling resistance [164]. It can be concluded that electrochemically treated electrodes have less electron transfer resistance, then promote the progress of electrochemical redox.

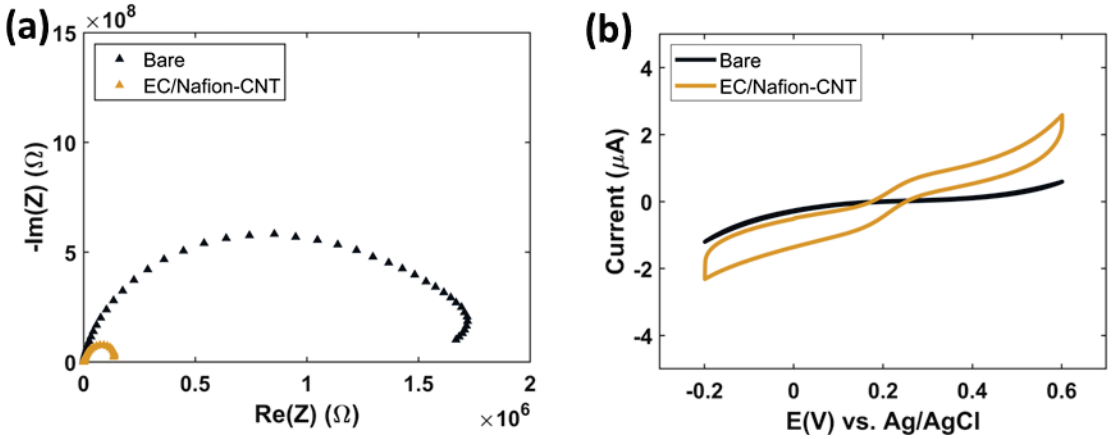

Figure 4-2 (a) EIS and (b) CV of bare and EC/Nafion-CNT CFMEs for 10 mM $[Fe(CN)_6]^{3-}$ /$[Fe(CN)_6]^{4-}$ in 0.1 M KCl solutions.

4.1.3 Improved Mechanical Strength

Previously developed CFMEs used a single carbon fiber as the substrate for sensitive and selective 5-HT measurements. However, due to the small size of the substrate material – a single fiber with a diameter of 7 µm – the microelectrodes were mechanically vulnerable and prone to failure during *in vivo* testing. To address this issue, multiple fiber bundles have been implemented as the substrate, with a diameter of approximately 70 µm.

Based on the mechanical characterizations, the single-fiber microelectrodes were only able to withstand up to 1 mN before breaking, while the multi-fiber microelectrodes remained intact even when a force of 30 mN was applied. These findings indicate that the multi-fiber microelectrodes

exhibit greater mechanical strength than their single-fiber counterparts, thereby demonstrating reliable measurement capabilities for *in vivo* applications.

4.1.4 Sensitivity

The surface-modified electrode for 5-HT and DA sensing are studied and presented in **Figure 4-3**. The EC/Nafion-CNT shows the Epas of DA and 5-HT were at 0.23 V and 0.4 V, respectively, and the Ipas of these analytes increased linearly with increased concentrations. The cyclic voltametric responses of EC/Nafion-CNT CFME to 5-HT concentrations are shown in **Figure 4-3a**. The calibration curve was plotted in **Figure 4-3b**, which shows the cyclic voltametric currents of 5-HT provided linear relationships with the 5-HT concentration in the range of 0.1 – 1 μM. The sensitivity was calculated to be 259.0 nA/μM. The LOD was 59.3 nM. **Figure 4-3c** shows the voltametric responses of the sensor to increasing DA concentration in the range of 0.1 – 1.5 μM. It is evidenced from **Figure 4-3d** that the sensor responds linearly to the DA concentrations in this range with a sensitivity of 129.9 nA/μM, and the LOD is 57.9 nM.

Furthermore, the EC/Nafion-CNT electrode was tested for simultaneous detection of 5-HT and DA (**Figure 4-3e**). Two well-defined oxidation peaks were observed, and their Epas remain unchanged. The voltametric Ipas of 5-HT and DA increased linearly with their concentration in the range of 0.1 – 1 μM. The sensitivity of 5-HT and DA were calculated to be 200.0 nA/μM and 68.1 nA/μM, with LOD of 44.0 nM and 67.7 nM, respectively (**Figure 4-3f**). These results indicate that clear simultaneous determination of 5-HT and DA was achieved using the EC/Nafion-CNT with high sensitivity.

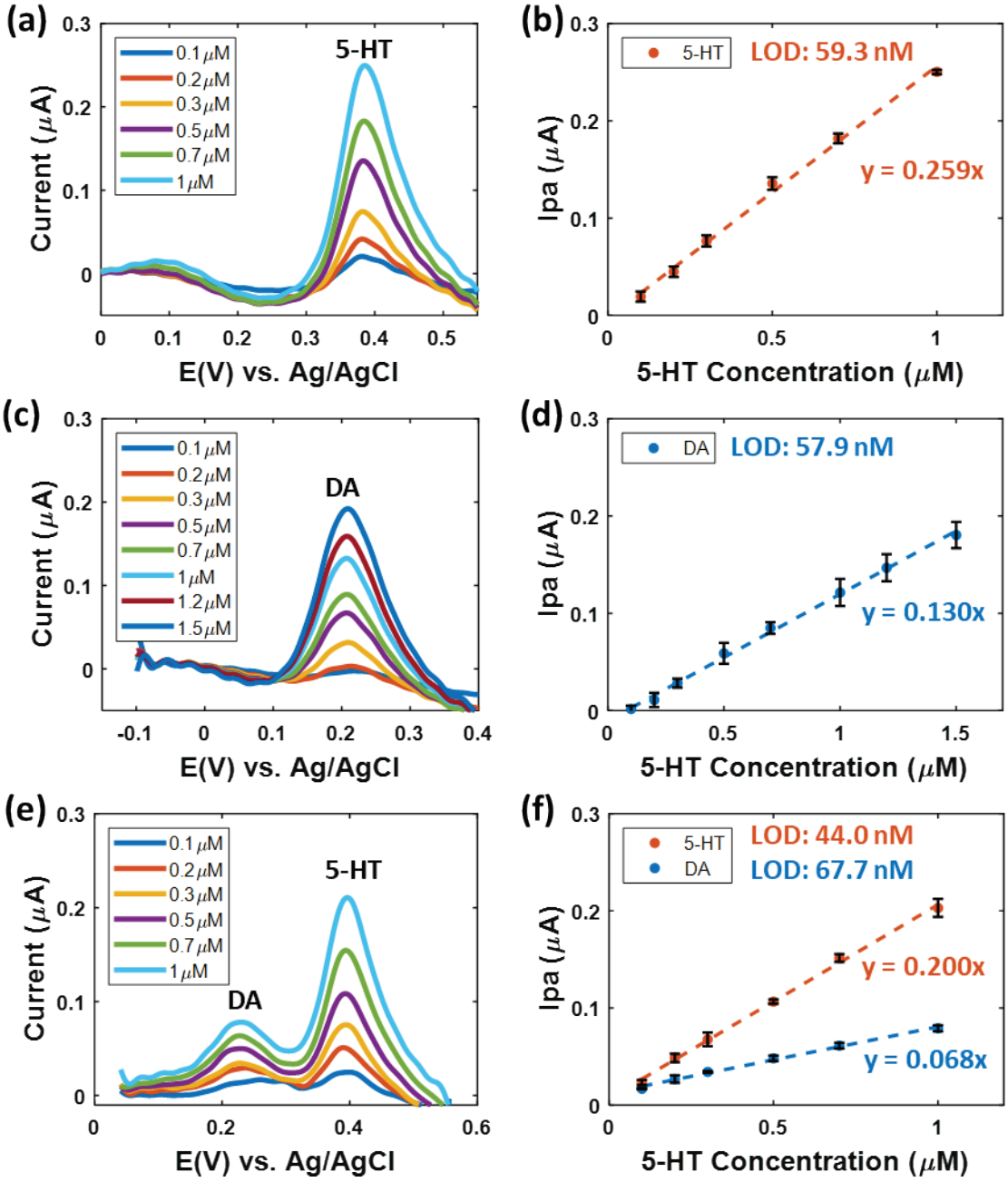

Figure 4-3 Sensitivity of EC/Nafion-CNT CFME for 5-HT and DA detection. (a) Representative CV curves within the linear range (0.1 to 1 μM) for 5-HT detection. (b) Calibration curves of 5-HT. (c) Representative CV curves within the linear range (0.1 to 1.5 μM) for DA detection. (b) Calibration curves of DA. (d) Representative CV curves within the linear range (0.1 to 1 μM) for 5-HT and DA detection. (b) Calibration curves of 5-HTand DA. All experiments were performed at the scan rate of 100 mV/s, with potential range from -0.1 to 0.6 V. Error bars denote standard error.

4.1.5 Selectivity

Accurate detection of DA and 5-HT *in vivo* is hindered by interference with high concentrations of electroactive molecules. To explore the selectivity of the sensor between DA, 5-HT and other possible interferential molecules in crayfish, CV measurements of 1 μM DA and 1 μM 5-HT were performed in the absence and presence of 20 μM UA, AA, 5-HIAA, OCT, and ADN. **Figure 4-4** illustrates that a 20-fold concentration of UA, AA, 5-HIAA, OCT, and ADN did not significantly influence the detection of DA and 5-HT, the results were within a 10% difference.

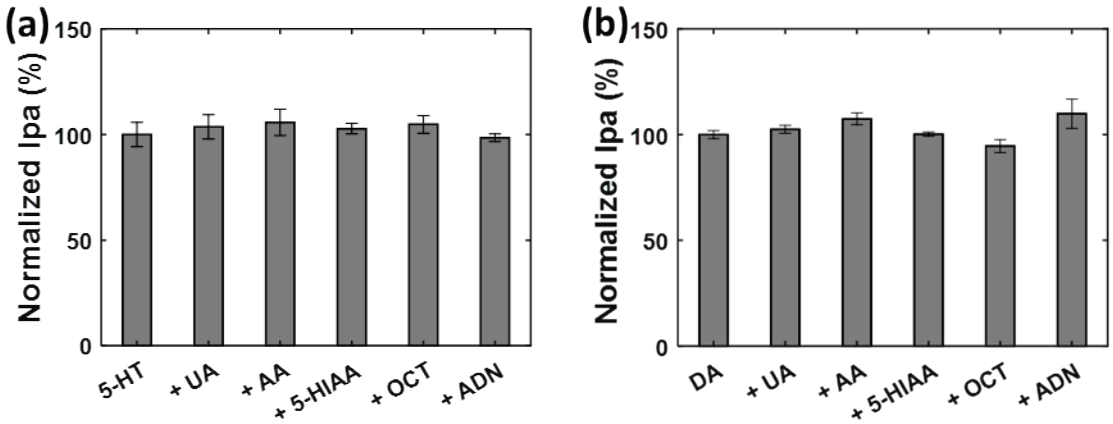

Figure 4-4 (a) The interference response of the EC/Nafion-CNT for the detection of 1.0 μM 5-HT in the presence of 20 μM UA, AA, 5-HIAA, OCT, and ADN. The oxidation peak currents are normalized to 1 μM 5-HT (n = 3). (b) The interference response of the EC/Nafion-CNT for the detection of 1.0 μM DA in the presence of 20 μM UA, AA, 5-HIAA, OCT, and ADN. The oxidation peak currents are normalized to 1 μM DA (n = 3).

4.1.6 Fouling Resistance

The stability of the CFME was tested by recording the response currents of electrode in 1 μM DA and 5-HT in PBS for 30 continuous cycles at 1 cycle per minute (**Figure 4-5**). The result indicated the current responses after 30 cycles were 107% and 85% of the initial current response for DA and 5-HT, respectively. The results demonstrate that the EC/Nafion-CNT CFMEs, with high sensitivity and selectivity, may have promising applications in electrochemical detection. The experimental results performed in beaker clearly demonstrate the utility of applying the

EC/Nafion-CNT electrode for simultaneous detection DA and 5-HT with high sensitivity, selectivity and stability.

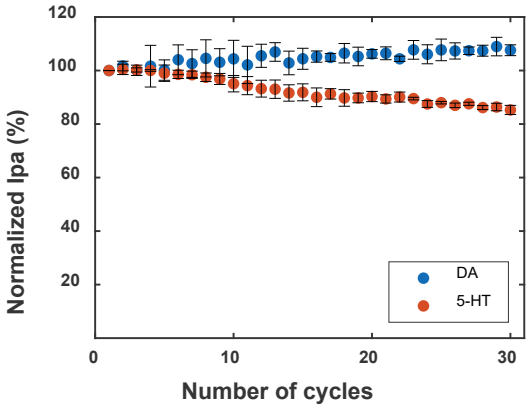

Figure 4-5 The oxidation peak currents of the EC/Nafion-CNT recoded in 1 μM DA and 1 μM 5-HT over 30 consecutive measurements. The oxidation peak currents are normalized to the value for the initial cycle (n = 3).

4.2 System Design and Integration

The overall wireless electrochemical DA and 5-HT monitoring system consisted of customized three-electrode configuration, flexible-rigid potentiostat module, and 3D printed package (**Figure 4-6**). Here, 3D printing technology was used for rapid prototyping of a wearable electrode package to attach to the crayfish. The 3D-printed package consists of two components: (i) an alignment connector printed with clear resin using digital light processing (DLP) (M50, CADWorks3D) to hold the electrodes and provide electrical connection between the electrodes and the PCB potentiostat, and (ii) an enclosure printed with PLA (Polylactic acid) using fused filament fabrication (FFF) (MK3S+, Prusa) to provide an interface with the crayfish. A small cutout (3 × 3 mm) on the enclosure allows the sensor electrodes to access the attached crayfish. A single 3 V coin cell lithium battery (2L76, Energizer, USA) powered the entire waterproof device, which is

capable of monitoring DA and 5-HT levels in freely behaving crayfish underwater and transmitting the data wirelessly to a smartphone.

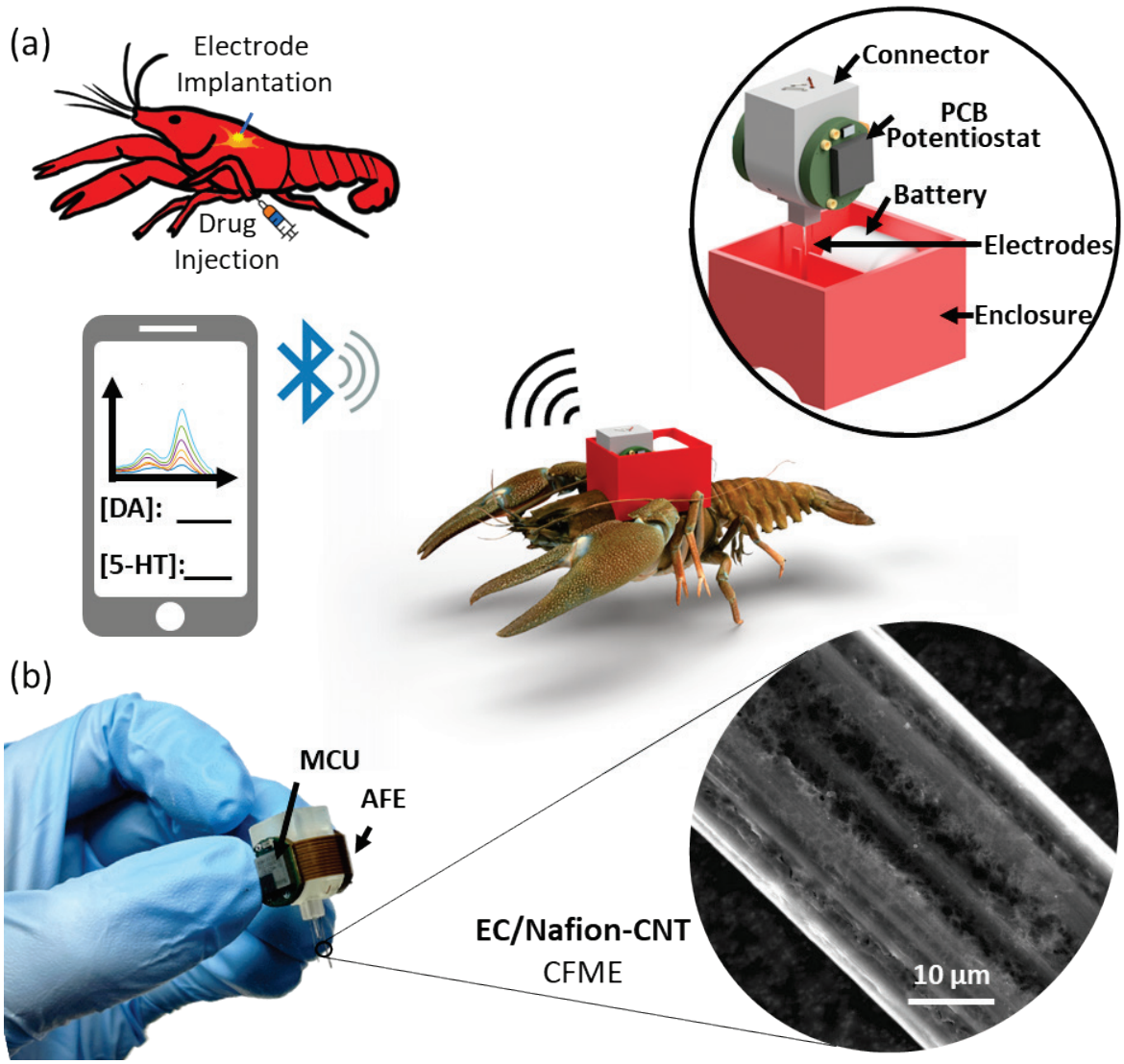

Figure 4-6 (a) Schematic illustrations depict the electrochemical sensing device and its capabilities for wireless simultaneous detection of DA and 5-HT. The CFME is implanted in the heart of a crayfish, while the drug is injected into the crayfish's ventral sinus cavity. (b) A photograph shows the integrated device hardware with a customized PCB, a 3D printed connector, and implantable electrodes. An SEM image of the CFME displays the surface-modified EC/Nafion-CNT CFME.

4.2.1 3D Printed Alignment Connector and Packaging

To facilitate the electrical connection between the PCB electronics and electrodes, an alignment connector was designed using Autodesk Inventor and fabricated using a DLP printer (M50, CADWorks3D) with clear microfluidics resin (V7.0a, CADWorks3D). The connector features three vertical channels in the center to hold glass capillaries with WE, RE, and CE. The extended metal wire from each electrode is threaded back into the connector and contacted with the corresponding pins on the PCB electronics. The schematic of the CAD design is shown in **Figure 4-7a**. The use of microfluidics resin was chosen for its compatibility with the glass capillaries and its high-resolution printing capabilities.

The enclosure for our device was printed using a FFF printer (MK3S+, Prusa, Czech Republic), with PLA filament material. PLA is known to be biodegradable and biocompatible, making it a suitable choice for our application. The enclosure provides housing for the connector, microelectrodes, and battery, as well as a contoured surface to interface with the crayfish (**Figure 4-7b**). The curvature on the bottom of the enclosure has a radius of 16 mm, which was designed to fit the shape of the crayfish carapace for physical attachment. A small cutout (3 × 3 mm) on the enclosure base allows the sensor electrodes to access the attached crayfish. The overall dimensions of the enclosure are 26 × 21 × 16.5 mm. The use of PLA material and an FFF printer allowed us to produce a cost-effective and customizable enclosure for our device.

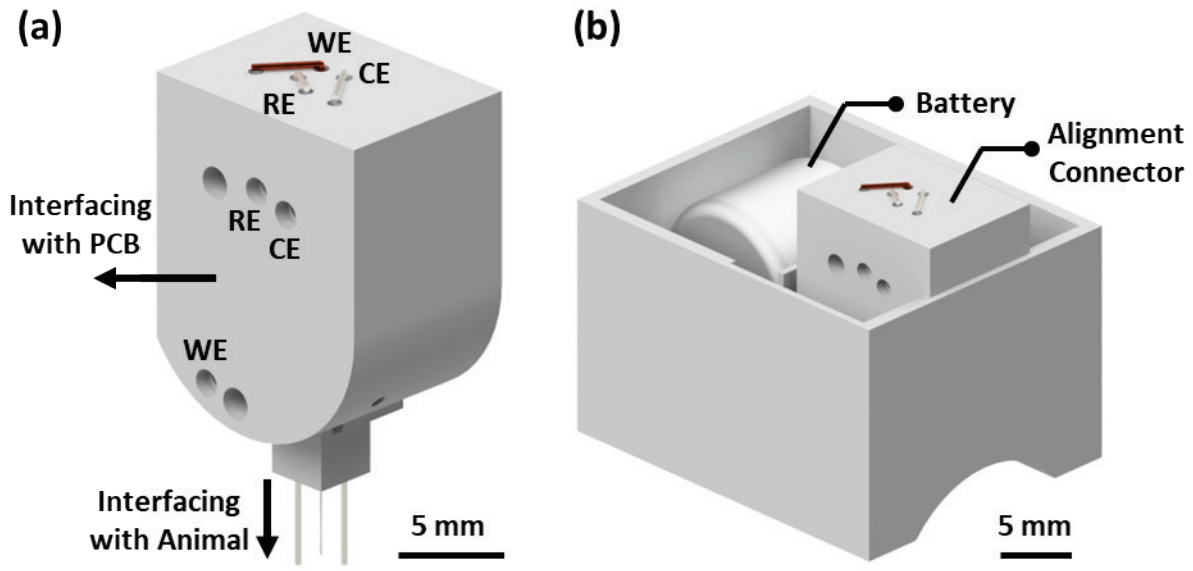

Figure 4-7 The CAD design of (a) DLP printed alignment connector for electrical connection between microelectrodes and PCB electronics, and (b)FFF printed device enclosure to house battery and alignment connector.

4.2.2 Wireless Communication Implementation

The wireless communication function was implemented on the BLE-MCU for wireless control and data output. With the Bluetooth 5 connectivity, the device can pair with a smartphone, and the command can be written to the MCU. Similarly, the measured signal can be transmitted to the smartphone in real time for analysis.

4.2.3 System Integration

The WE, RE, and CE were fabricated as described above. The glass capillaries were cut to 15 mm so that their length matched the height of the connector. The microelectrodes were pushed into the vertical channels in the connector, with all the top surfaces at the same level and the electrode tips extended out. The metal wire of each electrode was threaded back to the 3D printed connector. Connector pins were then pushed into the 3D printed connector to make electrical

connections with the microelectrodes. The electrode probes from the PCB electronics module were pushed into the connector pins for electrical contact and to fix their position. The PCB module was bent around the alignment connector and then lowered into the enclosure, with the electrodes extended from the bottom opening. The power wires of the PCB were soldered to the 2L76 battery for power supply. A FFF printed cap was used to fully encapsulate the whole device, and epoxy was used to seal the gap between printed parts to ensure water resistance. The system integration process is summarized in **Figure 4-8a**. **Figure 4-8b** shows an image of assembled device.

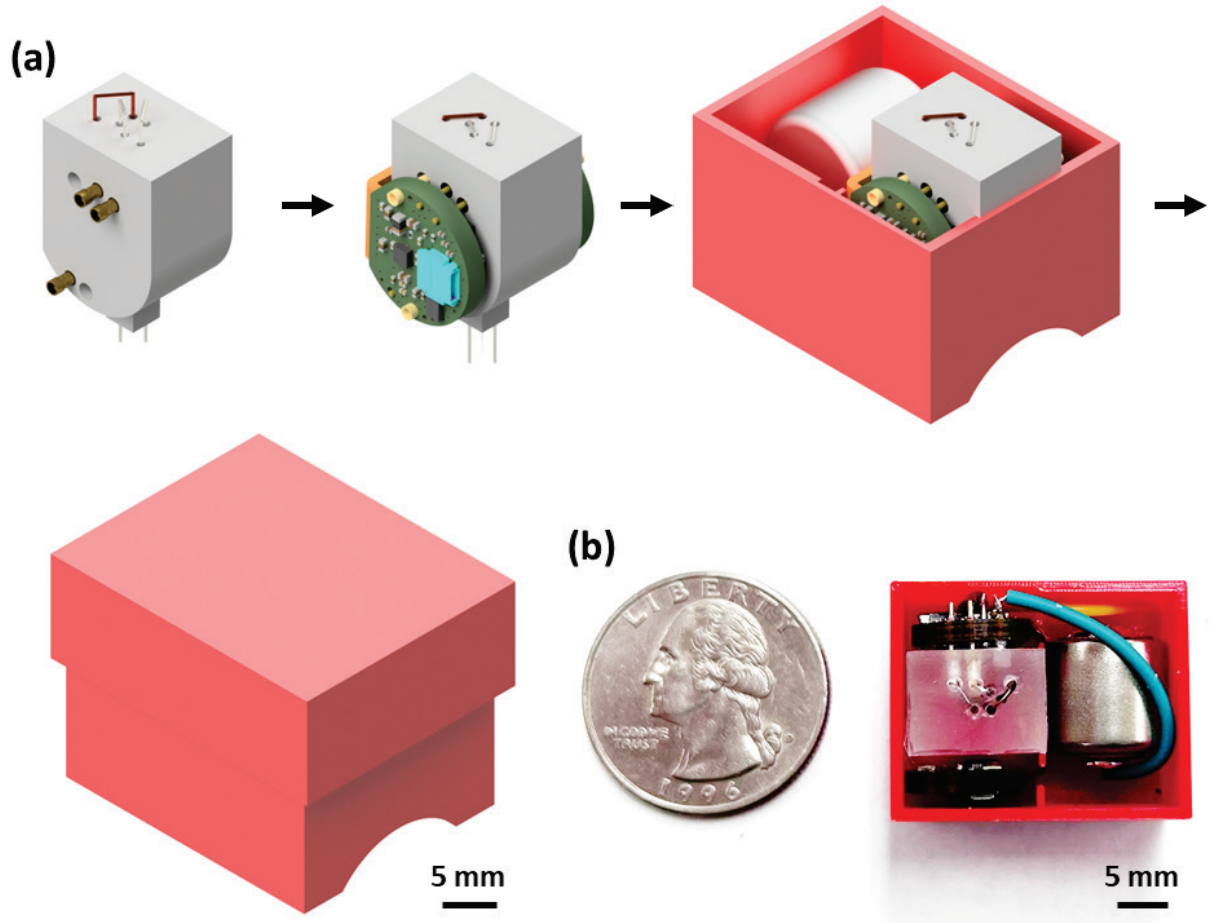

Figure 4-8 (a) Assembly process flow and (b) Image of assembled device.

4.3 Fully Integrated Device for Neurotransmitter Monitoring

5-HT is involved in a wide range of physiological and behavioral process [246]–[248]. Research also suggests the interaction between 5-HT and DA in regulating animal behaviors [249]. A number of studies indicate that 5-HT and DA systems interact closely at a basic neurophysiological level [253]–[255], and that impairment of the serotonin system function can lead to dysregulation of the DA system [249], [256].

Crayfish present an ideal model system to investigate the neurochemistry underlying neurobehavioral changes as their behaviors are well-characterized and quantifiable. In crayfish, injections of 5-HT into the circulatory system (hemolymph) can promote aggression and anxiety-like behavior [65], [238], [241], [257]. However, injections of DA resulted in an opposing effect on agonistic and phototactic behaviors as those seen with 5-HT [246], [258]. The underlying mechanisms remain poorly understood and require further investigation. One reason for this critical gap in knowledge is the lack of miniaturized technology to achieve real-time, wireless monitoring of neurotransmitter dynamics in freely behaving animals.

In this section, the performance of developed fully integrated device for simultaneous detection of both 5-HT and DA was verified by beaker level testing in comparison to the result obtained from benchtop equipment. The sensitivity of the device for 5-HT, DA and codetection were determined. The device was also being used for *in vivo* monitoring of 5-HT and DA dynamics simultaneously after injection events in freely moving crayfish.

4.3.1 Materials and Methods

Beaker Level Device Testing

DA (Sigma Aldrich, MO) and 5-HT (Alfa Aesar, MA) stock solutions was diluted to different concentrations with 1X PBS for beaker level characterizations. The electrochemical measurements were performed using either benchtop potentiostat VSP-300 with standard RE/CE or using PCB potentiostat module with customized RE/CE. CVs were obtained in the potential range from -0.1 to 0.6 V at a scan rate of 100mV/s with 1 minute holding time between each measurement.

The three-electrode electrochemical setup comprises a WE made of carbon fiber as previously described. The Ag/AgCl RE was fabricated by electrodepositing AgCl onto an Ag wire (A-M Systems, WA) in 3M KCl solution. A constant current bias of 0.15 mA was applied until a uniform AgCl coating was observed. The Pt wire CE was used as purchased (A-M Systems, WA).

Simultaneous *In Vivo* Detection of DA and 5-HT

In vivo experimentation was carried out on wild-caught adult red swamp crayfish (Procambarus clarkii) purchased from a commercial supplier (Niles Biological, CA). Crayfish were housed in aquarium tanks in a 21°C, 12hr/12hr light/dark cycle-controlled aquarium room and were fed ad libitum (an average of 2 pellets per animal) with formula one pellets (Ocean Nutrition, CA) twice a week. Crayfish with intact claws and no sign of body injury were anesthetized on ice for at least 15 minutes prior to surgery. Small incisions were then made through the dorsal carapace of the crayfish to expose the pericardial cavity, allowing direct implantation of electrodes into the heart. By injecting a drug into the ventral sinus cavity of crayfish, an animal with an open circulatory system, the drug enters the hemolymph, is being taken up by the heart and pumped into arteries. This allows detection of the drugs by the implanted electrode.

The device was glued onto the crayfish back, above the surgery site, and electrodes were implanted in the crayfish for CV measurements. The potential ranged from -0.1 to 0.6 V with a scan rate of 100 mV/s and 1 minute accumulation time. To test the system performance *in vivo*, the response currents of the crayfish hemolymph were initially recorded as the baseline. Then, the internal DA and 5-HT concentrations were changed by injecting the neurotransmitters into the animals, and the variations in the response current were continuously recorded.

4.3.2 Fully Integrated Device for In Vitro Testing

The sensitivity of the fully integrated electrochemical sensing system was tested in beaker. As described in the previous section, the overall system design was very small with a dimension of 2.8 cm × 2.3 cm, consisting of a customized three-electrode system, an PCB potentiostat, and a battery. To evaluate its electrochemical performance, the electrochemical system was compared to the benchtop potentiostat with standard RE/CE. Cyclic voltametric responses of the electrochemical device to DA and/or 5-HT in PBS were recorded on the phone application through BLE wireless data transmission and plotted in MATLAB. **Figure 4-9a** compares the cyclic voltammograms of 1 μM 5-HT that were recorded using a VSP-300 and our device. The Epas for 5-HT were observed to be 0.43 V using VSP-300, compared to 0.32 V recorded by the integrated system. The Ipas were measured as 122 nA and 118 nA from the benchtop and the device, respectively. Similarly, the cyclic voltammograms of 1 μM DA shows the Epa was 0.24 V from VSP-300 and 0.15 V using the developed device (**Figure 4-9b**). The Ipas were measured to be 120 nA for both setups. While the comparison demonstrates our sensing device had very similar Ipas, the Epa was shifted to a lower potential. The constant potential peak shift is likely due to the

difference in RE potentials between the commercial Ag/AgCl (3M KCl) RE and our customized Ag/AgCl RE.

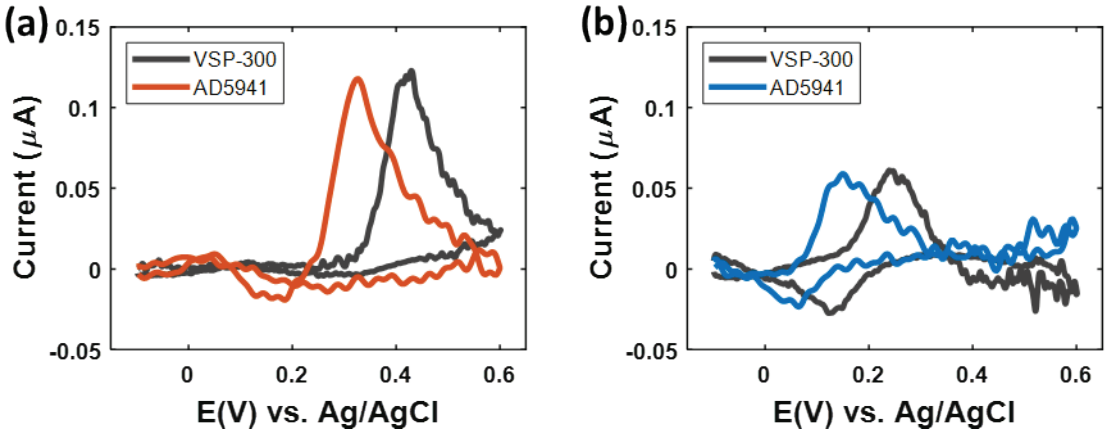

Figure 4-9 (a) Background subtracted cyclic voltammogram comparing the benchtop potentiostat and the electrochemical sensing system in (a) 1 μM 5-HT and (b) 1 μM DA. Potential range: -0.1 to 0.6 V. Scan rate: 100 mV/s.

Cyclic voltametric responses of the electrochemical device to the increasing 5-HT concentration are shown in **Figure 4-10ab**. The sensitivity was calculated to be 159.1 nA/μM with a LOD of 65.9 nM in the linear range of 0.1 – 1.0 μM. **Figure 4-10cd** shows the voltametric response of our electrochemical device for DA detection, providing a linear relationship in the range of 0.1 – 1.2 μM. The sensitivity was calculated to be 94.8 nA/μM with a LOD of 128.8 nM. The electrochemical system was also tested for simultaneous detection of DA and 5-HT in the range of 0.1 – 1.0 μM, showing a sensitivity of 133.0 nA/μM with a LOD of 112.9 nM for 5-HT and a sensitivity of 48.4 nA/μM with a LOD of 130.6 nM for DA.

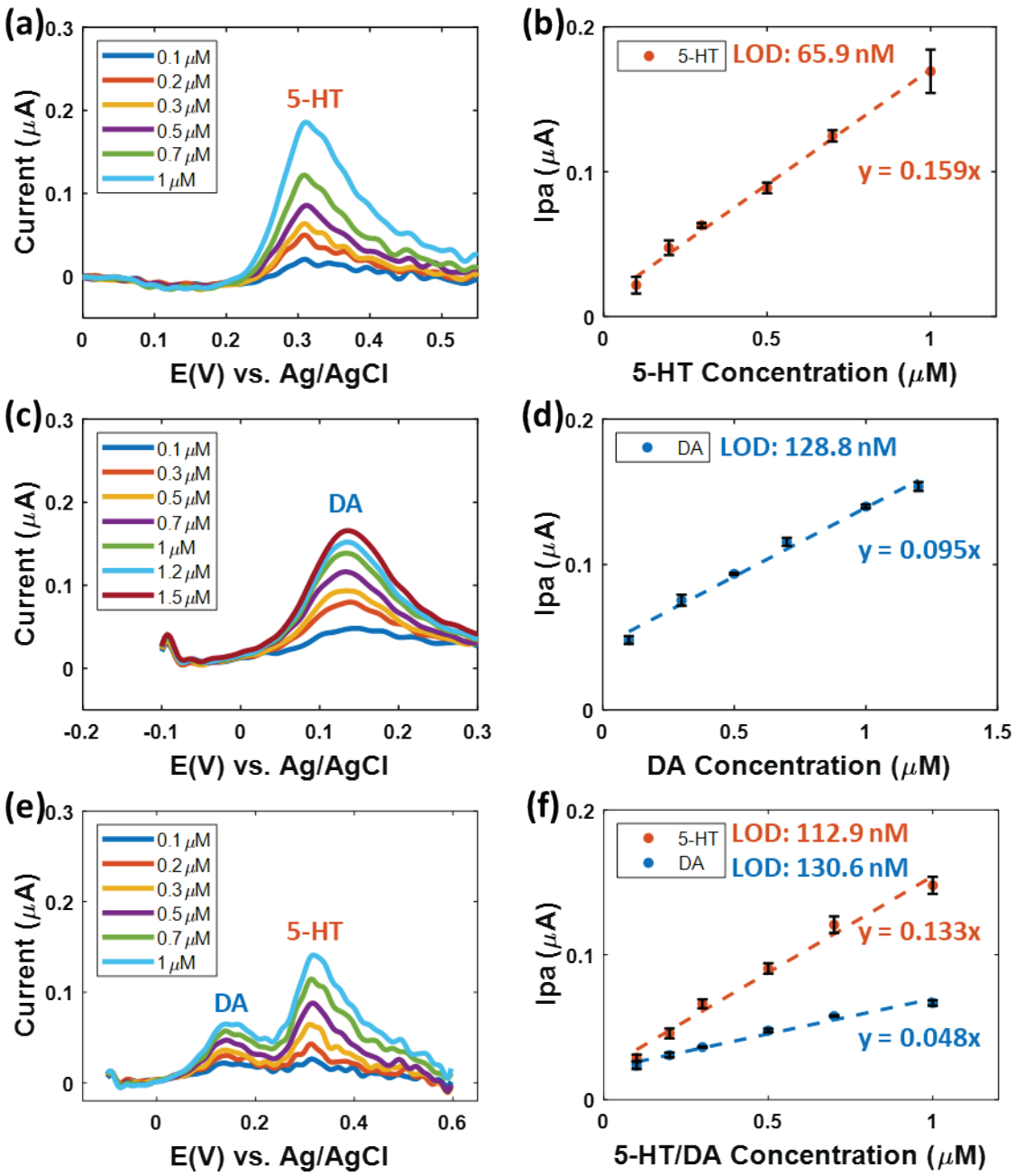

Figure 4-10 (a) Background subtracted voltametric response and calibration curve of the sensing system with 5-HT concentrations of 0.1 – 1.0 μM in 1X PBS. (b) The calibration curve of 5-HT, R^2 = 0.9943.(c) Background subtracted voltametric response and calibration curve of the sensing system with DA concentrations of 0.1 – 1.2 μM in 1X PBS. (d) The calibration curve of DA, R^2=0.9890. (e) Background subtracted voltametric response and calibration curve of the sensing system with DA and 5-HT concentrations of 0.1 – 1.0 μM in 1X PBS. (f) The calibration curve of DA (R^2=0.9804) and 5-HT (R^2=0.9853).

The analytical characterization of this wireless DA and 5-HT sensing system in comparison with other reported devices are summarized in **Table 4-1**. This reported device showed the ability to detect multiple neurotransmitters simultaneously with similar LODs compared to previously reported work. Although the weight is slightly heavier, which is mainly due to the waterproof design and battery required for the BLE communication. The BLE communication is more favorable than infrared (IR), as it does not require direct line-of-sight between devices, has longer communication range, and can be operated in a more complex environment.

Table 4-1 Comparative table of in vivo neurotransmitter sensing device.

Analytes	Technique	Wireless	Weigh	LOD	Ref
DA	CA	Yes, RF	2 g	100 nM	[31]
DA	CA	Yes, IR	49 mg	300 nM	[142]
DA	FSCV	Yes, RF	35 g	50 nM	[157]
DA and 5-HT	CV	Yes, BLE	7.8 g	152.4 nM (DA) 51.6 nM (5-HT)	My work

4.3.3 Monitoring *In Vivo* Neurotransmitter Levels in Freely Behaving Animals

In this section, the untethered electrochemical sensing system for simultaneous monitoring of DA and 5-HT was tested in freely moving crayfish. The untethered wearable system features a CFME interfaced with a miniaturized potentiostat module with wireless control and data acquisition through Bluetooth connection. The device enables real-time monitoring of DA and 5-HT dynamics *in viv*o and underwater through CV measurements in hemolymph without affecting crayfish behavior during its operation. By implanting electrodes into the crayfish heart, the device

can be used to facilitate a better understanding of the interaction between DA and 5-HT and their neuromodulation in animal behavior.

The performance of the wireless electrochemical sensing system was further verified through simultaneous *in vivo* detection of DA and 5-HT in crayfish. The device was attached to the crayfish carapace, with the electrodes implanted directly under the dorsal carapace into the heart to continuously monitor the response currents to DA and 5-HT in the crayfish hemolymph (**Figure 4-11a**). The total weight of the device was 7.8 g, which was designed to be neutrally buoyant and waterproof to minimize its impact on animal behavior in water. The device was first characterized with single injection of DA solution (0.5 mL of 3 mM) and 5-HT solution (0.5 mL of 3 mM). Representative cyclic voltammograms before and after the DA injection event (**Figure 4-11b**) and 5-HT injection event **(Figure 4-11c)** clearly show oxidation peak for DA (0.18 V) and 5-HT (0.4 V), respectively.

To simulate an elevated concentration of DA and 5-HT near the electrode implantation site, which might occur during natural behaviors in crayfish, and to examine the device's capability for co-detection in an *in vivo* environment, injections of 1X PBS (0.5 mL, as a negative control), and a DA&5-HT cocktail solution (0.5 mL of 300 μM) were respectively administered through the ventral sinus cavity of the crayfish and circulated through the heart [238]. During each experiment, five CV cycles were recorded, starting with the unaltered hemolymph (baseline), followed by three injection events. After each injection event, ten cycles were continuously recorded, with a 1-minute holding time between cycles. The monitoring results in crayfish are shown in **Figure 4-11d-f**. No change in Ipa was observed in the hemolymph measurements prior to any injections, and the administration of PBS did not result in an increase in Ipa at the DA potential or 5-HT potential (**Figure 4-11d**).

Representative cyclic voltammograms before and after a DA&5-HT cocktail injection event is shown in **Figure 4-11f**. No peaks were observed in the unaltered hemolymph, while two distinctive peaks were observed at 0.18 V (DA) and 0.38 V (5-HT) following the DA&5-HT cocktail injection, which was consistent with the beaker-level characterization. **Figure 4-11e** summarizes the CV oxidation peaks resulting from the continuous monitoring of crayfish hemolymph, depicting the dynamics of DA and 5-HT levels before and after the injection events. Immediately after the DA&5-HT cocktail injection, a clear increase in Ipa was observed, and the maximum measured Ipa reached 73.5 nA for DA and 181.1 nA for 5-HT 4 minutes after the injection. The Ipas decreased over time until the next injection event. A similar pattern was observed for the second and third injection events. For the second injection, the measured Ipa reached its maximum 5 minutes after injection, at 87.7 nA for DA and 177.3 nA for 5-HT. For the third injection, the maximum Ipas were 87.9 nA for DA and 145.1 nA for 5-HT. The successive reduction in Ipas following the injection potentially occurred due to a combination of chemical metabolism [239], dilution [238], and possible fouling of CFME fibers due to long cycling. These findings demonstrate that the wireless neurotransmitter sensing system can successfully monitor the *in vivo* dynamics of injected 5-HT and DA in the hemolymph of freely-behaving crayfish.

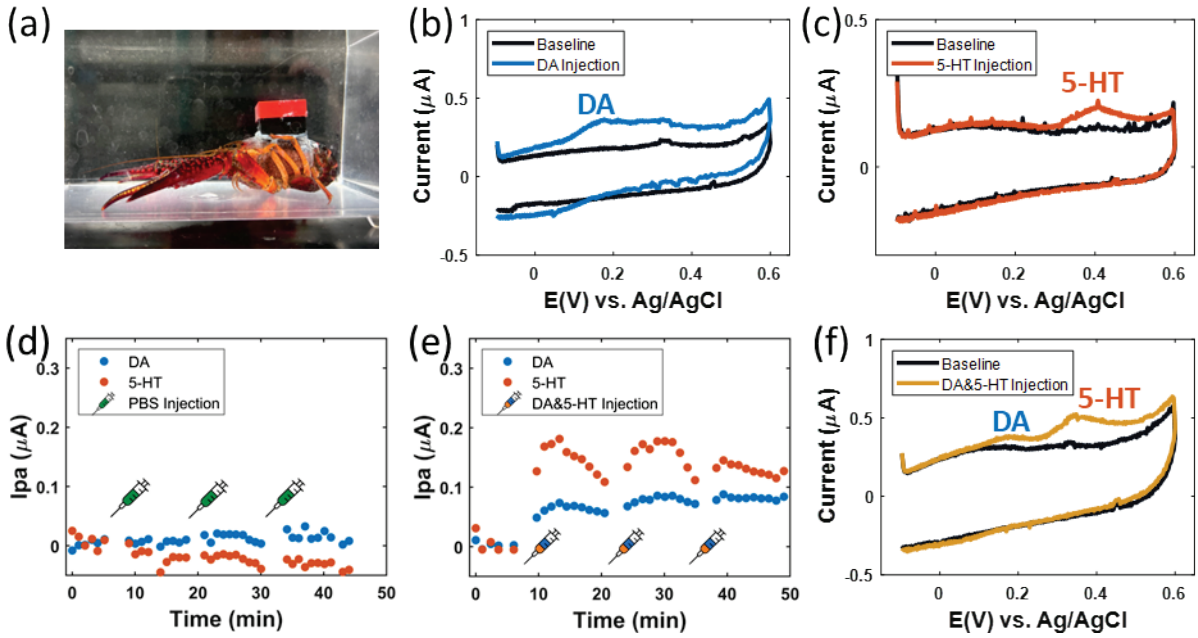

Figure 4-11 Simultaneous monitoring of DA and 5-HT in crayfish hemolymph. (a) Photograph of crayfish with the integrated electrochemical sensing device attached; (b) Representative response currents before and after DA-only injection (0.5 mL of 3 mM); (c) Representative response currents before and after 5-HT-only injection (0.5 mL of 3 mM); (b) Background-subtracted Ipas after three PBS injections (0.5 mL each; negative control); (d) Background-subtracted Ipas after three DA&5-HT cocktail injections (300 μM; 0.5 mL each); (f) Representative response currents before and after DA&5-HT cocktail injection (0.5 mL of 300 μM).

4.4 Chapter Summary

In conclusion, I have demonstrated a fully integrated untethered wireless electrochemical sensing device for the continuous monitoring of DA and 5-HT in hemolymph of freely behaving crayfish. This device utilizes surface-modified carbon fiber microelectrodes coupled with a miniaturized potentiostat module for wireless operation and data acquisition.

Section 4.1 describes an improved microelectrode surface modification protocol for *in vivo* application. Section 4.2 described the system design, system integration approach and rapid prototyping using 3D printing technology. Section 4.3 demonstrated the application of developed

miniaturized electrochemical system for wireless simultaneous monitoring of DA and 5-HT in freely moving crayfish.

The EC/Nafion-CNT CFMEs were based on multiple carbon fibers with electrochemical treatments, followed by Nafion-CNT coating. The surface morphology was characterized using SEM and EDS, confirming successful surface treatment. Electrochemical measurements using EIS and CV indicate improved electron transfer resistance and promoted electrochemical redox reactions. The mechanical tests also indicated improved mechanical robustness using a multi-fiber electrode compared to the single-fiber electrode. The EC/Nafion-CNT CFMEs were also characterized for their electrochemical performance for 5-HT and DA detection, showing a sensitivity of 259.0 nA/μM with a LOD of 59.2 nM for 5-HT and a sensitivity of 129.9 nA/μM with a LOD of 85.1 nM for DA. The CFMEs also exhibited excellent selectivity for DA and 5-HT among other potential interfering molecules, including UA, AA, 5-HIAA, OCT, and ADN, where less than 10% signal changes were observed with 20 times more concentrated interferent molecules. The novel electrodes also showed less than 15% signaling changes for 5-HT and 7% signal changes for DA over 30 consecutive cycles, indicating excellent repeatability.

Integrating the EC/Nafion-CNT CFMEs with previously developed miniaturized PCB potentiostat using 3D printing technology, the device exhibits high selectivity, sensitivity, and stability, while maintaining a small footprint to minimize its impact on animal behavior. The integrated electrochemical sensing system enables detection of DA and 5-HT with a sensitivity of 48.4 nA/μM and 133.0 nA/μM, respectively, within its sub-micromolar linear range. Further, the successful *in vivo* measurement demonstrates the simultaneous monitoring of DA and 5-HT dynamics in a freely-behaving aquatic animal. Quantifying the absolute concentration of DA and 5-HT *in vivo* in crayfish remains challenging due to variations in the carapace curvature and the

amount of hemolymph in the pericardial space, resulting in differences in the exposed area of the 5 mm sensing region of the electrode tip to the circulating hemolymph. To address this issue, a potential solution could involve customizing the 3D package design to better suit the size of the crayfish and allowing for adjustable electrode implantation depth to ensure consistency. Future work will focus on further optimizing hardware and software to achieve detection of endogenously released DA and 5-HT, which has been shown to orchestrate a suite of social behaviors in crayfish and other animals. This includes the initiation of fights, the decisions that lead to discrete social status (i.e., winning/losing), and the maintenance of such outcomes [11], [44], [239], [241], [248], [259], [260]. I envision that this device can also be employed to study neurohormonal DA and 5-HT associated with non-agonistic behaviors and enable chronic monitoring in crayfish and other aquatic (or terrestrial) animal species, potentially in their natural habitats (e.g., in a burrow or under a pond). Collectively, this work presents an engineered approach for the simultaneous monitoring of DA and 5-HT dynamics and holds the potential for adaptation to other model systems, contributing to the investigation of fundamental neurotransmitter-related research questions.

Chapter 5 Concluding Remarks

5.1 Highlights

- Surface-modified CFME was developed for electrochemical 5-HT detection.
    - Improved sensitivity was achieved with electrochemical treatment.
    - Improved selectivity and fouling resistance were achieved with Nafion-CNT coating.
    - Customized RE and CE were fabricated to use with surface-modified CFME for 5-HT detection in samples with small volume.
    - The linear range and LOD of 5-HT detection at microelectrodes were found to be within physiological 5-HT concentrations.
    - Detection of RIN14B-secreted 5-HT was successfully performed in supernatant.
    - Successful detection of 5-HT was achieved in homogenized crayfish nerve cord from pretreated crayfish.
    - The feasibility of using developed microelectrode for studying 5-HT signaling and modulation was demonstrated *in vitro* environments.
- Portable and customized potentiostat platforms were developed.
    - CV measurement functionality was implemented for both platforms.
    - Similar CV performance was achieved comparing benchtop and portable potentiostat system.
    - Sensitive 5-HT sensing was achieved by using a portable potentiostat platform with surface-modified carbon fiber.
    - 5-HT detection in artificial urine sample was measured at sub-micro molar concentration with high accuracy.

- Similar CV performance was achieved by using a benchtop and customized potentiostat system.
- Similar sensitivity was determined using the portable and miniaturized potentiostat systems.
- Successfully monitored *in vivo* 5-HT detection in crayfish hemolymph using customized potentiostat system.

- A fully integrated wearable 5-HT monitoring device was developed.
  - Simultaneous detection of 5-HT and DA was achieved.
  - *In vivo* monitoring of 5-HT and DA was achieved with implantable microelectrodes.
  - Increased 5-HT and DA levels were detected in hemolymph after drug injection.
  - The feasibility of using developed device for studying 5-HT dynamics with and serotonergic modulation in animal behaviors were demonstrated.

5.2 Summary

My dissertation has presented the development of minimally invasive electrochemical sensing systems to address challenges involved in 5-HT sensing and to facilitate neuroscience studies in investigating serotonergic modulation. **This thesis accomplishments involve:** (1) the development of novel surface-modified CFMEs for sensitive, selective 5-HT sensing with minimal fouling, (2) the implementation of a customized PCB for electrochemical measurement with wireless communication, and (3) the systematic integration for a miniaturized implantable device for continuous 5-HT monitoring in freely moving animals. The developed microelectrodes were validated for 5-HT detection in both a modeled gut epithelial cell culture environment and a homogenized nerve cord sample, demonstrating their potential to study 5-HT molecular transportation and serotonergic modulation in complex biological environments. The integrated

untethered implantable system demonstrated its capabilities for *in vivo* 5-HT monitoring and studying serotonergic modulation related to animal behaviors. Overall, this work presents minimally invasive neurochemical sensing systems that provide engineered approaches to facilitate the study of serotonergic modulations (**Figure 5-1**).

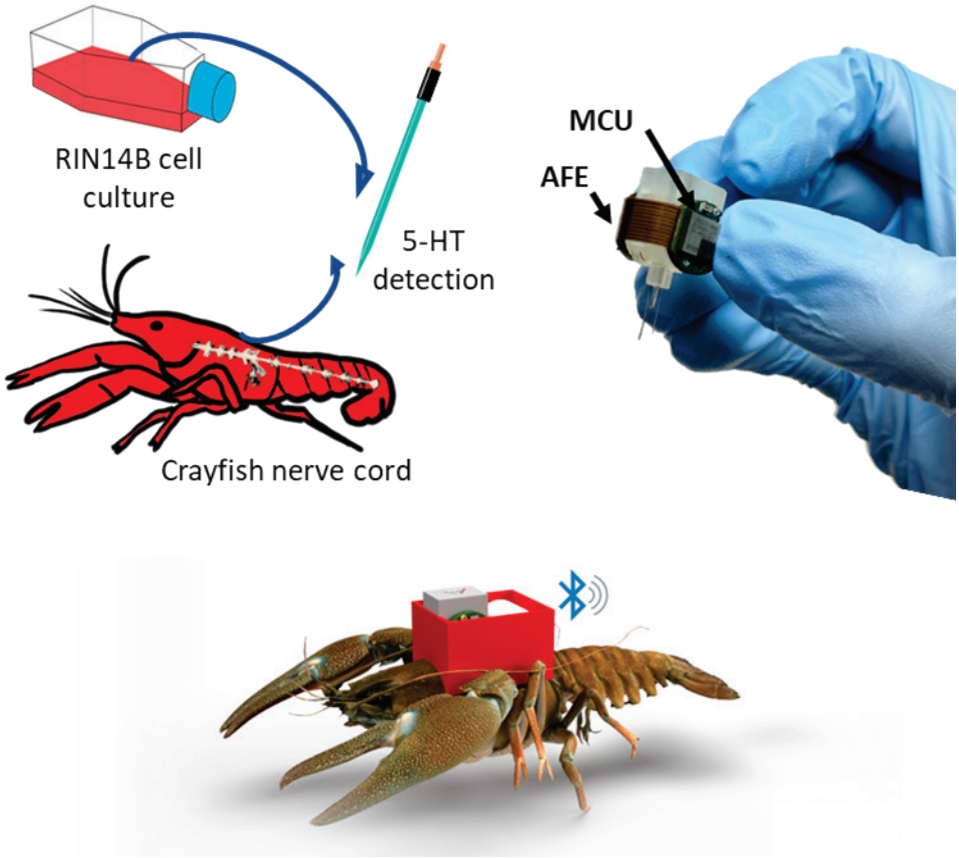

Figure 5-1 Schematic of the key contributions in this thesis. The Surface-Modified CFME and Customized PCB Potentiostat Platform were developed and integrated for Minimally Invasive Device for monitoring 5-HT signaling in animals.

I first developed a novel method for fabricating and surface-modifying CFMEs for 5-HT detection. The developed microelectrodes were first characterized using SEM, EDS, and electrochemical techniques to analyze the Nafion-CNT coating and electrochemical treatment. The results showed an increased surface area due to surface coating and electrochemical treatment. I then demonstrated the electrochemical performance of surface-modified CFMEs for 5-HT

detection, focusing primarily on sensitivity, selectivity, and 5-HT fouling. The results suggested that EC treatment significantly increased the electrode sensitivity to 5-HT due to the increased surface area. The Nafion-CNT coating showed improved selectivity and anti-fouling properties compared to non-coated counterparts. Based on these results, Nafion-CNT/EC electrodes were selected for further characterization and application due to their better sensitivity, selectivity, and fouling resistance. Furthermore, I demonstrated the application of the developed CFMEs, particularly Nafion-CNT/EC, for 5-HT detection in cell culture media and crayfish nerve cord. The novel surface-modification method allowed successful measurement of cell-released 5-HT in cell culture media and 5-HT in the crayfish nerve cord. The Nafion-CNT/EC microelectrode successfully detected AITC-treated RIN14B cell-released 5-HT from the cell-culture supernatant, indicating a release of 120.1 nM 5-HT based on the calibration curve method. The electrode also successfully detected 5-HT from a homogenized crayfish nerve cord after the crayfish was injected with 5-HT in the hemolymph. These results suggest that the injected 5-HT is uptaken by the nerve cord during hemolymph circulation. Overall, this novel surface-modified microelectrode provides a sensitive and reliable approach for 5-HT sensing with high time resolution, offering great potential for studying 5-HT signaling in the CNS and gastrointestinal environment and investigating downstream serotonergic modulations.

For hardware development, portable and miniaturized potentiostat systems have been developed for POC applications. Working towards the miniaturized potentiostat system, a commercially available portable potentiostat system was first selected to validate the hardware performance and functionality. I compared the CV functionality of these potentiostats using standard $Fe[(CN)_6]^{3-}$ and $Fe[(CN)_6]^{4-}$ electrochemical probes, as well as a standard 5-HT solution. The results suggest that both the portable potentiostat and the PCB potentiostat exhibit similar performance compared to the benchtop device.

I was able to demonstrate the application of a portable electrochemical sensing platform for 5-HT detection in artificial biological fluid. Using previously developed CFMEs, the portable platform showed a LOD of 140 nM with a sensitivity of 74 nA/mM (R^2 = 0.9968) in the linear range of 0.5 to 1.1 μM, which is physiologically relevant. The applicability of the platform in artificial urine was investigated, revealing excellent recovery rates. The experimental results indicate that the portable 5-HT detection system, based on a Nafion–CNT/EC electrode, provides sensitive electrochemical 5-HT measurements as a low-cost, simple, rapid, and versatile point-of-care solution for detecting 5-HT.

I also demonstrated the application of an implantable biosensing system for continuous monitoring of injected 5-HT in circulated hemolymph in freely behaving crayfish. The system integrates a customized PCB potentiostat module and modified implantable microelectrodes with a 3D-printed package to enable electrochemical CV measurements. The 5-HT detection capabilities were validated at the beaker-level with a sensitivity of 70 nA/μM in the linear range of 0.4 to 1.2 μM. This system also successfully achieved *in vivo* 5-HT detection in hemolymph through injections using the implantable device while allowing the crayfish to move freely in the underwater environment.

Overall, with previously developed CFMEs, the portable and miniaturized potentiostat circuits exhibit promising performance in the detection of 5-HT in different settings, including POC applications for diagnosing 5-HT syndrome, as well as monitoring 5-HT dynamics in animal models. Collectively, the portable and miniaturized potentiostat circuits offer a low-cost, sensitive, and rapid approach to 5-HT sensing. These advancements have the potential for various applications in instrumentation for 5-HT detection and monitoring, enabling further investigation into serotonergic modulation.

After characterizing subsystems, I demonstrated a fully integrated untethered wireless electrochemical sensing device for the continuous monitoring of DA and 5-HT in the hemolymph of freely behaving crayfish, using previously developed microelectrodes and hardware. This device utilizes surface-modified carbon fiber microelectrodes coupled with a miniaturized potentiostat module for wireless operation and data acquisition. The device exhibits high selectivity, sensitivity, and stability while maintaining a small footprint to minimize its impact on animal behavior. The integrated electrochemical sensing system enables the detection of DA and 5-HT with a sensitivity of 48.4 nA/μM and 133.0 nA/μM, respectively, within their sub-micromolar linear range. Furthermore, the successful *in vivo* measurement demonstrates the simultaneous monitoring of DA and 5-HT dynamics in a freely behaving aquatic animal. Upon drug injection into the animal, the device was able to capture the dynamic pattern following the injection, potentially occurring due to a combination of chemical metabolism, dilution, and possible fouling of CFME fibers due to long cycling. Overall, the results demonstrate that the wireless neurotransmitter sensing system can successfully monitor the *in vivo* dynamics of injected 5-HT and DA in the hemolymph of freely behaving crayfish.

5.2 Future works

The research presented in this dissertation serves as a significant step toward 5-HT monitoring in modeled and realistic environments for investigating serotonergic modulations. However, further work is needed to fully realize this goal.

Endogenous 5-HT Detection Using Carbon Fiber Microelectrodes

In vivo detection of 5-HT in crayfish hemolymph in Chapter 4 was achieved after drug injection. Injecting neurochemicals in invertebrates has commonly been used to study their neuronal and hormonal modulations. For example, 5-HT injection caused changes in both Pleurobranchaea and

Aplysia, leading to more active behavioral states identified by changes in posture and locomotion [261]. Injection of 5-HT in crayfish hemolymph also induced avoidance, indicating anxiety-like behavior [65]. These results have indicated serotonergic modulation in animal behaviors induced by 5-HT injections. However, the ability to detect naturally existing 5-HT levels and changes in 5-HT levels in response to stimuli will provide more information to understand serotonergic modulation in animal physiological and behavioral processes. Nevertheless, the naturally existing 5-HT concentration in invertebrates is low. According to the literature, the concentration of 5-HT in the hemolymph of blood-sucking bugs ranges from 7 to 100 nM, depending on feeding events [262]. The concentrations of 5-HT in the hemolymph of Aplysia ranges from 5 to 30 nM depending on animal variations, light/dark cycles, number of days after arrival to the laboratory, etc. [244]. The 5-HT concentration in crayfish (Orconectes limosus) hemolymph was reported to be below 10 nM [263]. Detecting naturally existing or naturally released 5-HT in crayfish hemolymph using the device developed in this research remains challenging. One of the future works will focus on improving device sensitivity to be able to detect naturally existing and released 5-HT.

An initial investigation has been conducted using a benchtop potentiostat (Interface 1010E, Gamry, PA) in combination with the surface-modified CFMEs to detect 5-HT levels in crayfish hemolymph. **Figure 5-2** shows an example of cyclic voltammetric responses in crayfish hemolymph without any treatment. A small but clear oxidation peak can be observed with an Epa of 0.32 V and an Ipa of 0.012 μA. According to the calibration curve, the 5-HT concentration can be estimated to be 20 nM, which is in the same order of magnitude as the values reported in the literature. However, other interference molecules, such as UA and 5-HIAA, may also result in an oxidation peak at a similar potential. In order to confirm that the oxidation peak is caused by the detection of 5-HT, a standard method, such as HPLC, is needed to verify the result. There was also

a large variation in the detected signal from animal to animal. In some cases, the oxidation peak was too small to be quantified. The results suggest that the 5-HT concentration in hemolymph was near the LOD of the electrode. Several methods can be used to further optimize the LOD of the system to achieve this goal. Additionally, the device can be expanded to other applications.

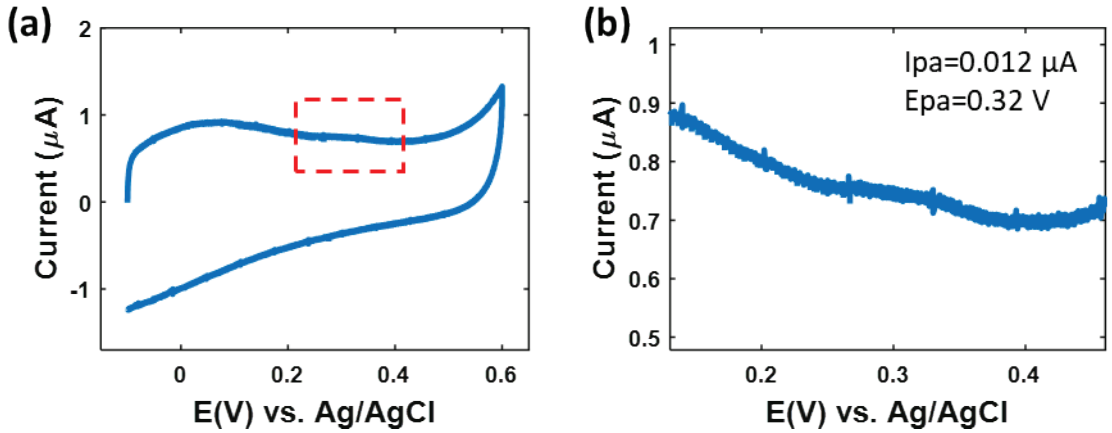

Figure 5-2 Representative in vivo CV measurement in crayfish hemolymph using developed EC/Nafion-CNT CFMEs and benchtop potentiostat. (a) Full cyclic voltammogram from -0.1 to 0.6 V and (b) cyclic voltammogram at selected region from 0.1 to 0.5 V.

Carbon Fiber Optimization

Based on the results reported in this work, the CFMEs with a single carbon fiber had a better LOD than the CFMEs with multiple fibers. However, the multi-fiber CFMEs are more mechanical robust, and have better sensitivity. In order to further enhance the overall performance of the microelectrodes, the surface modification protocol can be refined and fine-tuned. To achieve the optimal balance between LOD and robustness required for *in vivo* experiments, the number of fibers in the microelectrode can be carefully optimized. Increasing the number of fibers can potentially improve mechanical stability and durability, ensuring reliable performance during experiments. On the other hand, a higher number of fibers may slightly compromise the LOD. Therefore, it becomes crucial to strike a balance between LOD, sensitivity, and mechanical

robustness. By optimizing the surface modification protocol and carefully selecting the number of fibers in the microelectrode design, it is possible to achieve an ideal microelectrode configuration that meets the specific requirements of *in vivo* experiments.

Implementing Differential Pulse Voltammetry for Customized Potentiostat

CV was extensively employed in this work for 5-HT detection using both benchtop and customized potentiostats. However, for enhanced sensitivity, DPV can be utilized. In DPV, short pulses of small amplitude are overlaid on a linear ramp (**Figure 5-3a**). Current is measured before applying the pulse (indicated by red arrows in **Figure 5-3a**) and at the end of each pulse, enabling the calculation of the difference between the currents. This procedure effectively reduces the background current attributed to the DC ramp, resulting in a Faradaic current that is mostly free from capacitive components. The major advantage of DPV lies in its low capacitive current, which leads to heightened sensitivity. Additionally, the use of small step sizes in DPV produces narrower voltammetric peaks, making it a preferred method for distinguishing analytes with similar oxidation potentials [245] . **Figure 5-3b** illustrates the DPV response for dopamine, showcasing a narrower peak compared to cyclic voltammetry and its application in differentiating AA and DA [264]. Consequently, DPV presents an effective approach for achieving improved sensitivity and selectivity compared to CV. The DPV function can be programmed and implemented using AD5941.

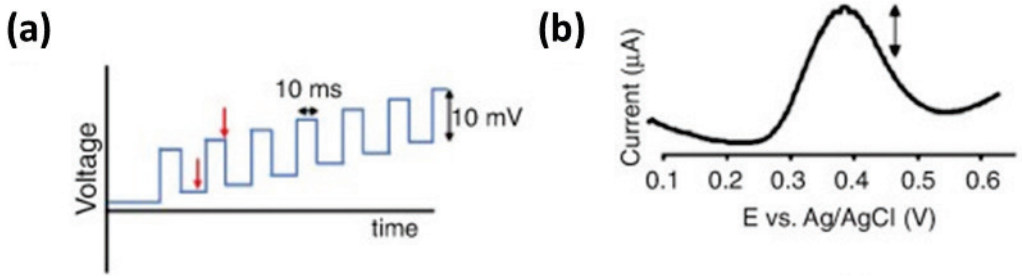

Figure 5-3 Schematic illustrating the waveform applied for DPV. (a) Applied waveform for DPV, with arrows indicating the points where differential current is measured at the end of each step. (b) Voltammogram obtained from DPV, showcasing the response of dopamine [245].

Detecting Serotonin or Dopamine with Electrochemical Impedance Spectroscopy

While CV has been applied in this work to characterize developed CFMEs and achieve in vitro and in vivo detection of 5-HT in biological samples, the EIS can be also used to detect 5-HT or DA without surface fouling. The basic principle of EIS involves applying a sine wave voltage at a DC level with a small amplitude (approximately 10 mV) to the WE and then measuring the resulting current at different frequencies, ranging from 1 MHz to 10 Hz. For EIS to work effectively, the voltage amplitude must be kept small to ensure a pseudo-linear behavior in the i-v plot, resulting in a current response that matches the frequency of the applied voltage. The measured current at each frequency is then used to calculate the impedance and establish a model circuit representing the chemical processes occurring at the electrode surface. The wide range of frequencies at which EIS can operate presents an opportunity to improve temporal resolution and consequently enhance sensitivity. Unlike CA and CV, EIS provides valuable information about the electrode's surface without the need for extensive potential sweeps or the oxidation of electroactive compounds. This characteristic has the potential to minimize 5-HT fouling. Notably, both 5-HT and DA are known to adsorb on CFME [199], [265], which makes EIS an effective tool for studying the impedance resulting from their adsorption without interference from desorption caused by oxidation. The use of EIS for detecting DA has been achieved in standard solutions, with high temporal resolution (10 ms with 100 Hz) and low LOD (1 nM) at 0 V DC bias to avoid molecule oxidation and surface fouling [265]. However, one evident challenge of this technique is its lack of selectivity. At sub-oxidation potential, any molecules that adsorb to the electrode can cause changes in impedance.

Nevertheless, additional surface modifications can be employed to enhance specific adsorption to targeted molecules, addressing this limitation. Overall, EIS proves to be an effective approach

for detecting both DA and 5-HT with high sensitivity and time resolution, while also preventing surface fouling, thereby improving electrode repeatability.

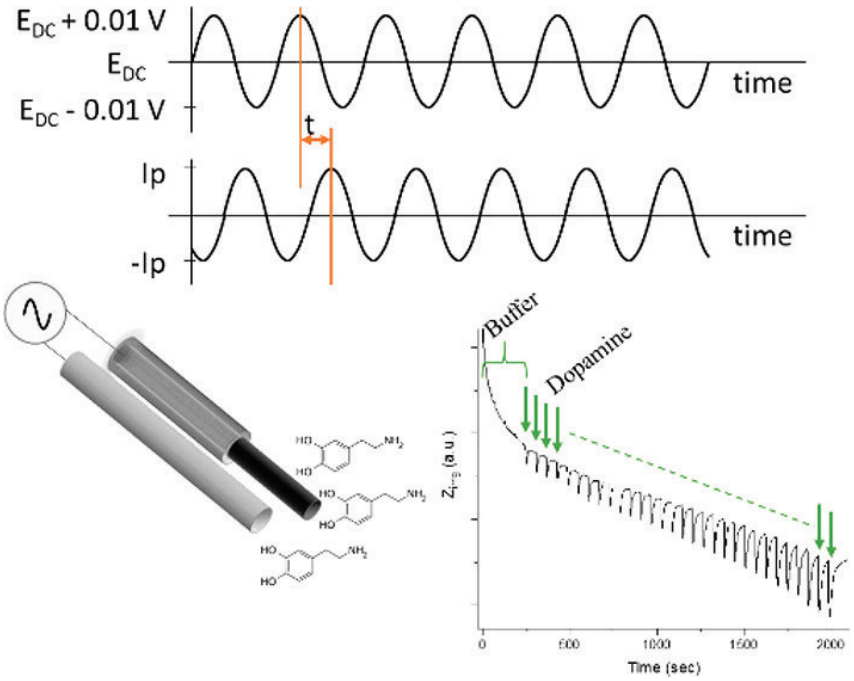

Figure 5-4 Diagram of the applied voltage signals used for EIS and measured current signals. The EIS has been used to detect DA with high sensitivity, time-resolution without oxidizing the molecules[265].

Serotonin Sensing in Crayfish Central Nervous System

Although this work only demonstrates *in vivo* 5-HT measurements in crayfish hemolymph, it holds potential applications for detecting 5-HT in other regions of crayfish or even in other animals. For example, 5-HT concentrations of 1 µM have been reported in crayfish brain regions, and they can reach up to 2 µM when treated with repeated electrical stimulations [65]. Implanting an electrode in the crayfish brain to directly detect released and uptaken 5-HT at serotonergic neurons would provide more information about 5-HT dynamics. However, this would require greater precision in electrode implantation surgery.

Using the *ex vivo* crayfish nerve cord is an alternative solution to study serotonergic modulation in nervous systems. In crayfish, the lateral giant escape circuit responds to sensory stimulation, which is found to be related to 5-HT concentration and the rate of application [66], [70], [73], [266]. These studies suggest that crayfish expresses 5-HT and behaves differently in response to social or environmental stimuli [267]. Moreover, the crayfish nerve cord can be removed from the crayfish but remains physiologically active ex vivo in saline. Therefore, crayfish nerve cords serve as an ideal experimental animal model to understand the principles of neurophysiology and serotonergic modulations in the CNS. The future work will also focus on applying optimized CFMEs and DPV for sensitive and selective 5-HT measurements in the ex vivo crayfish nerve cord with high spatiotemporal resolution to investigate 5-HT signaling and serotonergic modulation in the crayfish CNS.

Ingestible Capsule Device for Serotonin Sensing in Gastrointestinal Tract

As a major neurotransmitter mainly produced in enterochromaffin cells in the mucosa of the gastrointestinal tract, 5-HT plays an important role as a messenger molecule in the communication between the epithelium and the ENS. Enterochromaffin cells respond to a variety of luminal mechanical, osmotic, and chemical factors associated with the microbiome, diet, irritants, and immune-modulating cytokines by releasing the bulk of their 5-HT stores on the basolateral side of the epithelium [8], [268]. This released 5-HT is then available to stimulate enteric nerves, producing an effect on the surrounding ENS and potentially reaching the local musculature or the brain [269]. Since the majority of 5-HT is released on the basolateral side of the epithelium, it is important to have a sensor that provides direct accessibility to the local release site.

Carbon fiber microelectrodes can be utilized for neurotransmitter sensing applications due to their small size. However, they have limited penetration ability. To address this limitation, a 3-dimensional protective structure can be fabricated and integrated with carbon fiber microelectrodes, enhancing the penetration ability of the 5-HT microelectrodes. Recent advancements in 3D printing technologies, such as direct laser writing (DLW) or stereolithography (SLA), enable the fabrication of high-resolution 3D structures (**Figure 5-4a**) [270], [271]. Both techniques can be employed to create a hollowed microneedle structure capable of penetrating through the tissue layer [272]. The carbon fiber microelectrode can then be inserted into the hollowed channel for sensing beneath the tissue.

The microneedle will feature a central channel that guides the CFME into the intestinal tissue and will be designed to be porous, facilitating rapid fluid exchange between the sensor and biological material (**Figure 5-4b**). This fluid exchange is crucial for obtaining temporally resolved electrochemical measurements. The microelectrode-integrated microneedle will be securely attached to a spring actuator [273], enabling submucosal monitoring of 5-HT. The spring actuation mechanism will provide the necessary force to penetrate the colon tissue with the microelectrode. By leveraging simultaneous colorectal distention and real-time basolateral 5-HT measurements,

this approach facilitates the investigation of colonic 5-HT concentrations and serotonergic modulations.

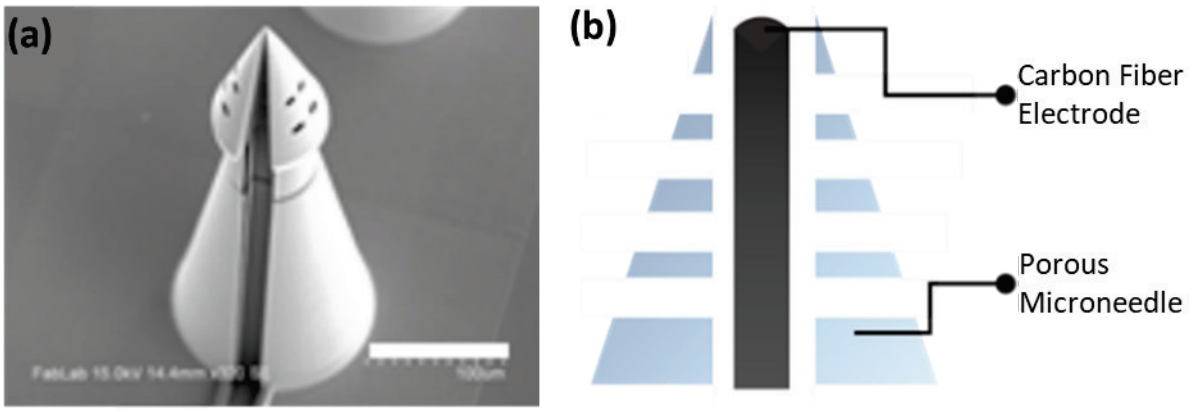

Figure 5-5 (a) DLW printed microneedle [270]. *(b) Schematic of microelectrode integrated microneedle design.*

In order to reach the targeted location in the gastrointestinal tract, ingestible capsule technologies will be used as they provide a localized method to target specific regions in the gastrointestinal tract for localized sensing or treatment. Ingestible capsule devices have been developed for sensing pH [155], [274], [275], gases [140], and other physiological parameters [156], [276]. However, none have been developed specifically for 5-HT sensing. In future work, the microneedle-based sensor can be integrated with an ingestible capsule platform to provide localized targeting capability in the gastrointestinal tract (**Figure 5-5**). The capsule device consists of an array of microneedle-based carbon fiber microelectrodes, a spring actuator, controlling electronics, and biocompatible package. The spring actuator and microneedle sensor remain compressed while traveling through the gastrointestinal tract. Upon reaching the targeted location, the onboard electronics will activate the actuator, causing the attached microelectrode to penetrate the tissue, thus allowing access to 5-HT in the targeted region. This device will provide localized sensing capability, which can be used to better understand 5-HT dynamics, serve as a diagnostic tool, and potentially be incorporated with drug delivery for a feedback loop-controlled device.

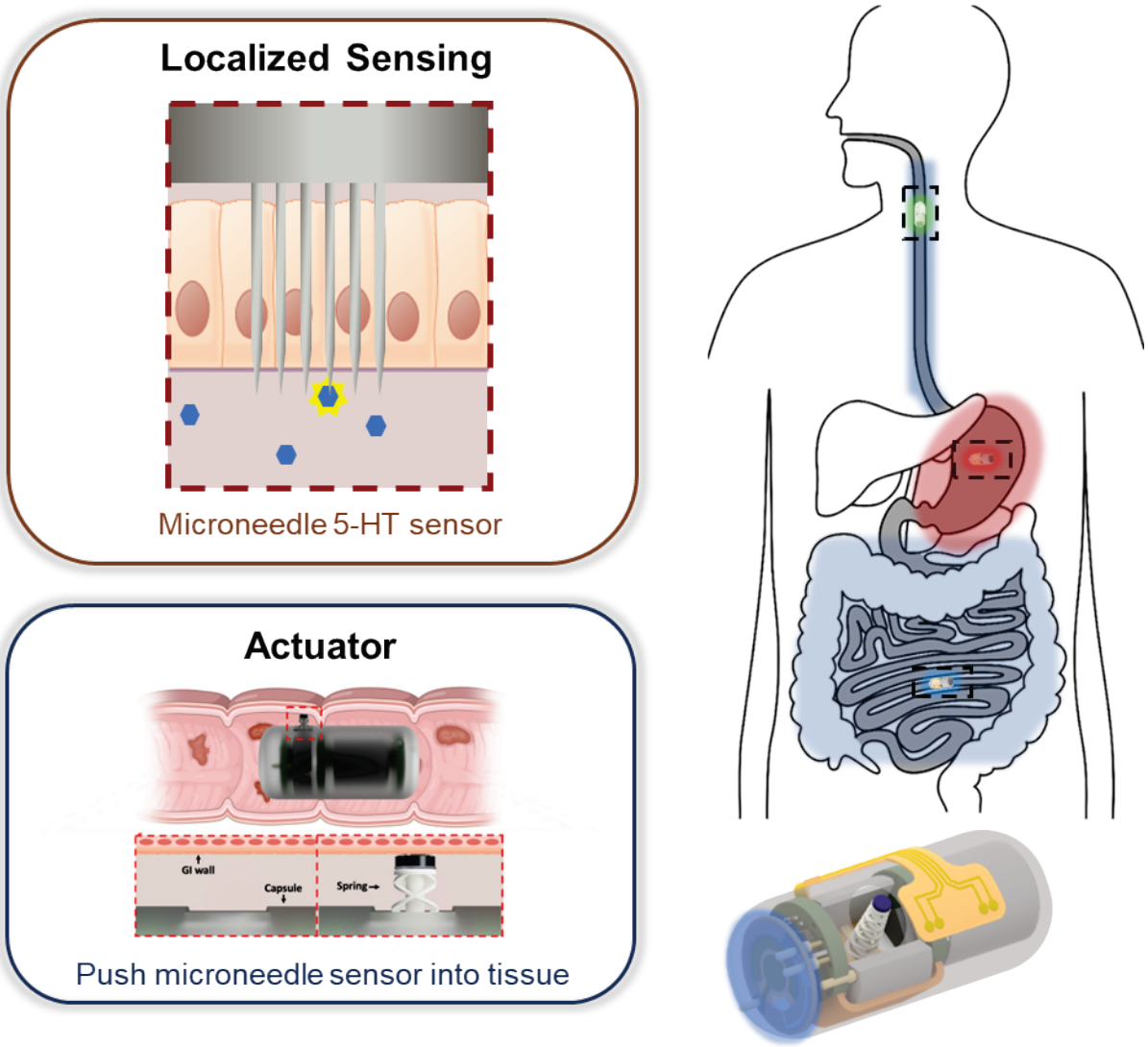

Figure 5-6 Schematics of ingestible capsule device with multimodal sensing capability. The microneedle 5-HT sensor is attached on the spring actuator. The actuator can be activated by the capsule electronics resulting in localized 5-HT detection in the submucosa layer [273].

5.3 Conclusion

My dissertation research has made significant contributions to relevant fields across the three main Chapters 2-4. One notable achievement is the development of a novel surface modification method for CFMEs, enabling sensitive and selective detection of 5-HT while minimizing surface fouling. By applying Nafion-CNT coating and electrochemical treatment, the modified CFMEs have been proven to be effective in detecting 5-HT at physiologically relevant concentrations in both modeled and realistic environments. The functionality of microelectrodes has been demonstrated for *in vitro* mammalian cell culture environments as well as animal tissue samples.

Furthermore, I have successfully implemented electrochemical measurements, particularly CV, using customized potentiostat electronics. This device provides a low-cost and miniaturized solution for wearable electrochemical sensing devices. I have integrated the developed microelectrodes with customized potentiostat electronics for a wearable device capable of detecting both *in vivo* DA and 5-HT in crayfish hemolymph. This represents the first wireless device developed for the simultaneous monitoring of neurotransmitter dynamics in freely moving crayfish using implanted microelectrodes.

In summary, the research presented in this dissertation provide a novel microelectrode sensor for sensitive, selective 5-HT measurements, a customized potentiostat electronics for miniaturized and portable electrochemical measurements, and a prototyped device for wireless DA and 5-HT monitoring. The device has the potential to expand its application to different animal models, enabling the monitoring of DA and 5-HT dynamics in various regions of interest. The real-time, *in situ* information provided by this device is unique and allows for correlation between animal behaviors and neurotransmitter dynamics to investigate neurochemical modulations. The prototyped device showcased in this dissertation serves as a foundation for the development of

diverse wearable electrochemical neurotransmitter sensing devices, which will facilitate future neuroscience research by enabling continuous, *in situ* monitoring of neurotransmitter dynamics without impacting animal behaviors.

APPENDIX A – MATLAB PROGRAM

```
% Matlab code to perform background subtraction for CV plot analysis
% Data was obtained from phone app
% Jinjing Han @ 01/08/2023

clear
close

% Enter all parameters here:
FileName_bg='HM-2.txt';              % Background signal file name
FileName_inj='HM-3.txt';             % After injection signal file name

NumData = 400;                       % number of data points
ScanRangeLow = -0.1;                 % Lower Scan Range
ScanRangeUp = 0.6;                   % Upper Scan Range

% Construct E
E=zeros(NumData,1);
for i=1:1:NumData
    if i <= NumData/2+1
        E(i)=ScanRangeLow + 2* (i-1)* (ScanRangeUp-ScanRangeLow)/ NumData;
    else
        E(i)=ScanRangeUp - 2* (i-NumData/2-1)* (ScanRangeUp-ScanRangeLow)/
NumData;
    end
end
E(1)=NaN;

% Import Data:
readFile = fopen(FileName_bg);
A=importdata(FileName_bg);           % Read text file in to a cell
fclose('all');
s=string(A);                         % Convert cell to string
data_bg=[];
for i = 1:size(s,1)                  % for each row in the cell
    if i>5 && mod(i,2) == 1
    temp1 = strsplit(s{i}, ', ');    % split by comma
    temp2=string(temp1(3));          % convert the last segment, (dec) data to
string
    temp3 = strsplit(temp2, ' ');    % split each number in (dec) data
    temp4 = str2double(temp3);       % convert to num
    temp5=temp4(2)*256+temp4(1);     % hex to dec
    temp6=-(temp5/1000-3);           % decode by rule in program
    data_bg=[data_bg;temp6];         % data is the current in uA
    else
        ;
    end
end
%%%%%%%%%%%%%%%%%%%%%%%%%%%%%%%%%%%%%%%%%%%%%%%%%%%%%%%%%%%%%%%%%%%%%%%
readFile = fopen(FileName_inj);
A=importdata(FileName_inj);          % Read text file in to a cell
fclose('all');
s=string(A);                         % Convert cell to string
```

```
data_inj=[];
for i = 1:size(s,1)                  % for each row in the cell
    if i>5 && mod(i,2) == 1
    temp1 = strsplit(s{i}, ', ');    % split by comma
    temp2=string(temp1(3));          % convert the last segment, (dec) data to
string
    temp3 = strsplit(temp2, ' ');    % split each number in (dec) data
    temp4 = str2double(temp3);       % convert to num
    temp5=temp4(2)*256+temp4(1);     % hex to dec
    temp6=-(temp5/1000-3);           % decode by rule in program
    data_inj=[data_inj;temp6];       % data is the current in uA
    else
        ;
    end
end

    I=data_inj-data_bg;
    plot (E,data_bg,'LineWidth',3)
    hold on
    plot (E,data_inj,'LineWidth',3)
    plot (E,I,'LineWidth',3)

% Plot Format
ax = gca;
ax.XAxis.LineWidth = 1;
ax.YAxis.LineWidth = 1;
ax.YAxis.FontWeight = 'bold';
ax.XAxis.FontWeight = 'bold';
set(gca,'FontSize',12);
xlabel('E(V) vs. Ag/AgCl','fontweight','bold','fontsize',16')
ylabel('Current (\muA)','fontweight','bold','fontsize',16')
set(gcf, 'Position',  [100, 100, 400, 300]);
title('DA/5HT injections')


xlim([-0.2 0.7])
ylim([-1.5 1.5])
yticks([-1.5 -1 -0.5   0  0.5 1 1.5])
```

APPENDIX B – MICROCONTROLLER FIRMWARE

```
/*
 * AD5940_Ramp.c
 *
 *  Created on: Feb 7, 2022
 *      Author: Justy /Jinjing
 *      Last modified: 09/23/2022
 */

#include "ad5940.h"
#include "RampTest.h"
#include "em_common.h"
#include "sl_bluetooth.h"
#include "gatt_db.h"
#include "app_assert.h"
#include "em_cmu.h"
#include "app_timer.h"

/**
   User could configure following parameters
**/

// Defines
#define TICKS_PER_SECOND 32768

static sl_sleeptimer_timer_handle_t ramp_timer;
static void ramp_timer_cb(sl_sleeptimer_timer_handle_t *handle, void *data);


#define APPBUFF_RAMP_SIZE 1024
uint32_t AppBuff_ramp[APPBUFF_RAMP_SIZE];
float LFOSCFreq_ramp;    /* Measured LFOSC frequency */
uint32_t DataCount_wireless;
uint32_t ramp_count = 0;
/**
 * @brief The general configuration to AD5940 like FIFO/Sequencer/Clock.
 * @note This function will firstly reset AD5940 using reset pin.
 * @return return 0.
*/

//TODO prototype of function in header file
static int32_t AD5940RAMPPlatformCfg(void)
{
  CLKCfg_Type clk_cfg;
  SEQCfg_Type seq_cfg;
  FIFOCfg_Type fifo_cfg;
  AGPIOCfg_Type gpio_cfg;
  LFOSCMeasure_Type LfoscMeasure;

  /* Use hardware reset */
  AD5940_HWReset();
  AD5940_Initialize();    /* Call this right after AFE reset */
```

```
  /* Platform configuration */

  /* Step1. Configure clock */
  clk_cfg.HFOSCEn = bTRUE;
  clk_cfg.HFXTALEn = bFALSE;
  clk_cfg.LFOSCEn = bTRUE;
  clk_cfg.HfOSC32MHzMode = bFALSE;
  clk_cfg.SysClkSrc = SYSCLKSRC_HFOSC;
  clk_cfg.SysClkDiv = SYSCLKDIV_1;
  clk_cfg.ADCCLkSrc = ADCCLKSRC_HFOSC;
  clk_cfg.ADCClkDiv = ADCCLKDIV_1;
  AD5940_CLKCfg(&clk_cfg);
  /* Step2. Configure FIFO and Sequencer*/
  /* Configure FIFO and Sequencer */
  fifo_cfg.FIFOEn = bTRUE;           /* We will enable FIFO after all parameters
configured */
  fifo_cfg.FIFOMode = FIFOMODE_FIFO;
  fifo_cfg.FIFOSize = FIFOSIZE_2KB;   /* 2kB for FIFO, The reset 4kB for sequencer */
  fifo_cfg.FIFOSrc = FIFOSRC_SINC3;   /* */
  fifo_cfg.FIFOThresh = 4;            /*  Don't care, set it by application parameter
*/
  AD5940_FIFOCfg(&fifo_cfg);
  seq_cfg.SeqMemSize = SEQMEMSIZE_4KB;  /* 4kB SRAM is used for sequencer, others for
data FIFO */
  seq_cfg.SeqBreakEn = bFALSE;
  seq_cfg.SeqIgnoreEn = bTRUE;
  seq_cfg.SeqCntCRCClr = bTRUE;
  seq_cfg.SeqEnable = bFALSE;
  seq_cfg.SeqWrTimer = 0;
  AD5940_SEQCfg(&seq_cfg);
  /* Step3. Interrupt controller */
  AD5940_INTCCfg(AFEINTC_1, AFEINTSRC_ALLINT, bTRUE);   /* Enable all interrupt in
INTC1, so we can check INTC flags */
  AD5940_INTCClrFlag(AFEINTSRC_ALLINT);
  AD5940_INTCCfg(AFEINTC_0,
AFEINTSRC_DATAFIFOTHRESH|AFEINTSRC_ENDSEQ|AFEINTSRC_CUSTOMINT0, bTRUE);
  AD5940_INTCClrFlag(AFEINTSRC_ALLINT);
  /* Step4: Configure GPIO */
  gpio_cfg.FuncSet = GP0_INT|GP1_SLEEP|GP2_SYNC;  /* GPIO1 indicates AFE is in sleep
state. GPIO2 indicates ADC is sampling. */
  gpio_cfg.InputEnSet = 0;
  gpio_cfg.OutputEnSet = AGPIO_Pin0|AGPIO_Pin1|AGPIO_Pin2;
  gpio_cfg.OutVal = 0;
  gpio_cfg.PullEnSet = 0;
  AD5940_AGPIOCfg(&gpio_cfg);
  /* Measure LFOSC frequency */
  /**@note Calibrate LFOSC using system clock. The system clock accuracy decides
measurement accuracy. Use XTAL to get better result. */
  LfoscMeasure.CalDuration = 1000.0;  /* 1000ms used for calibration. */
  LfoscMeasure.CalSeqAddr = 0;        /* Put sequence commands from start address of
SRAM */
  LfoscMeasure.SystemClkFreq = 16000000.0f; /* 16MHz in this firmware. */
  AD5940_LFOSCMeasure(&LfoscMeasure, &LFOSCFreq_ramp);
  printf("LFOSC Freq:%f\n", LFOSCFreq_ramp);
  AD5940_SleepKeyCtrlS(SLPKEY_UNLOCK);      /*  */
```

```
  return 0;
}

/**
 * @brief The interface for user to change application parameters.
 * @return return 0.
*/
void AD5940RampStructInit(void){
  //printf("Entering AD5940RampStructInit \n");

  AppRAMPCfg_Type *pRampCfg;
  AppRAMPGetCfg(&pRampCfg);
  /* Step1: configure general parameters */
  pRampCfg->SeqStartAddr = 0x10;                /* leave 16 commands for LFOSC
calibration.  */
  pRampCfg->MaxSeqLen = 1024-0x10;              /* 4kB/4 = 1024  */
  pRampCfg->RcalVal = 10000.0;                  /* 10kOhm RCAL */
  pRampCfg->ADCRefVolt = 1820.0f;               /* The real ADC reference voltage.
Measure it from capacitor C12 with DMM. */
  pRampCfg->FifoThresh = 480;                   /* Maximum value is 2kB/4-1 = 512-1.
Set it to higher value to save power. */
  pRampCfg->SysClkFreq = 16000000.0f;           /* System clock is 16MHz by default
*/
  pRampCfg->LFOSCClkFreq = LFOSCFreq_ramp;      /* LFOSC frequency */
  /* Configure ramp signal parameters */
  pRampCfg->RampStartVolt =  +100.0f;           /* -100mV */
  pRampCfg->RampPeakVolt = -600.0f;             /* +600mV */
  pRampCfg->VzeroStart = 1300.0f;               /* 1.3V */
  pRampCfg->VzeroPeak = 1300.0f;                /* 1.3V */
  pRampCfg->StepNumber = 400;                   /* Total steps. Equals to ADC sample
number */
  pRampCfg->RampDuration = 14*1000;             /* X * 1000, where x is total
duration of ramp signal. Unit is ms. 14s-> 100mV/s. */
  pRampCfg->SampleDelay = 7.0f;                 /* 7ms. Time between update DAC and
ADC sample. Unit is ms. */
  pRampCfg->LPTIARtiaSel = LPTIARTIA_512K;      /* Maximum current decides RTIA value
*/
  pRampCfg->LPTIARloadSel = LPTIARLOAD_SHORT;
  pRampCfg->AdcPgaGain = ADCPGA_1P5;

  pRampCfg->bTestFinished = bFALSE;             /* JH*/
}


void AD5940_Ramp_Start(void){
 // printf("Entering AD5940_Ramp_Start \n");
  AD5940RAMPPlatformCfg();
  AD5940RampStructInit();
  AppRAMPInit(AppBuff_ramp, APPBUFF_RAMP_SIZE);    /* Initialize RAMP application.
Provide a buffer, which is used to store sequencer commands */
  AppRAMPCtrl(RAMPCTRL_START, 0);                  /* Control IMP measurement to
start. Second parameter has no meaning with this command. */
  //TODO Check this repeat measurement
}
```

```
void AD5940_Ramp_Restart(void){
  AppRAMPInit (0, 0);               /* Initialize AMP application. Provide a buffer,
which is used to store sequencer commands */
  AppRAMPCtrl (RAMPCTRL_START, 0);  /* Control AMP measurement to start. Second
parameter has no meaning with this command. */
}

void AD5940_Ramp_Stop(void){
  AppRAMPCtrl (RAMPCTRL_STOPSYNC, 0); /* Stop measuring. Second parameter has no
meaning with this command. */
  AppRAMPCtrl (RAMPCTRL_SHUTDOWN, 0); /* Shut the sequencer measurement and amplifier
down. Second parameter has no meaning with this command. */
}

void AD5940_Ramp_StopSync(void){
  AppRAMPCtrl (RAMPCTRL_STOPSYNC, 0); /* Stop measuring. Second parameter has no
meaning with this command. */
}

void AD5940_Ramp_Record (uint8_t app){
  // printf("Enter AD5940_Ramp_Record \n");
  uint32_t temp;
  AppRAMPCfg_Type *pRampCfg;

  AppRAMPGetCfg(&pRampCfg);
  temp = APPBUFF_RAMP_SIZE;
  AppRAMPISR(AppBuff_ramp, &temp);

  if(app == 1){
       RampShowResult((float*)AppBuff_ramp, temp);

  }
  else {
       RampShowAppResult((float*)AppBuff_ramp, temp, connection);
  }
       if(pRampCfg->bTestFinished ==bTRUE){printf("done\n");}

//     /* Repeat Measurement continuously*/
//     if(pRampCfg->bTestFinished ==bTRUE){
//       AD5940_Delay10us(6000000); /* 200000=2s 60s */
//       pRampCfg->bTestFinished = bFALSE;
//       AD5940_SEQCtrlS(bTRUE);   /* Enable sequencer, and wait for trigger */
//       AppRAMPCtrl(RAMPCTRL_START, 0);
//     }
}


/**
 * @brief An example to deal with data read back from AD5940. Here we just print data
to UART
 * @note UART has limited speed, it has impact when sample rate is fast. Try to print
some of the data not all of them.
 * @param pData: the buffer stored data for this application. The data from FIFO has
been pre-processed.
 * @param DataCount: The available data count in buffer pData.
```

```
 * @return return 0.
*/

void RampShowResult(float *pData, uint32_t DataCount){
  static uint32_t index;
  /* Print data*/
  float *pFun = (float*)AppBuff_ramp;
  // printf("DataCount = %f \n", (float) DataCount);
  for(int i=0;i<DataCount;i++){
    printf("index:%d, %.3f\n", index++, (pFun[i]));
    //i += 10;  /* Print though UART consumes too much time. */
  }
}

void RampShowAppResult(float *pData, uint32_t DataCount, uint16_t connect){
  DataCount_wireless = DataCount;
  start_ramp_timer();
}


void start_ramp_timer(void){
  sl_status_t status;
  uint32_t timer_timeout = TICKS_PER_SECOND/100;

  status = sl_sleeptimer_start_periodic_timer(&ramp_timer,
                                      timer_timeout,
                                      ramp_timer_cb,
                                      NULL,
                                      1,
                                      0);
  if(status != SL_STATUS_OK) {
  }
}


void ramp_timer_cb(sl_sleeptimer_timer_handle_t *handle, void *data){
  (void)data;
  (void)handle;
  uint32_t buffer;
  float *pData = (float*)AppBuff_ramp;
  if(ramp_count < DataCount_wireless){
      buffer = (uint32_t) ((pData[ramp_count]+3) *1000);
      /*Send data buffer to phone app and notify. */
       sl_bt_gatt_server_write_attribute_value (gattdb_Sensor_1, 0, 4,
                                                (const uint8_t*) &buffer);
       sl_bt_gatt_server_send_notification (connection, gattdb_Sensor_1, 4,
                                           (const uint8_t*) &buffer);
       ramp_count++;
   }
  if (ramp_count == DataCount_wireless){
      (void) sl_sleeptimer_stop_timer(&ramp_timer);
      ramp_count = 0;
   }
}
```

REFERENCES

[1] M. Berger, J. A. Gray, and B. L. Roth, "The Expanded Biology of Serotonin," *Annu. Rev. Med.*, vol. 60, no. 1, pp. 355–366, Feb. 2009, doi: 10.1146/annurev.med.60.042307.110802.

[2] T. A. Jenkins, J. C. D. Nguyen, K. E. Polglaze, and P. P. Bertrand, "Influence of tryptophan and serotonin on mood and cognition with a possible role of the gut-brain axis," *Nutrients*, vol. 8, no. 1, p. 56, Jan. 2016, doi: 10.3390/nu8010056.

[3] R. G. Ruddell, D. A. Mann, and G. A. Ramm, "The function of serotonin within the liver," *J. Hepatol.*, vol. 48, no. 4, pp. 666–675, Apr. 2008, doi: 10.1016/j.jhep.2008.01.006.

[4] H. Wu, T. H. Denna, J. N. Storkersen, and V. A. Gerriets, "Beyond a neurotransmitter: The role of serotonin in inflammation and immunity," *Pharmacol. Res.*, vol. 140, pp. 100–114, Feb. 2019, doi: 10.1016/j.phrs.2018.06.015.

[5] D. M. Kendig and J. R. Grider, "Serotonin and colonic motility," *Neurogastroenterol. Motil.*, vol. 27, no. 7, pp. 899–905, Jul. 2015, doi: 10.1111/nmo.12617.

[6] M. D. Ferrari, J. Odink, C. Tapparelli, G. Van Kempen, E. Pennings, and G. W. Bruyn, "Serotonin metabolism in migraine," *Neurology*, vol. 39, no. 9, pp. 1239–1242, Sep. 1989, doi: 10.1212/wnl.39.9.1239.

[7] M. Camilleri, "Serotonin in the gastrointestinal tract," *Curr. Opin. Endocrinol. Diabetes Obes.*, vol. 16, no. 1, pp. 53–59, Feb. 2009, doi: 10.1097/MED.0b013e32831e9c8e.

[8] M. D. Gershon *et al.*, "The Serotonin Signaling System: From Basic Understanding To Drug Development for Functional GI Disorders," *Gastroenterology*, vol. 132, no. 1, pp. 397–414, Jan. 2007, doi: 10.1053/j.gastro.2006.11.002.

[9] J. Bacqué-cazenave *et al.*, "Serotonin in animal cognition and behavior," *Int. J. Mol. Sci.*, vol. 21, no. 5, p. 1649, Feb. 2020, doi: 10.3390/ijms21051649.

[10] E. R. Kandel and J. H. Schwartz, "Molecular biology of learning: Modulation of transmitter release," *Science*, vol. 218, no. 4571, pp. 433–443, Oct. 1982, doi: 10.1126/science.6289442.

[11] N. Jiménez-Morales, K. Mendoza-Ángeles, M. Porras-Villalobos, E. Ibarra-Coronado, G. Roldán-Roldán, and J. Hernández-Falcón, "Who is the boss? Individual recognition memory and social hierarchy formation in crayfish," *Neurobiol. Learn. Mem.*, vol. 147, pp. 79–89, Jan. 2018, doi: 10.1016/j.nlm.2017.11.017.

[12] D. Barbas, L. DesGroseillers, V. F. Castellucci, T. J. Carew, and S. Marinesco, "Multiple serotonergic mechanisms contributing to sensitization in Aplysia: Evidence of diverse serotonin receptor subtypes," *Learn. Mem.*, vol. 10, no. 5, pp. 373–386, 2003, doi: 10.1101/lm.66103.

[13] H. S. Ormsbee and J. D. Fondacaro, "Action of Serotonin on the Gastrointestinal Tract (42016)," *Proc. Soc. Exp. Biol. Med.*, vol. 178, no. 3, pp. 333–338, Mar. 1985, doi: 10.3181/00379727-178-42016.

[14] K. Pönicke, U. Gergs, I. B. Buchwalow, S. Hauptmann, and J. Neumann, "On the presence of serotonin in mammalian cardiomyocytes," *Mol. Cell. Biochem.*, vol. 365, no. 1–2, pp. 301–312, Jun. 2012, doi: 10.1007/s11010-012-1270-6.

[15] S. N. Spohn and G. M. Mawe, "Non-conventional features of peripheral serotonin signalling-the gut and beyond," *Nat. Rev. Gastroenterol. Hepatol.*, vol. 14, no. 7, pp. 412–420, Jul. 2017, doi:

10.1038/nrgastro.2017.51.

[16] R. El-Merahbi, M. Löffler, A. Mayer, and G. Sumara, “The roles of peripheral serotonin in metabolic homeostasis,” *FEBS Lett.*, vol. 589, no. 15, pp. 1728–1734, Jul. 2015, doi: 10.1016/j.febslet.2015.05.054.

[17] K. J. Ressler and C. B. Nemeroff, “Role of serotonergic and noradrenergic systems in the pathophysiology of depression and anxiety disorders.,” *Depress. Anxiety*, vol. 12 Suppl 1, no. SUPPL. 1, pp. 2–19, Jan. 2000, doi: 10.1002/1520-6394(2000)12:1+<2::AID-DA2>3.0.CO;2-4.

[18] M. J. Owens and C. B. Nemeroff, “Role of serotonin in the pathophysiology of depression: Focus on the serotonin transporter,” *Clin. Chem.*, vol. 40, no. 2, pp. 288–295, Feb. 1994, doi: 10.1093/clinchem/40.2.288.

[19] B. Roth, “Multiple Serotonin Receptors: Clinical and Experimental Aspects,” *Ann. Clin. Psychiatry*, vol. 6, no. 2, pp. 67–78, Jun. 1994, doi: 10.3109/10401239409148985.

[20] B. L. Roth and Z. Xia, “Molecular and Cellular Mechanisms for the Polarized Sorting of Serotonin Receptors: Relevance for Genesis and Treatment of Psychosis,” *Crit. Rev. Neurobiol.*, vol. 16, no. 4, pp. 229–236, 2004, doi: 10.1615/CritRevNeurobiol.v16.i4.10.

[21] J. D. C. Jeremy *et al.*, “Plasma anti-serotonin and serotonin anti-idiotypic antibodies are elevated in panic disorder,” *Neuropsychopharmacology*, vol. 20, no. 4, pp. 386–391, Apr. 1999, doi: 10.1016/S0893-133X(98)00130-4.

[22] B. J. Venton and R. M. Wightman, “Psychoanalytical electrochemistry: Dopamine and behavior,” *Analytical Chemistry*, vol. 75, no. 19. American Chemical Society, Oct. 01, 2003, doi: 10.1021/ac031421c.

[23] A. S. Darvesh *et al.*, “In vivo brain microdialysis: Advances in neuropsychopharmacology and drug discovery,” *Expert Opin. Drug Discov.*, vol. 6, no. 2, pp. 109–127, Feb. 2011, doi: 10.1517/17460441.2011.547189.

[24] Y. Su, S. Bian, and M. Sawan, “Real-time in vivo detection techniques for neurotransmitters: a review,” *Analyst*, vol. 145, no. 19, pp. 6193–6210, 2020, doi: 10.1039/D0AN01175D.

[25] B. H. C. Westerink, “Brain microdialysis and its application for the study of animal behaviour,” *Behav. Brain Res.*, vol. 70, no. 2, pp. 103–124, Oct. 1995, doi: 10.1016/0166-4328(95)80001-8.

[26] H. Yang, A. B. Thompson, B. J. McIntosh, S. C. Altieri, and A. M. Andrews, “Physiologically relevant changes in serotonin resolved by fast microdialysis,” *ACS Chem. Neurosci.*, vol. 4, no. 5, pp. 790–798, May 2013, doi: 10.1021/cn400072f.

[27] B. L. Sabatini and L. Tian, “Imaging Neurotransmitter and Neuromodulator Dynamics In Vivo with Genetically Encoded Indicators,” *Neuron*, vol. 108, no. 1, pp. 17–32, Oct. 2020, doi: 10.1016/j.neuron.2020.09.036.

[28] C. Tan, E. M. Robbins, B. Wu, and X. T. Cui, “Recent advances in in vivo neurochemical monitoring,” *Micromachines*, vol. 12, no. 2, p. 208, Feb. 2021, doi: 10.3390/mi12020208.

[29] J. E. Robinson *et al.*, “Optical dopamine monitoring with dLight1 reveals mesolimbic phenotypes in a mouse model of neurofibromatosis type 1,” *Elife*, vol. 8, Sep. 2019, doi: 10.7554/eLife.48983.

[30] P. Puthongkham, C. Yang, and B. J. Venton, “Carbon Nanohorn-modified Carbon Fiber Microelectrodes for Dopamine Detection,” *Electroanalysis*, vol. 30, no. 6, pp. 1073–1081, Jun. 2018, doi: 10.1002/elan.201700667.

[31] C. Liu *et al.*, “A wireless, implantable optoelectrochemical probe for optogenetic stimulation and dopamine detection,” *Microsystems Nanoeng.*, vol. 6, no. 1, p. 64, Aug. 2020, doi: 10.1038/s41378-020-0176-9.

[32] S. Banerjee *et al.*, “Electrochemical Detection of Neurotransmitters,” *Biosensors*, vol. 10, no. 8, p. 101, Aug. 2020, doi: 10.3390/bios10080101.

[33] M. L. Huffman and B. J. Venton, “Carbon-fiber microelectrodes for in vivo applications,” *Analyst*, vol. 134, no. 1, pp. 18–24, Dec. 2009, doi: 10.1039/b807563h.

[34] M. A. Johnson, “In vivo electrochemical measurements: Past, present and future,” *Bioanalysis*, vol. 5, no. 2. England, England, pp. 119–122, Jan. 2013, doi: 10.4155/bio.12.322.

[35] E. Castagnola *et al.*, “Real-Time Fast Scan Cyclic Voltammetry Detection and Quantification of Exogenously Administered Melatonin in Mice Brain,” *Front. Bioeng. Biotechnol.*, vol. 8, Nov. 2020, doi: 10.3389/fbioe.2020.602216.

[36] D. L. Robinson, B. J. Venton, M. L. A. V. Heien, and R. M. Wightman, “Detecting subsecond dopamine release with fast-scan cyclic voltammetry in vivo,” *Clin. Chem.*, vol. 49, no. 10, pp. 1763–1773, Oct. 2003, doi: 10.1373/49.10.1763.

[37] F. Sun *et al.*, “Next-generation GRAB sensors for monitoring dopaminergic activity in vivo,” *Nat. Methods*, vol. 17, no. 11, pp. 1156–1166, Nov. 2020, doi: 10.1038/s41592-020-00981-9.

[38] J. Wan *et al.*, “A genetically encoded sensor for measuring serotonin dynamics,” *Nat. Neurosci.*, vol. 24, no. 5, pp. 746–752, May 2021, doi: 10.1038/s41593-021-00823-7.

[39] B. Zhou *et al.*, “Plug-and-play fiber-optic sensors based on engineered cells for neurochemical monitoring at high specificity in freely moving animals,” *Sci. Adv.*, vol. 9, no. 22, p. eadg0218, Jun. 2023, doi: 10.1126/sciadv.adg0218.

[40] Z. Tavakolian-Ardakani, O. Hosu, C. Cristea, M. Mazloum-Ardakani, and G. Marrazza, “Latest trends in electrochemical sensors for neurotransmitters: A review,” *Sensors (Switzerland)*, vol. 19, no. 9, p. 2037, Apr. 2019, doi: 10.3390/s19092037.

[41] P. Hashemi, E. C. Dankoski, J. Petrovic, R. B. Keithley, and R. M. Wightman, “Voltammetric Detection of 5-Hydroxytryptamine Release in the Rat Brain,” *Anal. Chem.*, vol. 81, no. 22, pp. 9462–9471, Nov. 2009, doi: 10.1021/ac9018846.

[42] J. E. Baur, E. W. Kristensen, L. J. May, D. J. Wiedemann, and R. M. Wightman, “Fast-Scan Voltammetry of Biogenic Amines,” *Anal. Chem.*, vol. 60, no. 13, pp. 1268–1272, Jul. 1988, doi: 10.1021/ac00164a006.

[43] K. Nozawa *et al.*, “TRPA1 regulates gastrointestinal motility through serotonin release from enterochromaffin cells,” *Proc. Natl. Acad. Sci. U. S. A.*, vol. 106, no. 9, pp. 3408–3413, Mar. 2009, doi: 10.1073/pnas.0805323106.

[44] C. H. Summers and S. Winberg, “Interactions between the neural regulation of stress and aggression,” *J. Exp. Biol.*, vol. 209, no. 23, pp. 4581–4589, Dec. 2006, doi: 10.1242/jeb.02565.

[45] M. I. Nichkova, H. Huisman, P. M. Wynveen, D. T. Marc, K. L. Olson, and G. H. Kellermann, “Evaluation of a novel ELISA for serotonin: urinary serotonin as a potential biomarker for depression.,” *Anal. Bioanal. Chem.*, vol. 402, no. 4, pp. 1593–1600, Feb. 2012, doi: 10.1007/s00216-011-5583-1.

[46] D. T. Marc, J. W. Ailts, D. C. A. Campeau, M. J. Bull, and K. L. Olson, “Neurotransmitters

excreted in the urine as biomarkers of nervous system activity: Validity and clinical applicability," *Neurosci. Biobehav. Rev.*, vol. 35, no. 3, pp. 635–644, Jan. 2011, doi: 10.1016/j.neubiorev.2010.07.007.

[47] M. Brvar, D. Stajer, G. Kozelj, J. Osredkar, M. Mozina, and M. Bunc, "Urinary serotonin level is associated with serotonin syndrome after moclobemide, sertraline, and citalopram overdose," *Clin. Toxicol.*, vol. 45, no. 5, pp. 458–460, Jul. 2007, doi: 10.1080/15563650601118101.

[48] J. M. Feldman, "Urinary serotonin in the diagnosis of carcinoid tumors," *Clin. Chem.*, vol. 32, no. 5, pp. 840–844, May 1986, doi: 10.1093/clinchem/32.5.840.

[49] K. C. Berridge, T. E. Robinson, and J. W. Aldridge, "Dissecting components of reward: 'liking', 'wanting', and learning," *Curr. Opin. Pharmacol.*, vol. 9, no. 1, pp. 65–73, 2009, doi: 10.1016/j.coph.2008.12.014.

[50] Y. Liu, Y. A. Jiang, Y. Si, J. Y. Kim, Z. F. Chen, and Y. Rao, "Molecular regulation of sexual preference revealed by genetic studies of 5-HT in the brains of male mice," *Nature*, vol. 472, no. 7341, pp. 95–100, 2011, doi: 10.1038/nature09822.

[51] S. Nishizawa *et al.*, "Differences between males and females in rates of serotonin synthesis in human brain," *Proc. Natl. Acad. Sci. U. S. A.*, vol. 94, no. 10, pp. 5308–5313, 1997, doi: 10.1073/pnas.94.10.5308.

[52] R. M. A. Hirschfeld, "History and evolution of the monoamine hypothesis of depression," *J. Clin. Psychiatry*, vol. 61, no. SUPPL. 6, pp. 4–6, 2000, [Online]. Available: http://www.ncbi.nlm.nih.gov/pubmed/10775017.

[53] M. E. Molliver, "Serotonergic neuronal systems: What their anatomic organization tells us about function," *J. Clin. Psychopharmacol.*, vol. 7, no. 6, pp. 3S-23S, Dec. 1987, [Online]. Available: http://www.ncbi.nlm.nih.gov/pubmed/3323265.

[54] S. Athar, "Serotonin and Tryptophan," in *Encyclopedia of Movement Disorders*, Elsevier, 2010, pp. 104–108.

[55] C. Gross and R. Hen, "The developmental origins of anxiety," *Nat. Rev. Neurosci.*, vol. 5, no. 7, pp. 545–552, 2004, doi: 10.1038/nrn1429.

[56] K. P. Lesch, "Serotonergic gene inactivation in mice: Models for anxiety and aggression?," *Novartis Found. Symp.*, vol. 268, pp. 111–140, 2005, doi: 10.1002/0470010703.ch9.

[57] M. Giorgetti and L. H. Tecott, "Contributions of 5-HT2C receptors to multiple actions of central serotonin systems," *Eur. J. Pharmacol.*, vol. 488, no. 1–3, pp. 1–9, Mar. 2004, doi: 10.1016/j.ejphar.2004.01.036.

[58] A. Vidal-Gade *et al.*, "Caenorhabditis elegans selects distinct crawling and swimming gaits via dopamine and serotonin," *Proc. Natl. Acad. Sci. U. S. A.*, vol. 108, no. 42, pp. 17504–17509, 2011, doi: 10.1073/pnas.1108673108.

[59] J. F. Perrier and F. Cotel, "Serotonergic modulation of spinal motor control," *Curr. Opin. Neurobiol.*, vol. 33, pp. 1–7, 2015, doi: 10.1016/j.conb.2014.12.008.

[60] J. R. Strawn, W. S. Neckameyer, and R. L. Cooper, "The effects of 5-HT on sensory, central and motor neurons driving the abdominal superficial flexor muscles in the crayfish," *Comp. Biochem. Physiol. - B Biochem. Mol. Biol.*, vol. 127, no. 4, pp. 533–550, 2000, doi: 10.1016/S0305-0491(00)00287-X.

[61] Q. Yuan, F. Lin, X. Zheng, and A. Sehgal, “Serotonin modulates circadian entrainment in Drosophila,” *Neuron*, vol. 47, no. 1, pp. 115–127, 2005, doi: 10.1016/j.neuron.2005.05.027.

[62] F. Saudou and R. Hen, “5-Hydroxytryptamine receptor subtypes in vertebrates and invertebrates,” *Neurochem. Int.*, vol. 25, no. 6, pp. 503–532, 1994, doi: 10.1016/0197-0186(94)90150-3.

[63] D. H. Edwards and N. Spitzer, “Social Dominance and Serotonin Receptor Genes in Crayfish,” in *Current Topics in Developmental Biology*, vol. 74, Curr Top Dev Biol, 2006, pp. 177–199.

[64] C. Fachinelli, S. Sargo, R. Bataller, and E. L. Rodríguez Echandía, “Effect of 5-HTP and ketanserine on the aggressive reaction induced by food competition in dominant and submissive pigeons (Columba livia),” *Behav. Brain Res.*, vol. 35, no. 3, pp. 265–270, 1989, doi: 10.1016/S0166-4328(89)80146-9.

[65] P. Fossat, J. Bacqué-Cazenave, P. De Deurwaerdère, J.-P. P. Delbecque, and D. Cattaert, “Anxiety-like behavior in crayfish is controlled by serotonin,” *Science*, vol. 344, no. 6189, pp. 1293–1297, Jun. 2014, doi: 10.1126/science.1248811.

[66] S. R. Yeh, R. A. Fricke, and D. H. Edwards, “The effect of social experience on serotonergic modulation of the escape circuit of crayfish,” *Science*, vol. 271, no. 5247, pp. 366–369, 1996, doi: 10.1126/science.271.5247.366.

[67] W. Blenau and M. Thamm, “Distribution of serotonin (5-HT) and its receptors in the insect brain with focus on the mushroom bodies. Lessons from Drosophila melanogaster and Apis mellifera,” *Arthropod Struct. Dev.*, vol. 40, no. 5, pp. 381–394, Sep. 2011, doi: 10.1016/j.asd.2011.01.004.

[68] D. Mellon and C. J. Wheeler, “Coherent oscillations in membrane potential synchronize impulse bursts in central olfactory neurons of the crayfish,” *J. Neurophysiol.*, vol. 81, no. 3, pp. 1231–1241, 1999, doi: 10.1152/jn.1999.81.3.1231.

[69] S. Harzsch and B. S. Hansson, “Brain architecture in the terrestrial hermit crab Coenobita clypeatus (Anomura, Coenobitidae), a crustacean with a good aerial sense of smell,” *BMC Neurosci.*, vol. 9, no. 1, p. 58, Dec. 2008, doi: 10.1186/1471-2202-9-58.

[70] D. Edwards, “Crayfish Escape,” in *Oxford Research Encyclopedia of Neuroscience*, Oxford University Press, 2017.

[71] G. Calderón-Rosete, G. Flores, and L. Rodríguez-Sosa, “Diurnal rhythm in the levels of the serotonin 5-HT1A receptors in the crayfish eyestalk,” *Synapse*, vol. 59, no. 6, pp. 368–373, 2006, doi: 10.1002/syn.20252.

[72] A. J. Reisinger, L. S. Reisinger, E. K. Richmond, and E. J. Rosi, “Exposure to a common antidepressant alters crayfish behavior and has potential subsequent ecosystem impacts,” *Ecosphere*, vol. 12, no. 6, 2021, doi: 10.1002/ecs2.3527.

[73] S.-R. R. Yeh, B. E. Musolf, and D. H. Edwards, “Neuronal adaptations to changes in the social dominance status of crayfish,” *J. Neurosci.*, vol. 17, no. 2, pp. 697–708, Jan. 1997, doi: 10.1523/jneurosci.17-02-00697.1997.

[74] R. Huber and A. Delago, “Serotonin alters decisions to withdraw in fighting crayfish, Astacus astacus: The motivational concept revisited,” *J. Comp. Physiol. - A Sensory, Neural, Behav. Physiol.*, vol. 182, no. 5, pp. 573–583, Apr. 1998, doi: 10.1007/s003590050204.

[75] J. Bacqué-Cazenave, D. Cattaert, J. P. Delbecque, and P. Fossat, “Serotonin has opposite effects on the aggressiveness of crayfish, facing either a smaller or a larger rival: alteration of size perception,” *J. Exp. Biol.*, Jan. 2018, doi: 10.1242/jeb.177840.

[76] D. Chatterjee and R. Gerlai, “High precision liquid chromatography analysis of dopaminergic and serotoninergic responses to acute alcohol exposure in zebrafish,” *Behav. Brain Res.*, vol. 200, no. 1, pp. 208–213, Jun. 2009, doi: 10.1016/j.bbr.2009.01.016.

[77] A. Baranwal and P. Chandra, “Clinical implications and electrochemical biosensing of monoamine neurotransmitters in body fluids, in vitro, in vivo, and ex vivo models,” *Biosens. Bioelectron.*, vol. 121, pp. 137–152, Dec. 2018, doi: 10.1016/j.bios.2018.09.002.

[78] M. F. Hossain and G. Slaughter, “PtNPs decorated chemically derived graphene and carbon nanotubes for sensitive and selective glucose biosensing,” *J. Electroanal. Chem.*, vol. 861, p. 113990, 2020, doi: 10.1016/j.jelechem.2020.113990.

[79] Q. Cao, P. Puthongkham, and B. J. Venton, “Review: New insights into optimizing chemical and 3D surface structures of carbon electrodes for neurotransmitter detection,” *Anal. Methods*, vol. 11, no. 3, pp. 247–261, Jan. 2019, doi: 10.1039/c8ay02472c.

[80] M. Mirzaei and M. Sawan, “Microelectronics-based biosensors dedicated to the detection of neurotransmitters: A review,” *Sensors (Switzerland)*, vol. 14, no. 10, pp. 17981–18008, 2014, doi: 10.3390/s141017981.

[81] M. H. Naveen, N. G. Gurudatt, and Y. B. Shim, “Applications of conducting polymer composites to electrochemical sensors: A review,” *Appl. Mater. Today*, vol. 9, pp. 419–433, 2017, doi: 10.1016/j.apmt.2017.09.001.

[82] L. Xia, Z. Wei, and M. Wan, “Conducting polymer nanostructures and their application in biosensors,” *J. Colloid Interface Sci.*, vol. 341, no. 1, pp. 1–11, 2010, doi: 10.1016/j.jcis.2009.09.029.

[83] N. Chauhan, S. Chawla, C. S. Pundir, and U. Jain, “An electrochemical sensor for detection of neurotransmitter-acetylcholine using metal nanoparticles, 2D material and conducting polymer modified electrode,” *Biosens. Bioelectron.*, vol. 89, pp. 377–383, 2017, doi: 10.1016/j.bios.2016.06.047.

[84] G. Selvolini, I. Băjan, O. Hosu, C. Cristea, R. Săndulescu, and G. Marrazza, “DNA-based sensor for the detection of an organophosphorus pesticide: Profenofos,” *Sensors (Switzerland)*, vol. 18, no. 7, p. 2035, Jun. 2018, doi: 10.3390/s18072035.

[85] A. Ravalli, C. Rossi, and G. Marrazza, “Bio-inspired fish robot based on chemical sensors,” *Sensors Actuators, B Chem.*, vol. 239, pp. 325–329, 2017, doi: 10.1016/j.snb.2016.08.030.

[86] R. Rapini, A. Cincinelli, and G. Marrazza, “Acetamiprid multidetection by disposable electrochemical DNA aptasensor,” *Talanta*, vol. 161, pp. 15–21, 2016, doi: https://doi.org/10.1016/j.talanta.2016.08.026.

[87] L. F. Ferreira *et al.*, “Formation of novel polymeric films derived from 4-hydroxybenzoic acid,” *Mater. Chem. Phys.*, vol. 129, no. 1–2, pp. 46–52, 2011, doi: 10.1016/j.matchemphys.2011.03.053.

[88] D. C. Ferreira, A. E. D. H. MacHado, F. D. S. Tiago, J. M. Madurro, A. G. B. Madurro, and O. Abrahão, “Molecular modeling study on the possible polymers formed during the electropolymerization of 3-hydroxyphenylacetic acid,” *J. Mol. Graph. Model.*, vol. 34, pp. 18–27, 2012, doi: 10.1016/j.jmgm.2012.01.001.

[89] F. D. A. D. S. Silva, C. B. Lopes, L. T. Kubota, P. R. Lima, and M. O. F. Goulart, “Poly-xanthurenic acid modified electrodes: An amperometric sensor for the simultaneous determination of ascorbic and uric acids,” *Sensors Actuators, B Chem.*, vol. 168, pp. 289–296, 2012, doi:

10.1016/j.snb.2012.04.025.

[90] W. Song, Y. Chen, J. Xu, and D. B. Tian, “A selective voltammetric detection for dopamine using poly (gallic acid) film modified electrode,” *Chinese Chem. Lett.*, vol. 21, no. 3, pp. 349–352, 2010, doi: 10.1016/j.cclet.2009.10.008.

[91] G. Herzog, K. Gorgy, T. Gulon, and S. Cosnier, “Electrogeneration and characterization of photoactivable films and their application for enzyme grafting,” *Electrochem. commun.*, vol. 7, no. 8, pp. 808–814, 2005, doi: https://doi.org/10.1016/j.elecom.2005.05.002.

[92] O. Hosu *et al.*, “Nanostructured photoactivatable electrode surface based on pyrene diazirine,” *Electrochem. commun.*, vol. 80, pp. 5–8, 2017, doi: 10.1016/j.elecom.2017.05.002.

[93] O. Hosu, M. M. Bârsan, C. Cristea, R. Săndulescu, and C. M. A. Brett, “Nanostructured electropolymerized poly(methylene blue) films from deep eutectic solvents. Optimization and characterization,” *Electrochim. Acta*, vol. 232, pp. 285–295, 2017, doi: 10.1016/j.electacta.2017.02.142.

[94] M. M. Barsan, M. E. Ghica, and C. M. A. Brett, “Electrochemical sensors and biosensors based on redox polymer/carbon nanotube modified electrodes: A review,” *Anal. Chim. Acta*, vol. 881, pp. 1–23, 2015, doi: 10.1016/j.aca.2015.02.059.

[95] S. Ku, S. Palanisamy, and S.-M. Chen, “Highly selective dopamine electrochemical sensor based on electrochemically pretreated graphite and nafion composite modified screen printed carbon electrode,” *J. Colloid Interface Sci.*, vol. 411, pp. 182–186, 2013, doi: https://doi.org/10.1016/j.jcis.2013.08.029.

[96] F. S. Belaidi *et al.*, “PEDOT-modified integrated microelectrodes for the detection of ascorbic acid, dopamine and uric acid,” *Sensors Actuators B Chem.*, vol. 214, pp. 1–9, Jul. 2015, doi: 10.1016/j.snb.2015.03.005.

[97] S. Demuru and H. Deligianni, “Surface PEDOT:Nafion Coatings for Enhanced Dopamine, Serotonin and Adenosine Sensing,” *J. Electrochem. Soc.*, vol. 164, no. 14, pp. G129–G138, Dec. 2017, doi: 10.1149/2.1461714jes.

[98] R. F. Vreeland *et al.*, “Biocompatible PEDOT:Nafion composite electrode coatings for selective detection of neurotransmitters in vivo,” *Anal. Chem.*, vol. 87, no. 5, pp. 2600–2607, Mar. 2015, doi: 10.1021/ac502165f.

[99] Y. Liu, J. Zhang, Y. Cheng, and S. P. Jiang, “Effect of Carbon Nanotubes on Direct Electron Transfer and Electrocatalytic Activity of Immobilized Glucose Oxidase,” *ACS Omega*, vol. 3, no. 1, pp. 667–676, Jan. 2018, doi: 10.1021/acsomega.7b01633.

[100] Y. Wang and G. J. Weng, “Electrical conductivity of carbon nanotubeand graphene-based nanocomposites,” in *Micromechanics and Nanomechanics of Composite Solids*, Springer International Publishing, 2017, pp. 123–156.

[101] S. K. Vashist, D. Zheng, K. Al-Rubeaan, J. H. T. Luong, and F. S. Sheu, “Advances in carbon nanotube based electrochemical sensors for bioanalytical applications,” *Biotechnol. Adv.*, vol. 29, no. 2, pp. 169–188, Mar. 2011, doi: 10.1016/j.biotechadv.2010.10.002.

[102] S. Palanisamy, S. Ku, and S. M. Chen, “Dopamine sensor based on a glassy carbon electrode modified with a reduced graphene oxide and palladium nanoparticles composite,” *Microchim. Acta*, vol. 180, no. 11–12, pp. 1037–1042, 2013, doi: 10.1007/s00604-013-1028-1.

[103] K. Balasubramanian and M. Burghard, “Biosensors based on carbon nanotubes,” *Anal. Bioanal.*

Chem., vol. 385, no. 3, pp. 452–468, 2006, doi: 10.1007/s00216-006-0314-8.

[104] L. Agüí, P. Yáñez-Sedeño, and J. M. Pingarrón, "Role of carbon nanotubes in electroanalytical chemistry. A review," *Anal. Chim. Acta*, vol. 622, no. 1–2, pp. 11–47, 2008, doi: 10.1016/j.aca.2008.05.070.

[105] J. Li *et al.*, "Carbon nanotube nanoelectrode array for ultrasensitive DNA detection," *Nano Lett.*, vol. 3, no. 5, pp. 597–602, May 2003, doi: 10.1021/nl0340677.

[106] K. E. Geckeler and T. Premkumar, "Carbon nanotubes: Are they dispersed or dissolved in liquids?," *Nanoscale Res. Lett.*, vol. 6, no. 1, p. 136, 2011, doi: 10.1186/1556-276X-6-136.

[107] S. Hu and C. Hu, "Carbon nanotube-based electrochemical sensors: Principles and applications in biomedical systems," *J. Sensors*, vol. 2009, no. iv, 2009, doi: 10.1155/2009/187615.

[108] J. Wang, M. Musameh, and Y. Lin, "Solubilization of Carbon Nanotubes by Nafion toward the Preparation of Amperometric Biosensors," *J. AM. CHEM. SOC*, vol. 125, pp. 2408–2409, 2003, doi: 10.1021/ja028951v.

[109] Y. C. Tsai, J. M. Chen, S. C. Li, and F. Marken, "Electroanalytical thin film electrodes based on a Nafion™ - Multi-walled carbon nanotube composite," *Electrochem. commun.*, vol. 6, no. 9, pp. 917–922, 2004, doi: 10.1016/j.elecom.2004.07.003.

[110] K. B. Male, S. Hrapovic, Y. Liu, D. Wang, and J. H. T. Luong, "Electrochemical detection of carbohydrates using copper nanoparticles and carbon nanotubes," *Anal. Chim. Acta*, vol. 516, no. 1–2, pp. 35–41, 2004, doi: 10.1016/j.aca.2004.03.075.

[111] T. Wang, D. Zhao, X. Guo, J. Correa, B. L. Riehl, and W. R. Heineman, "Carbon nanotube-loaded nafion film electrochemical sensor for metal ions: Europium," *Anal. Chem.*, vol. 86, no. 9, pp. 4354–4361, May 2014, doi: 10.1021/ac500163f.

[112] K. Wu and S. Hu, "Electrochemical study and selective determination of dopamine at a multi-wall carbon nanotube-nafion film coated glassy carbon electrode," *Microchim. Acta*, vol. 144, no. 1–3, pp. 131–137, 2004, doi: 10.1007/s00604-003-0103-4.

[113] S. B. B. Hočevar *et al.*, "Carbon Nanotube Modified Microelectrode for Enhanced Voltammetric Detection of Dopamine in the Presence of Ascorbate," *Electroanalysis*, vol. 17, no. 5–6, pp. 417–422, Mar. 2005, doi: 10.1002/elan.200403175.

[114] B. E. K. K. Swamy and B. J. Venton, "Carbon nanotube-modified microelectrodes for simultaneous detection of dopamine and serotonin in vivo," *Analyst*, vol. 132, no. 9, pp. 876–884, Aug. 2007, doi: 10.1039/b705552h.

[115] A. G. Zestos, "Carbon Nanoelectrodes for the Electrochemical Detection of Neurotransmitters," *Int. J. Electrochem.*, vol. 2018, pp. 1–19, Aug. 2018, doi: 10.1155/2018/3679627.

[116] M. T. Shreenivas, B. E. Kumara Swamy, U. Chandra, and B. S. Sherigara, "Cyclic Voltammetric Investigation of Dopamine at Poly-(Gabapentin) Modified Carbon Paste Electrode," *Int. J. Electrochem.*, vol. 2011, pp. 1–5, 2011, doi: 10.4061/2011/386987.

[117] A. Hermans, R. B. Keithley, J. M. Kita, L. A. Sombers, and R. M. Wightman, "Dopamine detection with fast-scan cyclic voltammetry used with analog background subtraction," *Anal. Chem.*, vol. 80, no. 11, pp. 4040–4048, Jun. 2008, doi: 10.1021/ac800108j.

[118] M. K. Zachek, A. Hermans, R. M. Wightman, and G. S. McCarty, "Electrochemical dopamine detection: Comparing gold and carbon fiber microelectrodes using background subtracted fast scan

cyclic voltammetry," *J. Electroanal. Chem.*, vol. 614, no. 1–2, pp. 113–120, 2008, doi: 10.1016/j.jelechem.2007.11.007.

[119] J. Park, P. Takmakov, and R. M. Wightman, "In vivo comparison of norepinephrine and dopamine release in rat brain by simultaneous measurements with fast-scan cyclic voltammetry," *J. Neurochem.*, vol. 119, no. 5, pp. 932–944, Dec. 2011, doi: 10.1111/j.1471-4159.2011.07494.x.

[120] E. N. Nicolai *et al.*, "Detection of norepinephrine in whole blood via fast scan cyclic voltammetry," *2017 IEEE Int. Symp. Med. Meas. Appl. MeMeA 2017 - Proc.*, vol. 2017, pp. 111–116, May 2017, doi: 10.1109/MeMeA.2017.7985859.

[121] K. M. Wood and P. Hashemi, "Fast-scan cyclic voltammetry analysis of dynamic serotonin reponses to acute escitalopram," *ACS Chem. Neurosci.*, vol. 4, no. 5, pp. 715–720, May 2013, doi: 10.1021/cn4000378.

[122] E. C. Dankoski, R. Mark Wightman, and R. M. Wightman, "Monitoring serotonin signaling on a subsecond time scale," *Front. Integr. Neurosci.*, vol. 7, no. MAY, p. 44, May 2013, doi: 10.3389/fnint.2013.00044.

[123] K. Wu, J. Fei, and S. Hu, "Simultaneous determination of dopamine and serotonin on a glassy carbon electrode coated with a film of carbon nanotubes," *Anal. Biochem.*, vol. 318, no. 1, pp. 100–106, Jul. 2003, doi: 10.1016/S0003-2697(03)00174-X.

[124] P. P. Bertrand, "Real-time detection of serotonin release from enterochromaffin cells of the guinea-pig ileum," *Neurogastroenterol. Motil.*, vol. 16, no. 5, pp. 511–514, Oct. 2004, doi: 10.1111/j.1365-2982.2004.00572.x.

[125] A. D. Miller, G. L. Forster, J. S. Yeomans, and C. D. Blaha, "Midbrain muscarinic receptors modulate morphine-induced accumbal and striatal dopamine efflux in the rat," *Neuroscience*, vol. 136, no. 2, pp. 531–538, 2005, doi: 10.1016/j.neuroscience.2005.08.035.

[126] E. L. Unger *et al.*, "Locomotor hyperactivity and alterations in dopamine neurotransmission are associated with overexpression of A53T mutant human α-synuclein in mice," *Neurobiol. Dis.*, vol. 21, no. 2, pp. 431–443, Feb. 2006, doi: 10.1016/j.nbd.2005.08.005.

[127] W. T. Prater, M. Swamy, M. D. Beane, and D. B. Lester, "Examining the Effects of Common Laboratory Methods on the Sensitivity of Carbon Fiber Electrodes in Amperometric Recordings of Dopamine," *J. Behav. Brain Sci.*, vol. 08, no. 03, pp. 117–125, Jan. 2018, doi: 10.4236/jbbs.2018.83007.

[128] J. Kim and H. Ko, "A 1.2 v Low-Power CMOS Chopper-Stabilized Analog Front-End IC for Glucose Monitoring," *IEEE Sens. J.*, vol. 16, no. 17, pp. 6517–6518, Sep. 2016, doi: 10.1109/JSEN.2016.2591948.

[129] M. H. Nazari, H. Mazhab-Jafari, L. Leng, A. Guenther, and R. Genov, "CMOS neurotransmitter microarray: 96-channel integrated potentiostat with on-die microsensors," *IEEE Trans. Biomed. Circuits Syst.*, vol. 7, no. 3, pp. 338–348, 2013, doi: 10.1109/TBCAS.2012.2203597.

[130] J. M. Stine *et al.*, "Wireless Sensor-Integrated Platform for Localized Dissolved Oxygen Sensing in Bioreactors," *J. Microelectromechanical Syst.*, vol. 29, no. 5, pp. 713–719, Oct. 2020, doi: 10.1109/JMEMS.2020.2999089.

[131] C. Y. Huang, H. T. Huang, and R. T. Yuan, "Design of a portable mini potentiostat for electrochemical biosensors," in *Proceedings of 2017 IEEE 2nd Advanced Information Technology, Electronic and Automation Control Conference, IAEAC 2017*, Sep. 2017, pp. 200–203, doi: 10.1109/IAEAC.2017.8054006.

[132] F. Gao *et al.*, “Wearable and flexible electrochemical sensors for sweat analysis: a review,” *Microsystems Nanoeng.*, vol. 9, no. 1, p. 1, Jan. 2023, doi: 10.1038/s41378-022-00443-6.

[133] A. Heller and B. Feldman, “Electrochemical glucose sensors and their applications in diabetes management,” *Chem. Rev.*, vol. 108, no. 7, pp. 2482–2505, Jul. 2008, doi: 10.1021/cr068069y.

[134] S. Zhao *et al.*, “Recent advances of electrochemical sensors for detecting and monitoring ROS/RNS,” *Biosens. Bioelectron.*, vol. 179, p. 113052, Feb. 2021, doi: 10.1016/j.bios.2021.113052.

[135] C. Dincer *et al.*, “Disposable Sensors in Diagnostics, Food, and Environmental Monitoring,” *Adv. Mater.*, vol. 31, no. 30, p. 1806739, Jul. 2019, doi: 10.1002/adma.201806739.

[136] J. Kim, A. S. Campbell, B. Esteban-Fernández Ávila, J. Wang, B. E.-F. F. de Ávila, and J. Wang, “Wearable biosensors for healthcare monitoring,” *Nat. Biotechnol.*, vol. 37, no. 4, pp. 389–406, 2019, doi: 10.1038/s41587-019-0045-y.

[137] M. Wang *et al.*, “A wearable electrochemical biosensor for the monitoring of metabolites and nutrients,” *Nat. Biomed. Eng.*, vol. 6, no. 11, pp. 1225–1235, 2022, doi: 10.1038/s41551-022-00916-z.

[138] T. Arakawa *et al.*, “A Wearable Cellulose Acetate-Coated Mouthguard Biosensor for in Vivo Salivary Glucose Measurement,” *Anal. Chem.*, vol. 92, no. 18, pp. 12201–12207, 2020, doi: 10.1021/acs.analchem.0c01201.

[139] M. Senior, “Novartis signs up for Google smart lens,” *Nat. Biotechnol.*, vol. 32, no. 9, pp. 856–856, Sep. 2014, doi: 10.1038/nbt0914-856.

[140] K. Kalantar-Zadeh *et al.*, “A human pilot trial of ingestible electronic capsules capable of sensing different gases in the gut,” *Nat. Electron.*, vol. 1, no. 1, pp. 79–87, Jan. 2018, doi: 10.1038/s41928-017-0004-x.

[141] S. A. N. Gowers *et al.*, “Development of a Minimally Invasive Microneedle-Based Sensor for Continuous Monitoring of β-Lactam Antibiotic Concentrations in Vivo,” *ACS Sensors*, vol. 4, no. 4, pp. 1072–1080, Apr. 2019, doi: 10.1021/acssensors.9b00288.

[142] T. Stuart *et al.*, “Wireless, Battery-Free Implants for Electrochemical Catecholamine Sensing and Optogenetic Stimulation,” *ACS Nano*, vol. 17, no. 1, pp. 561–574, Jan. 2023, doi: 10.1021/acsnano.2c09475.

[143] M. Bariya, H. Y. Y. Nyein, and A. Javey, “Wearable sweat sensors,” *Nat. Electron.*, vol. 1, no. 3, pp. 160–171, Mar. 2018, doi: 10.1038/s41928-018-0043-y.

[144] Z. Sonner *et al.*, “The microfluidics of the eccrine sweat gland, including biomarker partitioning, transport, and biosensing implications,” *Biomicrofluidics*, vol. 9, no. 3, p. 031301, May 2015, doi: 10.1063/1.4921039.

[145] P. Swetha, U. Balijapalli, and S. P. Feng, “Wireless accessing of salivary biomarkers based wearable electrochemical sensors: A mini-review,” *Electrochem. commun.*, vol. 140, 2022, doi: 10.1016/j.elecom.2022.107314.

[146] G. Valdés-Ramírez *et al.*, “Non-invasive mouthguard biosensor for continuous salivary monitoring of metabolites,” *Analyst*, vol. 139, no. 7, pp. 1632–1636, 2014, doi: 10.1039/c3an02359a.

[147] J. Kim *et al.*, “Wearable salivary uric acid mouthguard biosensor with integrated wireless electronics,” *Biosens. Bioelectron.*, vol. 74, pp. 1061–1068, 2015, doi: 10.1016/j.bios.2015.07.039.

[148] Y. Lee *et al.*, “Wireless, intraoral hybrid electronics for real-time quantification of sodium intake toward hypertension management,” *Proc. Natl. Acad. Sci. U. S. A.*, vol. 115, no. 21, pp. 5377–5382, 2018, doi: 10.1073/pnas.1719573115.

[149] L. García-Carmona *et al.*, “Pacifier Biosensor: Toward Noninvasive Saliva Biomarker Monitoring,” *Anal. Chem.*, vol. 91, no. 21, pp. 13883–13891, 2019, doi: 10.1021/acs.analchem.9b03379.

[150] R. K. Mishra *et al.*, “Simultaneous detection of salivary Δ9-tetrahydrocannabinol and alcohol using a Wearable Electrochemical Ring Sensor,” *Talanta*, vol. 211, 2020, doi: 10.1016/j.talanta.2020.120757.

[151] N. Thomas, I. Lähdesmäki, and B. A. Parviz, “A contact lens with an integrated lactate sensor,” *Sensors Actuators, B Chem.*, vol. 162, no. 1, pp. 128–134, Feb. 2012, doi: 10.1016/j.snb.2011.12.049.

[152] L. A. Beardslee *et al.*, “Ingestible Sensors and Sensing Systems for Minimally Invasive Diagnosis and Monitoring: The Next Frontier in Minimally Invasive Screening,” *ACS Sensors*, vol. 5, no. 4, pp. 891–910, Apr. 2020, doi: 10.1021/acssensors.9b02263.

[153] G. E. Banis, L. A. Beardslee, J. M. Stine, and R. Ghodssi, “Enteric & 3D-printed hybrid package for sampling in digestive regions,” in *2018 Solid-State Sensors, Actuators and Microsystems Workshop, Hilton Head 2018*, May 2018, pp. 96–97, doi: 10.31438/trf.hh2018.27.

[154] A. S. Sharova, F. Melloni, G. Lanzani, C. J. Bettinger, and M. Caironi, “Edible Electronics: The Vision and the Challenge,” *Adv. Mater. Technol.*, vol. 6, no. 2, p. 2000757, Feb. 2021, doi: 10.1002/admt.202000757.

[155] C. Cheng *et al.*, “A wireless, ingestible pH sensing capsule system based on iridium oxide for monitoring gastrointestinal health,” *Sensors Actuators B Chem.*, vol. 349, p. 130781, Dec. 2021, doi: 10.1016/j.snb.2021.130781.

[156] K. Kalantar-zadeh, N. Ha, J. Z. Ou, and K. J. Berean, “Ingestible Sensors,” *ACS Sensors*, vol. 2, no. 4, pp. 468–483, Apr. 2017, doi: 10.1021/acssensors.7b00045.

[157] Y. T. Li, J. R. Wickens, Y. L. Huang, W. H. T. Pan, F. Y. B. Chen, and J. J. J. Chen, “Integrated wireless fast-scan cyclic voltammetry recording and electrical stimulation for reward-predictive learning in awake, freely moving rats,” *J. Neural Eng.*, vol. 10, no. 4, p. 046007, Aug. 2013, doi: 10.1088/1741-2560/10/4/046007.

[158] K. Khoshnevisan *et al.*, “Electrochemical detection of serotonin: A new approach,” *Clin. Chim. Acta*, vol. 501, pp. 112–119, Feb. 2020, doi: 10.1016/j.cca.2019.10.028.

[159] N. R. Ferreira, A. Ledo, J. Laranjinha, G. A. Gerhardt, and R. M. Barbosa, “Simultaneous measurements of ascorbate and glutamate in vivo in the rat brain using carbon fiber nanocomposite sensors and microbiosensor arrays,” *Bioelectrochemistry*, vol. 121, pp. 142–150, Jun. 2018, doi: 10.1016/j.bioelechem.2018.01.009.

[160] E. S. Bucher and R. M. Wightman, “Electrochemical Analysis of Neurotransmitters,” *Annu. Rev. Anal. Chem.*, vol. 8, pp. 239–261, Jul. 2015, doi: 10.1146/annurev-anchem-071114-040426.

[161] N. T. Rodeberg, S. G. Sandberg, J. A. Johnson, P. E. M. Phillips, and R. M. Wightman, “Hitchhiker’s Guide to Voltammetry: Acute and Chronic Electrodes for in Vivo Fast-Scan Cyclic Voltammetry,” *ACS Chem. Neurosci.*, vol. 8, no. 2, pp. 221–234, Feb. 2017, doi: 10.1021/acschemneuro.6b00393.

[162] S. Sharma, N. Singh, V. Tomar, and R. Chandra, “A review on electrochemical detection of serotonin based on surface modified electrodes,” *Biosens. Bioelectron.*, vol. 107, pp. 76–93, Jun. 2018, doi: 10.1016/j.bios.2018.02.013.

[163] M. E. Rice and C. Nicholson, “Measurement of nanomolar dopamine diffusion using low-noise perfluorinated lonomer coated carbon fiber microelectrodes and high-speed cyclic voltammetry,” *Anal. Chem.*, vol. 61, no. 17, pp. 1805–1810, 1989, doi: 10.1021/ac00192a005.

[164] M. E. Weese, R. A. Krevh, Y. Li, N. T. Alvarez, and A. E. Ross, “Defect Sites Modulate Fouling Resistance on Carbon-Nanotube Fiber Electrodes,” *ACS Sensors*, vol. 4, no. 4, pp. 1001–1007, Apr. 2019, doi: 10.1021/acssensors.9b00161.

[165] L. Lu, L. Liang, K. S. Teh, Y. Xie, Z. Wan, and Y. Tang, “The electrochemical behavior of carbon fiber microelectrodes modified with carbon nanotubes using a two-step electroless plating/chemical vapor deposition process,” *Sensors (Switzerland)*, vol. 17, no. 4, p. 725, Mar. 2017, doi: 10.3390/s17040725.

[166] R. Forster, “Micro- and Nanoelectrodes,” in *Encyclopedia of Applied Electrochemistry*, G. Kreysa, K. Ota, and R. F. Savinell, Eds. New York, NY: Springer New York, 2014, pp. 1248–1256.

[167] A. R. Pereira, J. C. P. de Souza, R. M. Iost, F. C. P. F. Sales, and F. N. Crespilho, “Application of carbon fibers to flexible enzyme electrodes,” *J. Electroanal. Chem.*, vol. 780, pp. 396–406, Nov. 2016, doi: 10.1016/j.jelechem.2016.01.004.

[168] A. E. Ross and B. J. Venton, “Nafion-CNT coated carbon-fiber microelectrodes for enhanced detection of adenosine.,” *Analyst*, vol. 137, no. 13, pp. 3045–3051, Jul. 2012, doi: 10.1039/c2an35297d.

[169] J. Wang, “Carbon-nanotube based electrochemical biosensors: A review,” *Electroanalysis*, vol. 17, no. 1, pp. 7–14, Jan. 2005, doi: 10.1002/elan.200403113.

[170] A. A. Chapin *et al.*, “Electrochemical measurement of serotonin by Au-CNT electrodes fabricated on microporous cell culture membranes,” *Microsystems Nanoeng.*, vol. 6, no. 1, pp. 1–13, Dec. 2020, doi: 10.1038/s41378-020-00184-4.

[171] R. C. Engstrom, “Electrochemical Pretreatment of Glassy Carbon Electrodes,” *Anal. Chem.*, vol. 54, no. 13, pp. 2310–2314, Nov. 1982, doi: 10.1021/ac00250a038.

[172] G. E. Cabaniss, A. A. Diamantis, W. R. Murphy, R. W. Linton, and T. J. Meyer, “Electrocatalysis of Proton-Coupled Electron-Transfer Reactions at Glassy Carbon Electrodes,” *J. Am. Chem. Soc.*, vol. 107, no. 7, pp. 1845–1853, Apr. 1985, doi: 10.1021/ja00293a007.

[173] J. Wang, X. Cai, C. Jonsson, and M. Balakrishnan, “Adsorptive Stripping Potentiometry of DNA at Electrochemically Pretreated Carbon Paste Electrodes,” *Electroanalysis*, vol. 8, no. 1, pp. 20–24, Jan. 1996, doi: 10.1002/elan.1140080105.

[174] Y. Li *et al.*, “Chemical nature of electrochemical activation of carbon electrodes,” *Biosens. Bioelectron.*, vol. 144, no. 44, p. 111534, Nov. 2019, doi: 10.1016/j.bios.2019.111534.

[175] R. L. McCreery, “Advanced carbon electrode materials for molecular electrochemistry,” *Chem. Rev.*, vol. 108, no. 7, pp. 2646–2687, Jul. 2008, doi: 10.1021/cr068076m.

[176] R. G. Compton, E. Laborda, and K. R. Ward, *Understanding voltammetry: Simulation of electrode processes*. IMPERIAL COLLEGE PRESS, 2013.

[177] V. Erspamer and B. Asero, “Identification of Enteramine, the Specific Hormone of the

Enterochromaffin Cell System, as 5-Hydroxytryptamine," *Nature*, vol. 169, no. 4306, pp. 800–801, May 1952, doi: 10.1038/169800b0.

[178] B. B. BRODIE, A. PLETSCHER, and P. A. SHORE, "Evidence That Serotonin Has a Role in Brain Function," *Science*, vol. 122, no. 3177, pp. 968–968, Nov. 1955, doi: 10.1126/science.122.3177.968.

[179] R. M. Hardisty and R. S. Stacey, "5-hydroxytryptamine in normal human platelets," *J. Physiol.*, vol. 130, no. 3, pp. 711–720, Dec. 1955, doi: 10.1113/jphysiol.1955.sp005437.

[180] D. Y. Kim and M. Camilleri, "Serotonin: A mediator of the brain-gut connection," *Am. J. Gastroenterol.*, vol. 95, no. 10, pp. 2698–2709, Oct. 2000, doi: 10.1111/j.1572-0241.2000.03177.x.

[181] P. P. Bertrand, X. Hu, J. Mach, and R. L. Bertrand, "Serotonin (5-HT) release and uptake measured by real-time electrochemical techniques in the rat ileum," *Am. J. Physiol. Liver Physiol.*, vol. 295, no. 6, pp. G1228–G1236, Dec. 2008, doi: 10.1152/ajpgi.90375.2008.

[182] T. Hata *et al.*, "Regulation of gut luminal serotonin by commensal microbiota in mice," *PLoS One*, vol. 12, no. 7, p. e0180745, Jul. 2017, doi: 10.1371/journal.pone.0180745.

[183] K. B. Gross and P. D. Sturkie, "Concentration of Serotonin in Intestine and Factors Affecting Its Release," *Exp. Biol. Med.*, vol. 148, no. 4, pp. 1261–1264, Apr. 1975, doi: 10.3181/00379727-148-38729.

[184] L. Ren *et al.*, "Loss of Ahi1 impairs neurotransmitter release and causes depressive behaviors in mice," *PLoS One*, vol. 9, no. 4, p. e93640, Apr. 2014, doi: 10.1371/journal.pone.0093640.

[185] W. Atkinson, S. Lockhart, P. J. Whorwell, B. Keevil, and L. A. Houghton, "Altered 5-hydroxytryptamine signaling in patients with constipation- and diarrhea-predominant irritable bowel syndrome," *Gastroenterology*, vol. 130, no. 1, pp. 34–43, 2006, doi: 10.1053/j.gastro.2005.09.031.

[186] A. Qasem, A. E. Naser, and S. A. Naser, "Enteropathogenic infections modulate intestinal serotonin transporter (SERT) function by activating Toll-like receptor 2 (TLR-2) in Crohn's disease," *Sci. Rep.*, vol. 11, no. 1, p. 22624, Nov. 2021, doi: 10.1038/s41598-021-02050-3.

[187] A. J. Steckl and P. Ray, "Stress Biomarkers in Biological Fluids and Their Point-of-Use Detection," *ACS Sensors*, vol. 3, no. 10, pp. 2025–2044, Oct. 2018, doi: 10.1021/acssensors.8b00726.

[188] M. Lindström, N. Tohmola, R. Renkonen, E. Hämäläinen, C. Schalin-Jäntti, and O. Itkonen, "Comparison of serum serotonin and serum 5-HIAA LC-MS/MS assays in the diagnosis of serotonin producing neuroendocrine neoplasms: A pilot study," *Clin. Chim. Acta*, vol. 482, pp. 78–83, Jul. 2018, doi: 10.1016/j.cca.2018.03.030.

[189] B. Wu, S. Yeasmin, Y. Liu, and L. J. Cheng, "Sensitive and selective electrochemical sensor for serotonin detection based on ferrocene-gold nanoparticles decorated multiwall carbon nanotubes," *Sensors Actuators B Chem.*, vol. 354, p. 131216, Mar. 2022, doi: 10.1016/j.snb.2021.131216.

[190] R. A. Jacob and G. Sotoudeh, "Vitamin C Function and Status in Chronic Disease," *Nutr. Clin. Care*, vol. 5, no. 2, pp. 66–74, Apr. 2002, doi: 10.1046/j.1523-5408.2002.00005.x.

[191] M. Samsel, K. Dzierzbicka, and P. Trzonkowski, "Adenosine, its analogues and conjugates," *Postepy Hig. Med. Dosw.*, vol. 67, pp. 1189–1203, Dec. 2013, doi: 10.5604/17322693.1078588.

[192] A. Anne, D. Lemordant, G. Dryhurst, and M. Z. Wrona, “Mechanism and products of electrochemical oxidation of 5, 7-dihydroxytryptamine,” *J. Am. Chem. Soc.*, vol. 111, no. 2, pp. 719–726, 1989, doi: 10.1021/ja00184a050.

[193] M. Z. Wrona and G. Dryhurst, “Electrochemical oxidation of 5-hydroxytryptamine in aqueous solution at physiological pH,” *Bioorg. Chem.*, vol. 18, no. 3, pp. 291–317, Sep. 1990, doi: 10.1016/0045-2068(90)90005-P.

[194] C. B. Jacobs, T. L. Vickrey, and B. J. Venton, “Functional groups modulate the sensitivity and electron transfer kinetics of neurochemicals at carbon nanotube modified microelectrodes,” *Analyst*, vol. 136, no. 17, pp. 3557–3565, 2011, doi: 10.1039/c0an00854k.

[195] Q. Cao, D. K. Hensley, N. V. Lavrik, and B. J. Venton, “Carbon nanospikes have better electrochemical properties than carbon nanotubes due to greater surface roughness and defect sites,” *Carbon N. Y.*, vol. 155, pp. 250–257, Dec. 2019, doi: 10.1016/j.carbon.2019.08.064.

[196] T. Huang *et al.*, “Oxidative polymerization of 5-hydroxytryptamine to physically and chemically immobilize glucose oxidase for electrochemical biosensing,” *Anal. Chim. Acta*, vol. 1013, pp. 26–35, Jul. 2018, doi: 10.1016/j.aca.2018.02.020.

[197] M. Z. Wrona and G. Dryhurst, “Oxidation of serotonin by superoxide radical: Implications to neurodegenerative brain disorders,” *Chem. Res. Toxicol.*, vol. 11, no. 6, pp. 639–650, Jun. 1998, doi: 10.1021/tx970185w.

[198] A. N. Patel, P. R. Unwin, and J. V. MacPherson, “Investigation of film formation properties during electrochemical oxidation of serotonin (5-HT) at polycrystalline boron doped diamond,” *Phys. Chem. Chem. Phys.*, vol. 15, no. 41, p. 18085, Nov. 2013, doi: 10.1039/c3cp53513d.

[199] A. A. Chapin, J. Han, and R. Ghodssi, “Adsorption Kinetic Model Predicts and Improves Reliability of Electrochemical Serotonin Detection,” *Methods Protoc.*, vol. 6, no. 1, p. 6, Jan. 2023, doi: 10.3390/mps6010006.

[200] R. Raghupathi *et al.*, “Identification of unique release kinetics of serotonin from guinea-pig and human enterochromaffin cells,” *J. Physiol.*, vol. 591, no. 23, pp. 5959–5975, Dec. 2013, doi: 10.1113/jphysiol.2013.259796.

[201] A. Ujike *et al.*, “IL-1β augments H2S-induced increase in intracellular Ca2+ through polysulfides generated from H2S/NO interaction,” *Eur. J. Pharmacol.*, vol. 821, pp. 88–96, Feb. 2018, doi: 10.1016/j.ejphar.2018.01.006.

[202] S. Lin and H. P. Cohen, “Crayfish ventral nerve cord and hemolymph: Content of free amino acids and other metabolites,” *Comp. Biochem. Physiol. -- Part B Biochem.*, vol. 45, no. 1, pp. 249–263, May 1973, doi: 10.1016/0305-0491(73)90305-2.

[203] J. Wang, “Electrochemical biosensors: Towards point-of-care cancer diagnostics,” *Biosens. Bioelectron.*, vol. 21, no. 10, pp. 1887–1892, Apr. 2006, doi: 10.1016/j.bios.2005.10.027.

[204] S. A. Soper *et al.*, “Point-of-care biosensor systems for cancer diagnostics/prognostics,” *Biosens. Bioelectron.*, vol. 21, no. 10, pp. 1932–1942, Apr. 2006, doi: 10.1016/j.bios.2006.01.006.

[205] C. Loncaric, Y. Tang, C. Ho, M. A. Parameswaran, and H.-Z. Yu, “A USB-based electrochemical biosensor prototype for point-of-care diagnosis,” *Sensors Actuators B Chem.*, vol. 161, no. 1, pp. 908–913, Jan. 2012, doi: 10.1016/j.snb.2011.11.061.

[206] V. Gubala, L. F. Harris, A. J. Ricco, M. X. Tan, and D. E. Williams, “Point of Care Diagnostics: Status and Future,” *Anal. Chem.*, vol. 84, no. 2, pp. 487–515, Jan. 2012, doi: 10.1021/ac2030199.

[207] E. T. S. G. da Silva, D. E. P. Souto, J. T. C. Barragan, J. de F. Giarola, A. C. M. de Moraes, and L. T. Kubota, "Electrochemical Biosensors in Point-of-Care Devices: Recent Advances and Future Trends," *ChemElectroChem*, vol. 4, no. 4, pp. 778–794, Apr. 2017, doi: 10.1002/celc.201600758.

[208] W. Li *et al.*, "The Impact of Recent Developments in Electrochemical POC Sensor for Blood Sugar Care," *Front. Chem.*, vol. 9, p. 723186, Jul. 2021, doi: 10.3389/fchem.2021.723186.

[209] C. I. L. Justino, T. A. P. Rocha-Santos, A. C. Duarte, and T. A. P. Rocha-Santos, "Advances in point-of-care technologies with biosensors based on carbon nanotubes," *TrAC Trends Anal. Chem.*, vol. 45, pp. 24–36, Apr. 2013, doi: 10.1016/j.trac.2012.12.012.

[210] A. Kaushik, A. Vasudev, S. K. Arya, S. K. Pasha, and S. Bhansali, "Recent advances in cortisol sensing technologies for point-of-care application," *Biosens. Bioelectron.*, vol. 53, pp. 499–512, Mar. 2014, doi: 10.1016/j.bios.2013.09.060.

[211] A. F. D. Cruz, N. Norena, A. Kaushik, and S. Bhansali, "A low-cost miniaturized potentiostat for point-of-care diagnosis," *Biosens. Bioelectron.*, vol. 62, pp. 249–254, Dec. 2014, doi: 10.1016/j.bios.2014.06.053.

[212] J. F. Rusling, C. V. Kumar, J. S. Gutkind, and V. Patel, "Measurement of biomarker proteins for point-of-care early detection and monitoring of cancer," *Analyst*, vol. 135, no. 10, p. 2496, 2010, doi: 10.1039/c0an00204f.

[213] C. Y. Huang, M. J. Syu, Y. S. Chang, C. H. Chang, T. C. Chou, and B. Da Liu, "A portable potentiostat for the bilirubin-specific sensor prepared from molecular imprinting," *Biosens. Bioelectron.*, vol. 22, no. 8, pp. 1694–1699, Mar. 2007, doi: 10.1016/j.bios.2006.07.036.

[214] S. C. Chow, J. Shao, H. Wang, and Y. Lokhnygina, *Sample size calculations in clinical research, third edition*, 3rd ed. 2017.

[215] R. J. Soto, J. R. Hall, M. D. Brown, J. B. Taylor, and M. H. Schoenfisch, "In Vivo Chemical Sensors: Role of Biocompatibility on Performance and Utility," *Anal. Chem.*, vol. 89, no. 1, pp. 276–299, Jan. 2017, doi: 10.1021/acs.analchem.6b04251.

[216] K. Tonyushkina and J. H. Nichols, "Glucose Meters: A Review of Technical Challenges to Obtaining Accurate Results," *J. Diabetes Sci. Technol.*, vol. 3, no. 4, pp. 971–980, Jul. 2009, doi: 10.1177/193229680900300446.

[217] J. B. Welsh, S. Psavko, X. Zhang, P. Gao, and A. K. Balo, "Comparisons of Fifth-, Sixth-, and Seventh-Generation Continuous Glucose Monitoring Systems," *J. Diabetes Sci. Technol.*, p. 193229682210998, Jun. 2022, doi: 10.1177/19322968221099879.

[218] Analog Devices, "Datasheet: AD5940/AD5941 High Precision, Impedance, and Electrochemical Front End," 2019. Accessed: Feb. 03, 2021. [Online]. Available: https://www.analog.com/en/products/ad5940.html?doc=AD5940-5941.pdf.

[219] Analog Devices, "AN-1563 APPLICATION NOTE Optimizing the AD5940 for Electrochemical Measurements by Micheál Lambe," 2019. Accessed: Jun. 29, 2023. [Online]. Available: www.analog.com.

[220] J. M. Stine, S. Botasini, L. A. Beardslee, J. A. Levy, and R. Ghodssi, "Miniaturized Capsule System for Hydrogen Sulfide Detection in the Gastrointestinal Tract," 2022.

[221] J. M. Stine, "Mesoscale Embedded Sensor-Integrated Systems for Localized Biomedical Monitoring," University of Maryland, 2023.

[222] S. Labs and Silicon Labs, *BGM121/BGM123 Blue Gecko Bluetooth SiP Module Data Sheet*. 2022, p. 142.

[223] R. C. Huiszoon, J. Han, S. Chu, J. M. Stine, L. A. Beardslee, and R. Ghodssi, "Integrated System for Bacterial Detection and Biofilm Treatment on Indwelling Urinary Catheters," *IEEE Trans. Biomed. Eng.*, vol. 68, no. 11, pp. 3241–3249, Nov. 2021, doi: 10.1109/TBME.2021.3066995.

[224] K. E. Dunham and B. J. Venton, "Improving serotonin fast-scan cyclic voltammetry detection: New waveforms to reduce electrode fouling," *Analyst*, vol. 145, no. 22, pp. 7437–7446, Nov. 2020, doi: 10.1039/d0an01406k.

[225] A. Abdalla *et al.*, "In Vivo Ambient Serotonin Measurements at Carbon-Fiber Microelectrodes," *Anal. Chem.*, vol. 89, no. 18, pp. 9703–9711, Sep. 2017, doi: 10.1021/acs.analchem.7b01257.

[226] M. Satyanarayana, K. Koteshwara Reddy, and K. Vengatajalabathy Gobi, "Nanobiocomposite Based Electrochemical Sensor for Sensitive Determination of Serotonin in Presence of Dopamine, Ascorbic Acid and Uric Acid In Vitro," *Electroanalysis*, vol. 26, no. 11, pp. 2365–2372, Nov. 2014, doi: 10.1002/elan.201400243.

[227] X. Shen, F. Ju, G. Li, and L. Ma, "Smartphone-based electrochemical potentiostat detection system using pedot: Pss/chitosan/graphene modified screen-printed electrodes for dopamine detection," *Sensors (Switzerland)*, vol. 20, no. 10, p. 2781, May 2020, doi: 10.3390/s20102781.

[228] L. O. Orzari, R. Cristina de Freitas, I. Aparecida de Araujo Andreotti, A. Gatti, and B. C. Janegitz, "A novel disposable self-adhesive inked paper device for electrochemical sensing of dopamine and serotonin neurotransmitters and biosensing of glucose," *Biosens. Bioelectron.*, vol. 138, p. 111310, Aug. 2019, doi: 10.1016/j.bios.2019.05.015.

[229] Y. Li *et al.*, "A Portable Electrochemical Platform Integrated with a 3D AuNPs/CNTs Sponge for Point-of-Care Testing of Neurotransmitters," *J. Electrochem. Soc.*, vol. 166, no. 6, pp. B524–B531, Apr. 2019, doi: 10.1149/2.1361906jes.

[230] J. E. Koehne *et al.*, "Carbon nanofiber electrode array for electrochemical detection of dopamine using fast scan cyclic voltammetry," *Analyst*, vol. 136, no. 9, pp. 1802–1805, 2011, doi: 10.1039/c1an15025a.

[231] S. D. Adams, E. H. Doeven, S. J. Tye, K. E. Bennet, M. Berk, and A. Z. Kouzani, "TinyFSCV: FSCV for the Masses," *IEEE Trans. Neural Syst. Rehabil. Eng.*, vol. 28, no. 1, pp. 133–142, Jan. 2020, doi: 10.1109/TNSRE.2019.2956479.

[232] S. Boonkaew, A. Dettlaff, M. Sobaszek, R. Bogdanowicz, and M. Jönsson-Niedziółka, "Electrochemical determination of neurotransmitter serotonin using boron/nitrogen co-doped diamond-graphene nanowall-structured particles," *J. Electroanal. Chem.*, vol. 926, p. 116938, Dec. 2022, doi: 10.1016/J.JELECHEM.2022.116938.

[233] Mayo Clinic Labtoratories, "SERU - Overview: Serotonin, 24 Hour, Urine." https://www.mayocliniclabs.com/test-catalog/Overview/87834.

[234] U. Andreasson *et al.*, "A practical guide to immunoassay method validation," *Front. Neurol.*, vol. 6, no. Aug, p. 179, Aug. 2015, doi: 10.3389/fneur.2015.00179.

[235] J. Han, J. M. Stine, A. A. Chapin, and R. Ghodssi, "A portable electrochemical sensing platform for serotonin detection based on surface-modified carbon fiber microelectrodes," *Anal. Methods*, vol. 15, no. 9, pp. 1096–1104, 2023, doi: 10.1039/d2ay01627c.

[236] J. M. Stine, "Mesoscale Embedded Sensor-Integrated Systems for Localized Biomedical

Monitoring. Ph.D. Thesis," University of Maryland, 2023.

[237] K. P. Curran and S. H. Chalasani, "Serotonin circuits and anxiety: What can invertebrates teach us?," *Invertebr. Neurosci.*, vol. 12, no. 2, pp. 81–92, Dec. 2012, doi: 10.1007/s10158-012-0140-y.

[238] J. B. Panksepp, Z. Yue, C. Drerup, and R. Huber, "Amine neurochemistry and aggression in crayfish," *Microsc. Res. Tech.*, vol. 60, no. 3, pp. 360–368, Feb. 2003, doi: 10.1002/jemt.10274.

[239] R. Huber, K. Smith, A. Delago, K. Isaksson, and E. A. Kravitz, "Serotonin and aggressive motivation in crustaceans: Altering the decision to retreat," *Proc. Natl. Acad. Sci. U. S. A.*, vol. 94, no. 11, pp. 5939–5942, May 1997, doi: 10.1073/pnas.94.11.5939.

[240] X. Liu and J. Liu, "Biosensors and sensors for dopamine detection," *View*, vol. 2, no. 1, p. 20200102, Feb. 2021, doi: 10.1002/VIW.20200102.

[241] R. Huber, J. B. B. Panksepp, Z. Yue, A. Delago, and P. Moore, "Dynamic interactions of behavior and amine neurochemistry in acquisition and maintenance of social rank in crayfish," *Brain. Behav. Evol.*, vol. 57, no. 5, pp. 271–282, 2001, doi: 10.1159/000047245.

[242] C. Xu, F. Wu, P. Yu, and L. Mao, "In Vivo Electrochemical Sensors for Neurochemicals: Recent Update," *ACS Sensors*, vol. 4, no. 12, pp. 3102–3118, Dec. 2019, doi: 10.1021/acssensors.9b01713.

[243] B. L. Hanssen, S. Siraj, and D. K. Y. Wong, "Recent strategies to minimise fouling in electrochemical detection systems," *Rev. Anal. Chem.*, vol. 35, no. 1, pp. 1–28, Apr. 2016, doi: 10.1515/revac-2015-0008.

[244] J. Levenson, J. H. Byrne, and A. Eskin, "Levels of Serotonin in the Hemolymph of Aplysia Are Modulated by Light/Dark Cycles and Sensitization Training," *J. Neurosci.*, vol. 19, no. 18, pp. 8094–8103, Sep. 1999, doi: 10.1523/JNEUROSCI.19-18-08094.1999.

[245] B. J. Venton and D. J. DiScenza, "Voltammetry," in *Electrochemistry for Bioanalysis*, Elsevier, 2020, pp. 27–50.

[246] K. Ibuchi and T. Nagayama, "Opposing effects of dopamine on agonistic behaviour in crayfish," *J. Exp. Biol.*, vol. 224, no. 12, Jun. 2021, doi: 10.1242/JEB.242057.

[247] E. A. Kravitz, "Serotonin and aggression: Insights gained from a lobster model system and speculations on the role of amine neurons in a complex behavior," *J. Comp. Physiol. - A Sensory, Neural, Behav. Physiol.*, vol. 186, no. 3, pp. 221–238, Mar. 2000, doi: 10.1007/s003590050423.

[248] N. Watanabe and M. Yamamoto, "Neural mechanisms of social dominance," *Front. Neurosci.*, vol. 9, no. APR, p. 154, Jun. 2015, doi: 10.3389/fnins.2015.00154.

[249] D. Seo, C. J. Patrick, and P. J. Kennealy, "Role of serotonin and dopamine system interactions in the neurobiology of impulsive aggression and its comorbidity with other clinical disorders," *Aggress. Violent Behav.*, vol. 13, no. 5, pp. 383–395, Oct. 2008, doi: 10.1016/j.avb.2008.06.003.

[250] Y. Su, S. Bian, and M. Sawan, "Real-time: In vivo detection techniques for neurotransmitters: A review," *Analyst*, vol. 145, no. 19, pp. 6193–6210, 2020, doi: 10.1039/d0an01175d.

[251] C. Xu, F. Wu, P. Yu, and L. Mao, "In Vivo Electrochemical Sensors for Neurochemicals: Recent Update," *ACS Sensors*, vol. 4, no. 12. American Chemical Society, pp. 3102–3118, Dec. 27, 2019, doi: 10.1021/acssensors.9b01713.

[252] K. Kashish, S. Gupta, S. K. Dubey, and R. Prakash, "Genosensor based on a nanostructured, platinum-modified glassy carbon electrode for Listeria detection," *Anal. Methods*, vol. 7, no. 6, pp.

2616–2622, 2015, doi: 10.1039/c5ay00167f.

[253] N. D. Daw, S. Kakade, and P. Dayan, “Opponent interactions between serotonin and dopamine,” *Neural Networks*, vol. 15, no. 4–6, pp. 603–616, Jun. 2002, doi: 10.1016/S0893-6080(02)00052-7.

[254] S. Kapur and G. Remington, “Serotonin-dopamine interaction and its relevance to schizophrenia,” *Am. J. Psychiatry*, vol. 153, no. 4, pp. 466–476, Apr. 1996, doi: 10.1176/ajp.153.4.466.

[255] P. T.-H. Wong, H. Feng, and W. L. Teo, “Interaction of the dopaminergic and serotonergic systems in the rat striatum: effects of selective antagonists and uptake inhibitors,” *Neurosci. Res.*, vol. 23, no. 1, pp. 115–119, Aug. 1995, doi: 10.1016/0168-0102(95)90023-3.

[256] M. G. De Simoni, G. Dal Toso, F. Fodritto, A. Sokola, and S. Algeri, “Modulation of striatal dopamine metabolism by the activity of dorsal raphe serotonergic afferences,” *Brain Res.*, vol. 411, no. 1, pp. 81–88, May 1987, doi: 10.1016/0006-8993(87)90683-4.

[257] M. S. Livingstone, R. M. Harris-Warrick, and E. A. Kravitz, “Serotonin and octopamine produce opposite postures in lobsters,” *Science*, vol. 208, no. 4439, pp. 76–79, Apr. 1980, doi: 10.1126/science.208.4439.76.

[258] C. Shiratori, N. Suzuki, Y. Momohara, K. Shiraishi, H. Aonuma, and T. Nagayama, “Cyclic AMP-regulated opposing and parallel effects of serotonin and dopamine on phototaxis in the Marmorkrebs (marbled crayfish),” *Eur. J. Neurosci.*, vol. 46, no. 3, pp. 1863–1874, Aug. 2017, doi: 10.1111/ejn.13632.

[259] D. Sato and T. Nagayama, “Development of agonistic encounters in dominance hierarchy formation in juvenile crayfish,” *J. Exp. Biol.*, vol. 215, no. 7, pp. 1210–1217, Apr. 2012, doi: 10.1242/jeb.066191.

[260] Y. Yamaguchi, Y. A. Lee, A. Kato, E. Jas, and Y. Goto, “The roles of dopamine D2 receptor in the social hierarchy of rodents and primates,” *Sci. Rep.*, vol. 7, no. 1, p. 43348, Feb. 2017, doi: 10.1038/srep43348.

[261] R. A. Palovcik, B. A. Basberg, and J. L. Ram, “Behavioral state changes induced in Pleurobranchaea and Aplysia by serotonin,” *Behav. Neural Biol.*, vol. 35, no. 4, pp. 383–394, Aug. 1982, doi: 10.1016/S0163-1047(82)91034-2.

[262] A. B. Lange, I. Orchard, and F. Michael Barrett, “Changes in haemolymph serotonin levels associated with feeding in the blood-sucking bug, Rhodnius prolixus,” *J. Insect Physiol.*, vol. 35, no. 5, pp. 393–399, Jan. 1989, doi: 10.1016/0022-1910(89)90113-3.

[263] U. Hoeger, “Fate of Circulating Serotonin in the Hemolymph of the Crayfish, Orconectes limosus,” *Zeitschrift fur Naturforsch. - Sect. C J. Biosci.*, vol. 45, no. 9–10, pp. 1053–1059, Oct. 1990, doi: 10.1515/znc-1990-9-1018.

[264] S. Alwarappan, A. Erdem, C. Liu, and C.-Z. Li, “Probing the Electrochemical Properties of Graphene Nanosheets for Biosensing Applications,” *J. Phys. Chem. C*, vol. 113, no. 20, pp. 8853–8857, May 2009, doi: 10.1021/jp9010313.

[265] N. Rivera-Serrano *et al.*, “Static and Dynamic Measurement of Dopamine Adsorption in Carbon Fiber Microelectrodes Using Electrochemical Impedance Spectroscopy,” *Anal. Chem.*, vol. 90, no. 3, pp. 2293–2301, Feb. 2018, doi: 10.1021/acs.analchem.7b04692.

[266] T. Teshiba, A. Shamsian, B. Yashar, S. R. Yeh, D. H. Edwards, and F. B. Krasne, “Dual and opposing modulatory effects of serotonin on crayfish lateral giant escape command neurons,” *J. Neurosci.*, vol. 21, no. 12, pp. 4523–4529, 2001, doi: 10.1523/jneurosci.21-12-04523.2001.

[267] N. Spitzer, D. H. Edwards, and D. J. Baro, “Conservation of structure, signaling and pharmacology between two serotonin receptor subtypes from decapod crustaceans, Panulirus interruptus and Procambarus clarkii,” *J. Exp. Biol.*, vol. 211, no. 1, pp. 92–105, 2008, doi: 10.1242/jeb.012450.

[268] A. Linan-Rico *et al.*, “Mechanosensory signaling in enterochromaffin cells and 5-HT release: Potential implications for gut inflammation,” *Front. Neurosci.*, vol. 10, no. DEC, p. 564, Dec. 2016, doi: 10.3389/fnins.2016.00564.

[269] J. A. Foster and K.-A. McVey Neufeld, “Gut–brain axis: how the microbiome influences anxiety and depression,” *Trends Neurosci.*, vol. 36, no. 5, pp. 305–312, May 2013, doi: 10.1016/j.tins.2013.01.005.

[270] S. Chu, N. Uplekar, S. Liu, and R. Ghodssi, “Complementary Capillary System Integrated Microneedles for Autonomously Localized Therapeutics Loading,” *J. Microelectromechanical Syst.*, vol. 29, no. 5, pp. 912–917, Oct. 2020, doi: 10.1109/JMEMS.2020.2999255.

[271] S. Liu, S. Chu, L. A. Beardslee, and R. Ghodssi, “Hybrid and Passive Tissue-Anchoring Mechanism for Ingestible Resident Devices,” *J. Microelectromechanical Syst.*, vol. 29, no. 5, pp. 706–712, Oct. 2020, doi: 10.1109/JMEMS.2020.2999448.

[272] Á. Cárcamo-Martínez, B. Mallon, J. Domínguez-Robles, L. K. Vora, Q. K. Anjani, and R. F. Donnelly, “Hollow microneedles: A perspective in biomedical applications,” *Int. J. Pharm.*, vol. 599, p. 120455, Apr. 2021, doi: 10.1016/j.ijpharm.2021.120455.

[273] J. A. Levy, M. A. Straker, J. M. Stine, L. A. Beardslee, V. Borbash, and R. Ghodssi, “Thermomechanical Soft Actuator for Targeted Delivery of Anchoring Drug Deposits to the GI Tract,” *Adv. Mater. Technol.*, vol. 8, no. 2, Jan. 2023, doi: 10.1002/admt.202201365.

[274] S. Roman, F. Mion, F. Zerbib, R. Benamouzig, J. Letard, and S. Bruley des Varannes, “Wireless pH capsule – yield in clinical practice,” *Endoscopy*, vol. 44, no. 03, pp. 270–276, Jan. 2012, doi: 10.1055/s-0031-1291541.

[275] Hung Cao *et al.*, “An Implantable, Batteryless, and Wireless Capsule With Integrated Impedance and pH Sensors for Gastroesophageal Reflux Monitoring,” *IEEE Trans. Biomed. Eng.*, vol. 59, no. 11, pp. 3131–3139, Nov. 2012, doi: 10.1109/TBME.2012.2214773.

[276] E. De la Paz *et al.*, “A self-powered ingestible wireless biosensing system for real-time in situ monitoring of gastrointestinal tract metabolites,” *Nat. Commun.*, vol. 13, no. 1, p. 7405, Dec. 2022, doi: 10.1038/s41467-022-35074-y.